Nano Today 24 (2019) 15–47

Contents lists available at ScienceDirect

Nano Today

journal homepage: www.elsevier.com/locate/nanotoday

Review

Colloidal nanocrystals for heterogeneous catalysis

Pit Losch[a,b,1], Weixin Huang[a,1], Emmett D. Goodman[a], Cody J. Wrasman[a], Alexander Holm[a], Andrew R. Riscoe[a], Jay A. Schwalbe[a], Matteo Cargnello[a,*]

[a] Department of Chemical Engineering and SUNCAT Center for Interface Science and Catalysis, Stanford University, Stanford, CA, 94304, USA
[b] Max-Planck-Institut für Kohlenforschung, Kaiser-Wilhelm-Platz, 1, D-45470, Mülheim an der Ruhr, Germany

ARTICLE INFO

Article history:
Received 2 June 2018
Received in revised form
14 November 2018
Accepted 24 December 2018
Available online 17 January 2019

Keywords:
Colloidal nanocrystals
Heterogeneous catalyst
Thermal catalysis
Electrocatalysis
Photocatalysis
Uniform nanostructures

ABSTRACT

Catalytic materials are an essential component of the chemical industry. They find applications in everything from fine chemical manufacturing to greenhouse gas mitigation. They are indispensable for developing a sustainable future. Their development has been continuous, from early trial and error efforts to the first fundamental insights gained through surface science, to modern in-situ characterization and computational predictions. The accumulation of knowledge on the working principles of catalytic surfaces allowed designing and producing better systems with improved performance. Even though tremendous progress has been made thanks to surface science techniques, these studies are usually performed under ultra-high vacuum and are therefore limited in their applicability to more relevant industrial conditions. The control over size, shape and composition in colloidal nanocrystals makes them formidable precursors for model heterogeneous catalysts. These model systems enable linking the insights from surface science studies via in-situ and operando studies to realistic catalytic reaction conditions. In this review, colloidal nanocrystals are presented as powerful building blocks for catalytic materials in the quest for fundamental understanding. A review of the principal methods to produce colloidal nanocrystals with a high level of control is reported, complemented by procedures for how to prepare active catalysts from these particles. Examples and guidelines for the catalytic applications of these materials revolve around the three guiding objectives in catalysis science: activity, selectivity and stability. This work will be limited to examples of this colloidal approach in the areas of thermal, electro- and photocatalysis. The exposed approaches can be used and extended to many other areas of catalysis science, thus providing a new avenue to explore fundamentals and applications of catalytic materials.

Contents

Introduction 16
Scope of this review 17
Overview of the synthesis of colloidal catalysts 17
Synthesis of colloidal materials: size control 18
The use of reducing agents 18
Hot-injection and thermal decomposition methods 18
Soft-templated growth 20
Electrochemical synthesis with size control 21
Shape-control 21
Use of capping agents and surfactants 21
Seed-mediated growth 22
Light-mediated shape control 22
Selective etching and post-synthesis shape control 23

* Corresponding author.
E-mail address: mcargnello@stanford.edu (M. Cargnello).
[1] These authors contributed equally to this work.

https://doi.org/10.1016/j.nantod.2018.12.002
1748-0132/

Compositional control 24
One-pot reduction/thermal decomposition 24
Seed-mediated approaches 25
Template-directed compositional control 26
Nanocrystal-based composites 26
Inorganic hybrids 26
Organic-inorganic hybrids 29
Preparation of colloidal heterogeneous catalysts: deposition, removal of capping agents, activation 30
Advanced tools for characterization 32
Applications of colloidal materials in catalysis 32
Impact of particle size 32
Particle size effects in thermal catalysis 32
Particle size effects in electrocatalysis 34
Particle size effects in photocatalysis 34
Impact of nanocrystal shape 36
Particle shape effects in thermal catalysis 36
Particle shape effects in electrocatalysis 38
Particle shape effects in photocatalysis 38
Impact of nanocrystal composition 38
Particle composition effects in thermal catalysis 38
Particle composition effects in electrocatalysis and photocatalysis 40
Impact of nanocrystal-based composite structure 40
Conclusions and outlook 43
Acknowledgements 43
References 43

Introduction

Catalytic processes are a central technology for a sustainable future. By lowering the energy required for the production and separation of chemicals, and by reducing the emission of pollutants and greenhouse gases, catalytic processes have been crucial in providing and utilizing chemicals at lower environmental cost. These achievements have been made thanks to continuously improving activity and selectivity of novel generations of catalysts. 100 years ago, when the first important catalytic processes (such as the Haber-Bosch process) were investigated, catalysis was practically alchemy. With time, catalysis developed into a science, driven by innovations in characterization techniques, synthesis methods, and computational advances that have allowed to gather crucial information unimaginable to access a century ago, about reaction mechanisms and catalytic materials [1,2]. These improvements unveiled details about the chemical reactivity of catalytic systems that would have been unthinkable in the past. Model systems such as single-crystal surfaces played an important role in transforming catalysis from an art into a science, and novel synthesis techniques have been developed to turn the knowledge gained by surface science studies into engineering and industrial practice. Certainly, it is even more necessary at present that humanity is facing energy shortcomings and global warming, to explore catalytic processes, to understand their very fundamental properties and thereby to refine their activity, selectivity and stability. To this aim, the use and study of catalytic materials under conditions that are as close to the final application as possible are highly desirable.

Colloidal materials are emerging as a valuable tool in the study of fundamental properties of heterogeneous catalysts in industrially relevant conditions [3–6]. Techniques to prepare colloidal particles can provide exquisite control over size, shape and composition such that the heterogeneity of catalytic materials can be drastically decreased, even to the level of atomically-precise materials [7]. Colloidal nanocrystals can be used as building blocks for preparing high-performing heterogeneous catalysts with well-defined structures [8], and the active sites can be encoded within the initial building blocks to further control secondary parameters to affect their reactivity (e.g. support, distance, promoting phases). This level of control allows varying one single parameter at the time providing the opportunity to perform accurate structure-property relationship studies. Through these studies, it is possible to gain crucial knowledge for assembling catalysts with improved activity, stability and selectivity.

Although the discovery and synthesis of colloidal materials is well-known and has been exhaustively documented in past reviews [5,8], recent advances in synthesis and characterization have allowed scientists to find applications for colloidal materials in many new fields, especially catalysis. By looking at publication records, it is clear that the rapid growth of publications involving colloidal materials in heterogeneous catalysts parallels the growth of techniques for nanoparticle (NP) synthesis and structural characterization (i.e. the documentation on improvements in electron microscopy has preceded the exponential growth in nanoparticle science by 10–20 years, Fig. 1). In this still young field, discussion over appropriate terminology has only recently emerged; special attention has to be given to reporting experimental data. For improved description and comparability, best practices have been proposed: [9] a sample shall be described as monodisperse only if the standard deviation in the size (diameter, edge length etc.) is less than 5%; for non-spherical nanocrystals, the overall yield of particles should be treated separately from shape yield (90% shape yield is when an interesting shape is observed in 90% of the observed electron microscopy region), and concentrations should be given in molarities in order to permit comparison with molecular data.

Uniform nanocrystal building blocks have therefore emerged as novel supramolecular precursors to prepare heterogeneous catalysts. This “precursor concept” for the manufacture of solid metal colloid catalysts was already proposed by H. Bönnemann in the 1990s [10]. Compared to conventional salt-impregnation or precipitation methods, colloidal building blocks allow for support-independent synthetic control of size, shape and composition of the metal active phase. In stark contrast to the heterogeneous mixtures obtained by wetness impregnations, colloidally synthesized materials applied permit the study of a homogeneous material with well-defined properties. These materials have attracted industrial attention, and have even been recently commercialized by BASF [11]: catalysts for selective hydrogenation reactions are prepared

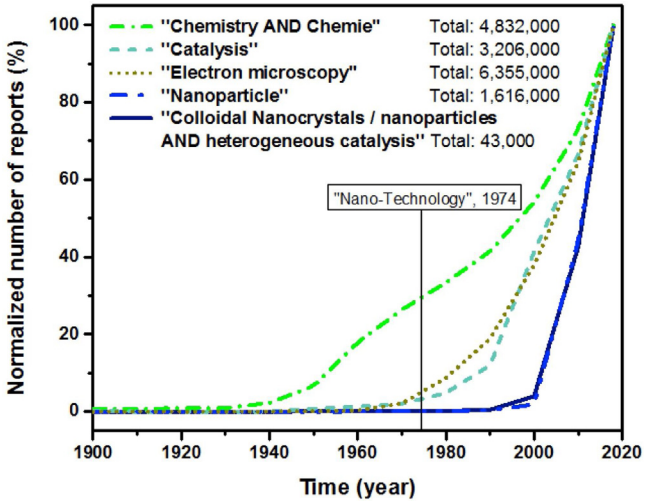

Fig. 1. The normalized number of reports in different related research fields over the last century. Compared to the slow and steady growth of reports citing "chemistry AND Chemie" (the German word was added for completeness), publications involving "catalysis" and "electron microscopy" recently encountered an exponential growth, preceding and enabling the present exponential evolution of "nanoparticles" in general, and "colloidal nanocrystals / nanoparticles AND heterogeneous catalysis" in particular. The term "nanotechnology", often related to the birth of nanosciences, was coined in 1974 by N. Taniguchi. [9] He also correctly predicted the evolution of characterization technique accuracies by the 1980s, to allow for the controlled manipulation of materials at the nanoscale.

by formation of a solution of either Pd or Pt nanocrystals and their subsequent one-pot deposition onto supports. BASF researchers showed that Pd catalysts are active and selective for the hydrogenation of alkynes to alkenes, replacing a previously utilized lead-containing catalyst; and that Pt materials are selective for the hydrogenation of nitroarenes. However, widespread applicability of colloidal materials in the production of commodity chemicals is still lacking due to high synthesis costs and challenges in scalability. Further industrial application hinges on engineering colloidal catalysts, which boast activity and/or selectivity advantages, where decreased operation and separation costs compensate for an increased cost of fabrication.

Scope of this review

The goal of this review is to demonstrate that colloidal catalysts can provide fundamental understanding of catalytic reactions, and ultimately improves catalytic performance. Through colloidal syntheses, where nanocrystal size, shape and composition are carefully controlled and tuned, it is possible to create a class of heterogeneous catalysts with specific and well-defined characteristics.

The study of catalytic behavior on size-controlled active phases is an approach to understand the complex atomic dynamics of catalytic reactions. Nanocrystal size often has a dramatic effect on the activity, selectivity, and stability for a given reaction, as different nanoparticle sizes have different surface area to volume ratios, facet, and electronic structures. Size-dependent activity and selectivity often stems from the relative proportion of differently coordinated sites, or different geometric features, as a function of nanocrystal size. Size-dependent stability relates to the varying surface free energies of different nanocrystal sizes, with the general trend of larger nanocrystals having lower, more stable surface energetics. Colloidally-synthesized, size-selected nanocrystals allow for interrogation of size-dependent properties in model powder catalysts under realistic conditions. Using these tools, researchers have begun to deconvolute the active sites involved in increasingly complex catalytic reactions.

In addition to size, tools have been developed to control the shape of nanocrystals. Metal nanoparticles of different shapes expose different facets and crystal planes. Each facet often has a distinct coordination number and atomic arrangement, which leads to varied adsorption energies of adsorbates and catalytic intermediates. Colloidal synthesis of nanocrystals with well-defined shapes makes the study of reactivity on particular facets possible [11]. Tuning nanocrystal shape allows researchers to study the effect of particular crystal facets on activity, selectivity and stability for various reactions [4,12,13]. In the past, important structure-sensitive discoveries in catalysis were made only under ultra-high vacuum using specially cut crystallographic planes. Although such fundamental work is important, it is still far removed from practical, powder catalysts. High-surface area, colloidally-synthesized nanocrystals of different shapes help bridge the gap between single-crystal studies and practical industrial catalysts. Despite the ability of colloidal synthesis to create nanocrystals (NCs) with specific facets, it is critical to be aware of the stability of the nanocrystal shapes under reaction conditions. Reconstruction of facets under reaction conditions often occurs, especially for those with high surface energy and/or in the presence of strongly binding compounds [14]. It is crucial to verify that a particular shape is maintained after catalytic reactions, if accurate structure-property relationships are to be studied. Colloidal nanocrystals with well-defined facets and shapes can help design structure-property relationship studies that can bridge fundamental work on single crystal surfaces and realistic materials used in industrial applications [13].

Finally, composition causes changes in both electronic states of the surface atoms and atomic arrangement. For example, alloy and intermetallic materials can show very different properties from their corresponding pure components, and even from each other. The binding of adsorbates on their surfaces is likely quite different. Other bimetallic nanostructures such as core-shell geometries can further change surface properties. The geometric positioning of atoms on a surface can be crucial for reactivity, as it is known that some components of an alloy may prefer a certain position on the surface (e.g. steps rather than terraces) in order to minimize surface energy. Compared to traditional catalyst synthesis techniques, which result in ranges of sizes and compositions in a single material, colloidal synthesis of multimetallic nanoparticles provides unprecedented control over both multimetallic composition and specific single-particle geometry. In this way, the impact of each metal in a multimetallic system can be systematically investigated. By varying one parameter at a time, it is possible to draw useful structure-property relationships that can provide a better understanding about reaction mechanisms [15].

Overview of the synthesis of colloidal catalysts

Bottom-up synthesis of colloidal nanoparticles can be carried out both in aqueous and non-aqueous media. These methods usually involve the use of inorganic or organometallic precursors for the particular metal synthesis, and organic ligands, surfactants and polymers to control the size, shape and composition of the synthesized nanostructures [16]. Top-down approaches involving physical methods are also viable strategies to produce controlled nanoparticles, but often do not provide the degree of uniformity, control, flexibility, and scalability provided by colloidal approaches.

Colloidal nanocrystals prepared by wet chemical methods often involve the reduction of metal salts or the decomposition of organometallic precursors under controlled conditions. The key concept in the preparation of uniform colloidal nanoparticles is the controlled temporal separation of particle nucleation and growth. This separation can be achieved by fast addition of a key component, such as a reactant or a reducing agent [17,18], or by the fast

decomposition of a precursor during heat-up of the solution [19]. Other methods, such as electrochemical and photochemical methods in the presence of ligands, can also lead to the production of colloidal nanomaterials with some degree of control.

It is worth mentioning that a benefit of colloidal catalyst synthesis is control over metal loading. After synthesis of a colloidal solution, methods such as thermogravimetric analysis (TGA) are used to determine the concentration of metal nanoparticles in that solution. The addition of a specific solution volume to a catalyst support allows for control over the exact metal weight loading of the catalyst, independent of the specific catalyst support. Other methods such as incipient wetness impregnation might result in metal loss during a high-temperature calcination step, due to volatile metal species (i.e. PtO_2, RuO_4) [20,21].

Herein we will describe various ways of synthesizing colloidal nanocrystals, with special emphasis on the control of their structure. The parameters that can be controlled and are influential for catalytic processes encompass particle size, shape, and elemental composition. Organic ligands used to control the nanocrystals during their synthesis need to be removed in order to fully exploit their potential for catalysis. Therefore, different options for depositing the particles on supports and for removing organic ligands to prepare supported or encapsulated heterogeneous catalysts will be presented. The final part consists of a brief introduction on emerging advanced tools for characterizing and understanding of the formation of these particles.

Synthesis of colloidal materials: size control

The use of reducing agents

The first report of colloidal synthesis using reducing agents goes back to Faraday in 1857 [22], when he recognized that colloidal gold nanoparticles could be prepared from the reduction of $HAuCl_4$ with highly reactive white phosphorus (P_4). Nowadays, various reductants are used to synthesize colloidal nanocrystals, mostly metals, including sodium borohydride, alcohols and gaseous hydrogen. As a general approach, a reducing agent is added to the metal precursor salt in the presence of stabilizing agents (ligands, polymers or surfactants). By controlling the preparation conditions (e.g. concentration of stabilizers/reducing agents, pH, temperature), a variety of colloidal particles with controlled sizes may be obtained.

The strength of the reducing agent is related to the reducing potential required for the metal reduction step: more noble metals such as Au and Pd tend to be reduced more easily, whereas less noble metals such as Cu and Co require stronger reducing agents. The choice of reducing agent also depends on other compounds present in solution, such as ligands, ions and complexing agents that can drastically change the metal reduction potential.

In the early 1950s, Turkevich described the size-selective synthesis of Au colloids by using sodium citrate as both mild reductant and stabilizer [23]. During the synthesis, the metal ions (Au^{3+}) of chloroauric acid are reduced to metallic atoms (Au°) by the reducing agent (sodium citrate). The reaction occurs at mild temperatures in water. By manipulating the concentration of sodium citrate, Au nanoparticles with different size distribution are synthesized. Similar reaction conditions were found to be easily extended to other metals, such as Pd [24]. This method has become very popular, and much interest has arisen in improving particle size distributions and especially in extending the particle size range. Au particles in the whole size range between 1 and 300 nm are nowadays accessible via colloidal synthetic routes. Among recent developments, Peng and colleagues showed that pH value of the medium is a crucial parameter in this chemical reduction route [25]. The solution pH was determined by the concentrations of $HAuCl_4$ and sodium citrate. When pH increased from 3.7 to 6.5, the reactive Au ions ($[AuCl_3(OH)]^-$) would be converted to less reactive $[AuCl_2(OH)_2]^-$ and $[AuCl(OH)_3]^-$ and thus lead to the formation of monodisperse gold nanocrystals. By varying the solution pH between 6.5–7.4, particle size distributions can be tuned in the nanoscale range of 20 to 40 nm. Very recently, Puntes and coworkers further perfected the citrate reduction method to precisely control colloidal Au nanocrystals with narrow size distributions [26,27]. The method takes advantage of a procedure where small ~3.5 nm Au seeds are formed first using trace amounts of tannic acid, which can then be grown into Au NPs larger sizes (Fig. 2). Controlled nucleation of highly monodisperse 3.5 nm Au involves the combined use of two competing reducing agents: tannic acid and sodium citrate. The particles with larger sizes are obtained from the controlled growth of these seeds. In contrast to the seed synthesis, the growth process is achieved by the exclusive use of sodium citrate. The growth of initial seeds mediated by sodium citrate determines their final size. The procedure was also extended to Ag nanocrystals by the same group [28]. By precisely controlling the amount of two reducing agents and other synthetic parameters (temperature of the solution, and the Ag seeds to Ag precursor ratio), Ag nanoparticle sizes from 10 to 300 nm could be obtained.

Metals that are harder to reduce require stronger reducing agents, especially in the presence of ligands that can further increase their reduction potential. Sun and Murray showed that monodisperse Co NPs can be synthesized by reduction of cobalt ions with superhydride ($LiBEt_3H$, Et = ethyl) at 200 °C in dioctylether [18]. This synthesis method combines the use of a reducing agent, and the practice of hot injection. The control of particle size between 2 and 11 nm was demonstrated by using stabilizing trialkylphosphine ligands with different bulkyness: steric hindrance in trioctylphosphine leads to smaller particles (more nuclei are formed, less growth), whereas larger particles are obtained when using a less sterically hindered phosphine such as tributylphosphine.

Hot-injection and thermal decomposition methods

The separation of nucleation and growth in order to obtain uniform nanocrystals can be induced by a rapid supersaturation of monomers in solution. This can be achieved either by rapid addition of a necessary compound during the synthesis ("hot injection" methods), or by a fast decomposition of a precursor in solution during the rapid heat up of the synthesis mixture ("heat-up" methods).

The hot-injection method was first reported by Bawendi's group for the synthesis of cadmium chalcogenide nanocrystals [17]. The rapid injection of precursors into the solvent at a high temperature causes the fast nucleation of NPs, which is followed by growth on the existing nuclei to form monodisperse nanocrystals. This synthetic route enabled the preparation of CdSe nanocrystals with controllable sizes from 2 to 12 nm and narrow size distributions (~10%). The nanocrystals can be further refined by size-selective precipitation. More recently, the hot-injection method was extended to synthesize colloidal nanoparticles of various other metals and metal alloys coupled to the use of reducing agents, including the cobalt nanocrystals that were discussed above [17,29,30].

Inspired by the hot-injection method, synthesis processes to induce a burst nucleation have been developed and the thermal decomposition method gained much traction because of its easier implementation (one-pot as opposed to quick injection of chemicals at elevated temperatures) [19]. Furthermore, this method has been easily extended to many more materials, such as metals, metal oxides, and chalcogenides. In this method, all reagents (i.e. precursors, solvents and surfactants) are mixed at room temperature and the mixture is then heated at a controlled rate to a desired temperature to induce the nucleation and growth of nanoparticles. In this case, ligands are crucial to control the thermal decomposition; common ligands (e.g. organic amines, phosphines, alcohols and

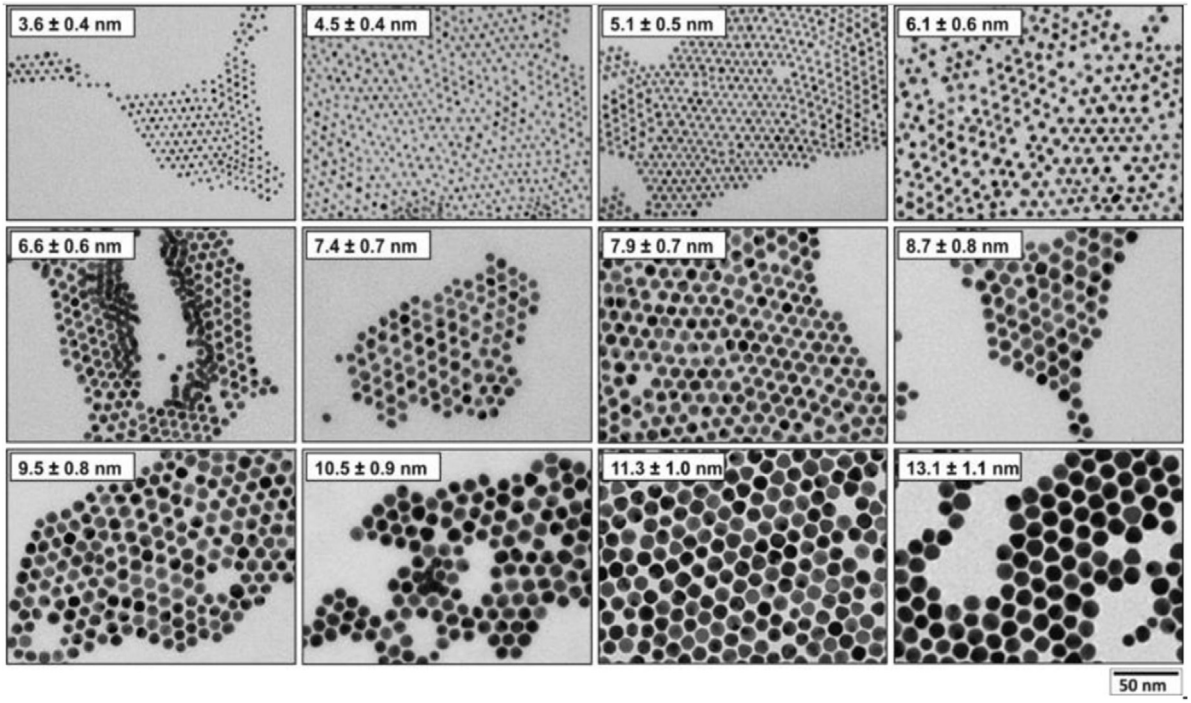

Fig. 2. Transmission electron microscopy images of an improved citrate-based Au nanocrystal synthesis using seed particles (3.6 nm) and further growing them in solution. The particle size can be tuned from 3.6 ± 0.4 nm of the seeds to 13.1 ± 1.1 nm, with narrow particles size distributions of 10% dispersion or less.
Reprinted with permission from Ref. [26] Copyright (2016) American Chemical Society.

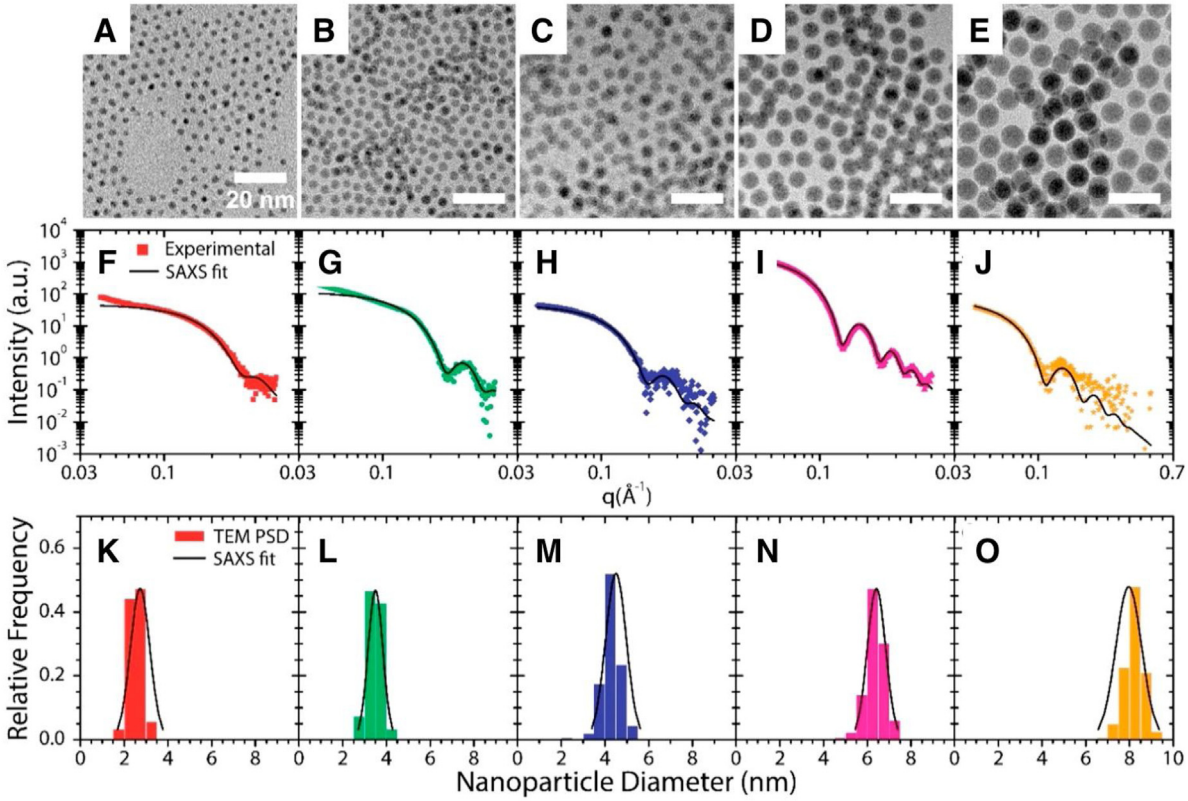

Fig. 3. Representative TEM images (A – E), small-angle X-ray scattering patterns (F – J), and particle size distributions (K – O) for uniform Pd NCs obtained by heat-up methods.
Reprinted with permission from Ref. [36] Copyright (2017) American Chemical Society.

carboxylic acids) are utilized to tune the conditions of nucleation and growth during synthesis. Furthermore, reactions of amines or alcohols and acids at high temperature lead to the formation of oxide materials through the slow release of water by amide or ester forming reaction [31]. This method was first demonstrated for the synthesis of FePt nanocrystals by using oleylamine (OLAM)

and oleic acid (OLAC) as stabilizers [32]. The synthesis is based on the reduction of platinum acetylacetonate and decomposition of iron pentacarbonyl precursors. $Fe(CO)_5$ is thermally unstable and decomposes to Fe and carbon monoxide at high temperature, while $Pt(acac)_2$ is readily reduced by a mild reducing agent, 1,2-alkanediol, to Pt. Thus, Fe and Pt atoms combine to form bimetallic [Fe–Pt] clusters acting as seeds. The growth process proceeds as more Fe–Pt atoms deposit on the seeds for obtaining the desired sizes. By further controlling the growth of the particles using a combination of oleic acid and oleylamine, sizes between 3 and 10 nm could be obtained, eventually using a seed-mediated approach for the larger particle sizes. This decomposition reaction was further extended to demonstrate its utility in large scale synthesis of iron oxide nanocrystals [33]. Often, the role of different parameters (temperature, time, concentrations, surfactants) on the synthesis of nanocrystals by heat-up methods is hard to parse out from simple ex-situ analysis of the final materials [34]. In-situ techniques for the study of reaction mechanisms and nanocrystal formation are important to provide knowledge on how the colloidal materials are formed. In a recent study, our group quantitatively studied the roles of three common ligands (trioctylphosphine (TOP), oleylamine, and oleic acid) in the colloidal synthesis of Pd nanocrystals [35]. Using small-angle x-ray scattering (SAXS) throughout the synthesis, we quantitatively describe how TOP significantly slowed down the precursor decomposition and the nucleation rate so to cause the formation of larger (and eventually more polydisperse) NCs. Oleylamine facilitated the conversion of the Pd-TOP complex into monomers, leading to smaller NPs due to stronger binding with the growing Pd NCs. In contrast, oleic acid strongly influenced the nucleation kinetics, and the presence of more oleic acid resulted in larger Pd NCs. By rationally combining the different surfactants and reaction conditions, the synthesis of monodisperse Pd NPs with a wide size range from 3 to 11 nm and control at the nanometer level was demonstrated. This set of particles, depicted in Fig. 3, proved useful to explain structure-property relationships in methane combustion catalysts [36].

Soft-templated growth

In the examples outlined above, surfactants serve as ligands to control the nucleation and growth of colloidal materials in solution acting as what could be considered soft templates. The final material structure is dictated by chemical interactions between them and the transition metal precursors. There are methods to control the size of colloidal nanocrystals that rely instead on physical barriers to template the synthesis of nanomaterials. Micelles can be considered as soft templates, whereas inorganic material templates can also be used and will be discussed more in detail. Micelles are structures formed in solution, where surfactants assemble into agglomerates (spherical shape is the most common, but others are possible) to maximize the interactions between hydrophilic heads and hydrophobic tails with solvents. Due to the possibility of segregating small volumes of one solvent in another, they have been used for the synthesis of colloidal materials, where the micellar droplets act as nanoreactors [37–39].

Micelles, with a hydrophilic (referred to as inverse or reverse micelles) or hydrophobic (direct micelles) internal volume dispersed in a solvent phase with opposite polarity, form small vesicles as a non-continuous phase separation. The preference for the formation of direct over reverse micelles can be predicted by the critical packing parameter (CPP) of constituent surfactants [39]. This parameter indicates the geometrical / entropical ability of a surfactant molecule to preferentially form inverse micelles (CPP > 1) or normal micelles (CPP < 1). Apart from entropy, factors such as temperature and pressure, as well as surfactant concentration (important threshold is the critical micellar concentration) affect the formation and size of micelles. The optimization of a micellar size-controlled synthesis usually is a challenging undertaking. Nevertheless, the adaptability of the polarity in the micellar cavity, its size and various other parameters render the technique very attractive.

As early as 1982, reverse micelles (where water is contained within the emulsion droplets and organic solvents make up the continuous phase) were used as a soft template for the synthesis of Pt, Rh, Pd and Ir metal nanoparticles [40]. In this method, the dissolution and enrichment of metal salts within micelles precede the reduction of metal salts with hydrogen or hydrazine. Instead of monomeric surfactants, micelles can also be composed of polymer polyvinylpyrrolidone (PVP) dispersed in toluene and used as nanocompartments for the size-controlled growth of various metallic or metal oxide nanoparticles (Fig. 4) [41]. The size of the colloidal gold particles could for example be varied from 1 to 15 nm depending on the concentration of the metal salt. Supported Au nanoclusters have also been synthesized from diblock (PVP)-copolymer micelles. The advantage of this size-selective method, is that the particles can be deposited onto flat supports with control over interparticle distance [42], which can represent an important element to investigate in model catalytic materials.

Reverse micellar templating is the most common method for the size-controlled synthesis of metal (oxide) nanoparticles as it allows for control of the concentration of metal salts in the spherical polar pockets of the micelles. Noteworthy examples include the synthesis of cobalt nanoparticles with sizes from 6.5 to 21 nm in diameter, which could be efficiently deposited on supports and subsequently turned into cobalt oxide for the application in Fischer-Tropsch catalysis [43,44]. There are quantitative models for the dependence of size of non-ionic reverse micelles on parameters such as molecular structure of the surfactant, the type of oil, the total concentration of surfactant, the ratio of surfactant to total surfactant, the water to surfactant molar ratio, temperature, salt concentration, and polar phase [45]. In these studies, authors disclosed that the best approach for size control is in varying temperature, water concentration, and the water-to-surfactant molar ratio, as well as the proportion of short and long chain surfactants.

In addition to solid-core metal nanoparticles, whose growth can be controlled by micelles, nanoporous crystals such as zeolites, metal organic frameworks (MOFs) and covalent organic frameworks (COFs) can also be produced in the form of very small colloidal crystallites using highly complex surfactant templates. In this way, classical catalyst supports can become colloidal particles themselves. The group of R. Ryoo has reported pioneering advances in this field by developing surfactants containing a zeolite structure-directing moiety. [46] Such syntheses are performed under hydrothermal conditions, where silicon and aluminum (or another tetrahedral atom) sources become concentrated, forming lamellar micelles. In these confined spaces, nanosized zeolite crystals are formed upon self-assembly and condensation reactions. Depending on the type of micelles, the dimensionality of the final particles could be tuned to form 2D zeolite nanosheets or nanorods [46,47]. It is worth mentioning that, as in the case of metal nanoparticles, the micellar size control of a crystallising inorganic-organic hybrid (i.e., the zeolite-surfactant pair) requires insights at the molecular and supramolecular level to enable a feedback loop optimization of the synthesis. Small angle x-ray scattering (SAXS), is a powerful technique to acquire such knowledge at the molecular and supramolecular level, and NMR has proven as a valuable complementary method [48,49]. One remaining technical limitation is the instrumental difficulty or even inability to perform such measurements under in-situ conditions (high pressures of water steam).

A similar trend can be observed for partially or fully organic nanoporous frameworks such as metal organic frameworks (MOFs) for coordination porous crystals or covalent organic frameworks

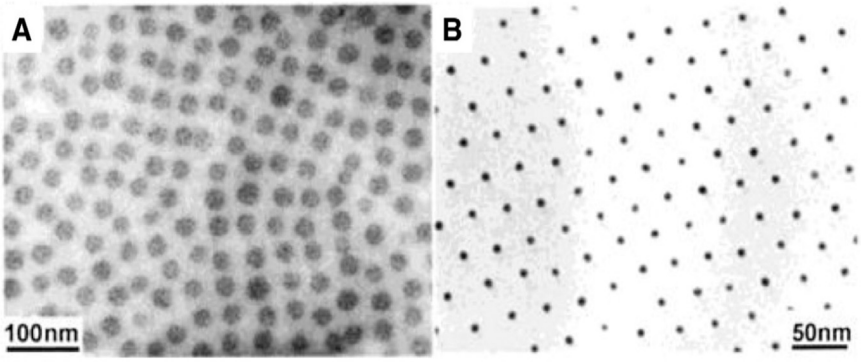

Fig. 4. Au nanoparticles prepared in micelles for the PVP-in-toluene system. Two striking features are shown: the micelle forms a pocket guiding the size-selective growth of a particle (A), and particles in micelles will deposit as films on supports with precise interparticle distances (B). The surfactant chain length governs the latter effect. Reprinted with permission from Ref. [41] Copyright (2000) American Chemical Society.

(COFs) for fully polymerized porous networks [50,51]. There are potential benefits in conceiving such porous materials at sizes of colloidal nanoparticles. In particular, in applications such as catalysis, gas separation or membrane technology, the size control of such crystals allows one to tune internal mass transport with respect to external mass transport. The synthesis of such porous partial or fully organic frameworks remains rather complex: multiple parameters need to be adapted to guarantee size control. Their formation, as for zeolites, is determined via sometimes rather slow crystallization or polymerization reactions.

Electrochemical synthesis with size control

While many of the colloidal nanoparticle preparations described above rely on chemical or thermal reduction of metal precursors, it is also possible to directly use electrons to the same effect. Electrodeposition, the reduction of metal ions onto an electrode, is a common way to prepare rough films of varying composition and textural properties [52–54]. It is frequently done in aqueous solutions.

However, when the deposition is done in non-aqueous electrolytes and in the presence of a surfactant, colloidal metal nanoparticles can be produced instead of a film. In this process, a sacrificial anode is used to supply metal ions that transport to the cathode where they are recombined with electrons to produce metallic nanoparticles. Polar aprotic solvents, such as tetrahydrofuran and dimethylformamide are employed. As in previously described chemical syntheses, a surfactant is used to stabilize the particles in solution [55]. By manipulating the current density during synthesis, metal particles within size range from 1.4 to 4.8 nm could be obtained. Later this method has been extended to the use of metal salts that can be directly added to the solution in addition or instead of the sacrificial anodes [56]. Thereby this method allowed for the size selective synthesis of, amongst others, Pt, Rh, Ru, Mn but also nanoalloy samples (e.g. PtSn or PdPt). The use of a non-traditional cell incorporating two anodes of different metals allows for compositional control [57,58]. The coulombic efficiencies reported for these processes are typically in the vicinity of 50%, and this method could be a way to avoid the use of expensive and/or dangerous reducing agents, such as inorganic and organic hydrides, in colloidal nanocrystal synthesis. Electrical energy can also be used to make colloidal nanoparticles through electrical explosion of a wire in an organic solvent [59]. In this unique approach, a high current causes a wire to abruptly disintegrate in organic solvent. Depending on the reactivity of the metal, this can form a carbide or a metal nanoparticle. The particles are capped by in-situ polymerized capping agents.

Shape-control

Use of capping agents and surfactants

Due to preferential binding of ligands to different crystal planes, surface-capping agents are routinely used to alter the distribution of exposed nanocrystal facets, which results in different nanocrystal shapes. The crystal planes, which are passivated by strongly bound ligands, are those commonly found in the final nanocrystal product. This method is by far the most commonly used to obtain shape control in colloidal materials.

In a pioneering work, researchers demonstrated how preferential binding of fluoride to {001} facets of TiO_2 particles can induce the formation of anatase TiO_2 with these exposed reactive facets [60]. Mechanistically, these were synthesized through the in-situ release of hydrofluoric acid (HF) formed from a TiF_4 precursor (Fig. 5) [61]. Because F^- acts as a capping agent, which strongly adsorbs on {001} planes of anatase TiO_2, selective growth occurred on the usually more stable {101} facet, leaving the protected {001} facet unchanged. The amount of HF released during the synthesis can be adapted by tuning the amount of fluoride precursor used (by mixing in TiF_4 and $TiCl_4$), or by changing the TiF_4/oleylamine ratio. The authors therefore demonstrated the control of small TiO_2, crystallites, where the exposed facets could be tuned from almost only {101} to near exclusively {001} (Fig. 5).

In addition to metal oxides, there is clear interest in shaping colloidal nanocrystals such to compare small particles to single-crystalline surfaces that have been long-studied using ultra high vacuum techniques [62–64]. Halogen ions (F^-, Cl^-, Br^-, and I^-) have been utilized in the synthesis of shape-control metals and alloys, since these ions can strongly adsorb on certain planes and thus stabilize specific facets during the growth process. The case of Pd is particularly interesting, where many different shapes can be obtained by varying the concentration of halogenides, capping ligands and seed morphology [65]. More recently, by introducing NaCl and NaI as capping agents, two distinct shapes of PtPd nanocrystals were prepared with selective exposure of {111} and {100} facets respectively [66]. The absence of halide ions (Cl^- and I^-) resulted in the formation of the nanocrystals with uncontrolled sizes and shapes, proving that the choice of halide was the major factor in controlling the shape of PtPd nanocrystals.

In the case of palladium, different surfactants can also be added to stabilize or block specific facets, meanwhile permitting others to grow [67]. Gaseous carbon monoxide (CO) is a classic example of a strong-binding agent that directs the growth of specific facets. It is known that CO strongly binds to metallic surfaces and may therefore be used as structure-directing agent. Gaseous CO could directly be flown into the reaction flask [68], but because of the hazards of handling toxic pure CO gas, convenient methods rely on the use

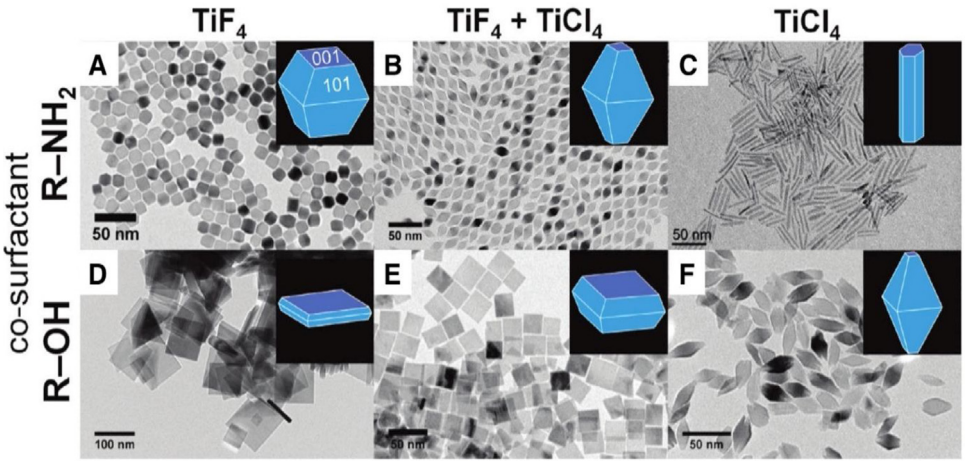

Fig. 5. Representation of TEM micrographs of TiO_2 nanocrystals synthesized using the precursor TiF_4 (A, D), a mixed precursor of TiF_4 and $TiCl_4$ (B, E), and $TiCl_4$ (C, F). Reprinted with permission from Ref. [61] Copyright (2012) American Chemical Society.

of carbonyl precursors that decompose at high temperatures and can therefore be used in conjunction with heat-up methods to produce colloidal nanocrystals. A recent study showed that bimetallic Pt-Mn nanocubes were obtained using manganese decacarbonyl [$Mn_2(CO)_{10}$] as precursor [69]. The in-situ formation of CO from the decomposition of Mn precursor that binds to the (100) facets of growing Pt nuclei leads to the stabilization of certain facets and therefore to shape control to make cubic particles.

Pioneering work by Younan Xia and co-workers on the preparation of several materials with specific geometries inspired many works involving tunable nanocrystal facets [70]. In early works, his group showed that polyol methods could be adapted to using capping agents, such as poly(vinylpirrolidone) (PVP), to shape the growth of Ag and Au nanoparticles [70]. Usually, these synthesis methods use a seed-mediated approach, where small nanocrystals (seeds) are used to trigger the heterogeneous nucleation of metals on the surface of the pre-formed seeds (see also below in this section). The main parameters for tuning the shape of the nanocrystals were the transition metal salt concentration, amount of capping agent, and temperature. It was found that a narrow set of conditions would provide cubes, presumably due to the particular interactions between PVP chains and Ag facets (highly dependent on the parameters cited before) that would change the surface energy of different facets in solution.

Tuning the pH of the media can also control the growth of metal oxides, due to their hydroxylated surfaces, such that OH^- or H^+ ions are used as selective capping agents on specific facets with acid-base properties. The acid–base balance (pH) in the solution, which modulates the surface potential of nanoparticles, leads to different stabilities of metal oxide and metal hydroxide surfaces, and ultimately affects the synthesis of specific facets in ceria materials [71].

Seed-mediated growth

An additional advantage of colloidal nanocrystals is that they can be used as starting building blocks to further increase their structural complexity in seed-mediated synthesis. This method has seen great successes in the synthesis of gold nanorods and has been adapted for many other materials [72]. Seed-mediated synthesis often removes the nucleation step of nanocrystal formation, which can introduce polydispersity, and thus enables more uniform particles to be produced. In many cases, the introduction of pre-formed seeds allows for particle geometries not possible via traditional one step synthetic routes. New shapes are achieved by the favored addition of nanocrystal precursors to specific facets of the seeds. This is accomplished either by addition to those facets being energetically favorable or by the addition of surfactants to change the surface energies of specific facets as described above. Preferential facet growth is utilized in the synthesis of long brookite titania rods where favored growth in the axial direction results in a rod geometry [73,74]. The size of these rods can be tuned by changing the amounts of precursors added. In many cases, the concentration of precursor and its relation to the number of seeds also determines the final particle geometry. The precursor to particle ratio can be controlled either by adding different levels of precursor at once or by adding a constant stream of precursor. For example, Au nanocrystals with a variety of shapes from spheres to cubes can be produced using different concentrations of precursor [75]. On the other hand, several different types of Au coverages between Au shells and Au heterodimers can be added to Pd seeds by changing the injection rate of Au precursors [76]. The concentration of precursor is important because higher concentrations favor faster deposition, which often forms uniform shells, while low concentrations favor deposition on energetically favorable sites, leading to more complex shapes like heterodimers or islands on corner sites depending on the epitaxial relationship between seeds and precursor materials and the experimental conditions [77]. These methods can also provide complex architectures that would otherwise be very difficult to synthesize. In this respect, C.L. Lu et al. used this method to produce highly complex structures composed of Au-Pd core-shell nanocrystals by taking advantage of preferential etching and what they claimed to be Au-Pd mismatch at the low temperatures of the synthesis [78].

Along this line of thought, H.-C. Peng's group proved that it is possible to separate the two discrete phenomena of particle growth and nucleation when well-defined seeds are used [79]. They could thereby analyze the explicit roles of thermodynamic (temperature, pressure and respective concentrations etc.) and kinetic (e.g. ligands) parameters in directing the evolution of colloidal metal nanocrystals into specific shapes during the particle growth phenomenon. For example, starting from single-crystal seeds exposing {100}, {111}, and {110} facets, colloidal nanocrystals with diversified shapes were obtained by adjusting various thermodynamic or kinetic parameters. They also claim that these mechanistic insights can be extended to predict the products of conventional one-pot syntheses, which involve self-nucleation.

Light-mediated shape control

Alongside chemical interactions and physical barriers, the interaction between light and matter via surface plasmonic effects has

also gained increasing interest in the community. In a landmark study, R. Jin and co-workers developed a photoinduced method to shape silver nanospheres into triangular silver nanocrystals [80]. Later, they reported an extension of their methodology to synthesize relatively monodisperse nanoprisms with desired edge lengths in the 30–120 nm range [81]. According to their reports, the particle growth process is governed by surface plasmon excitations. Depending on the illumination wavelengths chosen, the excitations of the localized surface plasmon resonance (LSPR) led either to fusion of nanoprisms in an edge-selective manner resulting in a bimodal particle size distribution, or to the growth of the nanoprisms until they reached their light-controlled final size. Follow-up research on plasmon-mediated solution synthesis permitted accessing tremendous control over size in addition to shape, via adapting the wavelength of monochromatic light [82]. One such later study by V. Bastys et al. led to the proposition of an alternative particle growth mechanism postulating the formation of Ag nanoprisms consuming preformed Ag seeds, instead of edge-selective fusion as described earlier [82]. Even more recent in-situ STEM studies on such growing Ag-nanoprisms from nanoparticulate seeds were performed, and the authors, thanks to irradiation with white light inside the electron microscope setup, were able to visualize the processes of prism-formation with temporal resolution [83]. The crystalline edge growth was attributed to local plasmonic hotspots.

The surface plasmon-driven shape control has later also been successfully extended to other shapes. Two related studies reported silver nanoparticles with respectively bipyramidal, truncated bipyramidal, prismatic and truncated bi-tetrahedral shapes by investigating and controlling the kinetics of the plasmon-driven growth [84,85]. The relative rates of deposition of silver onto Ag(111), as opposed to Ag(100), facets is governed by pH and the Bis-(p-sulfonatophenyl)phenylphosphine dihydrate dipotassium salt (BSPP)-to-silver cation-ratio. To exemplify their approach as depicted in Fig. 6A (for path a), they proved that a fast reaction rate favors the growth of (100)-faceted right triangular bipyramids by preferential Ag deposition on (111) facets compared to (100) facets converting the planar-twinned seeds into small right bipyramids. The subsequent growth of the latter forms the final right triangular bipyramids. This growth is guaranteed by a continuous, fast reaction rate achieved by a high pH (10 or 11) and a relatively low [BSPP]/[Ag^+] ratio (close to 1.0). The same group, led by C. Mirkin, synthesized Ag-nanorods by using penta-twinned nanorod seeds, whereas the surface plasmon chemistry was adapted from the previously described phenomenology [86].

Recently, extensions to the field of plasmon-driven shape selective metal nanoparticle synthesis were made for gold, an important achievement since earlier reports were all based on silver [87]. In order to tailor the syntheses of gold particles such as hexagonal and triangular prisms, interactions between light, surfactant (PVP), and nanocrystal twinning were taken into account to optimize synthesis conditions. In particular, a special role was found for the surfactant PVP, which, according to the authors, adsorbed at the perimeter of the growing nanoprisms, thus providing guidance in the anisotropic plasmon-driven growth of the nanostructures.

It is worth mentioning that the potential field of application of tailored silver and gold nanoparticles exceeds the field of catalysis. Their spectral response can be tailored over the whole spectrum of visible light to red light and near infrared (NIR) light. Therefore, they are discussed as promising bio-markers/-probes as body tissue is transparent to this light [88].

Along all these mentioned tunable parameters one limitation needs to be mentioned. Since the light mediated shaping mechanism is based on localized surface plasmon resonance (LSPR), it remains confined to the application to plasmonic materials, mainly Au and Ag.

Selective etching and post-synthesis shape control

Nanocrystals can be treated following synthesis to enable more complex geometries. This result can be achieved through several methods: ligand treatments that promote the growth of a specific facet, preferential etching of a specific facet or metal in an alloy, or by causing phase changes in the nanocrystals. For example, treating Co particles in an oxidizing environment will result in cobalt oxide particles with a void at their center [89]. This is a result of the Kirkendall effect where two species, e.g. first oxygen atoms, then vacancies move inward and cobalt atoms diffuse in the opposite direction at a different rate. A similar effect can be obtained by adding sulfur to the nanocrystal solution and producing cobalt sulfide nanocrystals with the same void structure. In many cases the voids of these particles can be accessed by pores in the shell, thereby increasing the effective accessible surface area of the material.

Another possible way to increase the surface area of nanocrystals is to remove a metal from the synthesized nanocrystal, leaving it porous. In the case of $PtNi_3$, this can be done preferentially to remove Ni and leave a nanoframe of a Pt rich alloy [90]. This technique takes advantage of the fact that Ni is the less noble metal and can be etched preferably. Dissolved oxygen in the system oxidizes Ni°, while oleylamine acts as a ligand and selectively extracts Ni cations thereby turning $PtNi_3$ particles into Pt_3Ni frames. Frames are produced because of the segregation of Pt to the edges and center of a rhombic dodecahedron, initially providing nanostructures where Pt preferentially stays at the core with a Ni-rich shell. However, at longer reaction times the further segregation of Pt to the outer shells leads to the final frames with enriched Pt skin [91]. In addition to increased surface area, these frames also have an increased fraction of under-coordinated atoms, which are most active for many reactions.

Post synthesis treatments can also be used to create new particle geometries from existing bimetallic particles. For example, it has been shown that exposing AuMn particles to high temperature oxidizing treatments leads to several heterostructures of MnO/Au from MnO shells on Au to MnO/Au heterodimers [92]. The deciding factor for the final particle shape is the composition of the seed with higher Mn fractions favoring heterodimers. This transformation takes advantage of the higher affinity for oxygen of Mn as compared to Au. High temperatures and an oxygen environment enable Mn to exsolve from the alloy nanocrystal and become MnO. Similar results have been found when starting with AuNi and AuCu (Fig. 7) [93,94].

Au is a common component of these pairs due to its very low affinity for oxygen. It has been shown that in some cases high temperature oxidizing conditions result in metal segregation, while high temperature reducing environments favor their re-integration into alloys [94]. While it is common to create these post-treated particles using gas environments, it is also possible to perform similar transformations in the liquid phase. For example, exposing AuCu nanocrystals to a solution containing dissolved sulfur will result in Au/CuS_2 heterodimers [95]. Similar observations were reported by Wang et al. who explored the controlled synthesis of silver octahedral particles from cubic and quasi-spherical single crystal Ag seeds. The selection of the capping agent, citrate, which blocks the {111} facet and facilitates growth at the {100} facet, was key to forming the octahedra regardless of the seed structure. The structure of the particle was dependent on the concentration of metallic precursor and capping agent used, though growth was similar regardless of seed structure. The size of the particle was related to the size of seed (dependent on the solvent/reductant used) and octahedra over the range 15–200 nm were successfully made [96]. In many

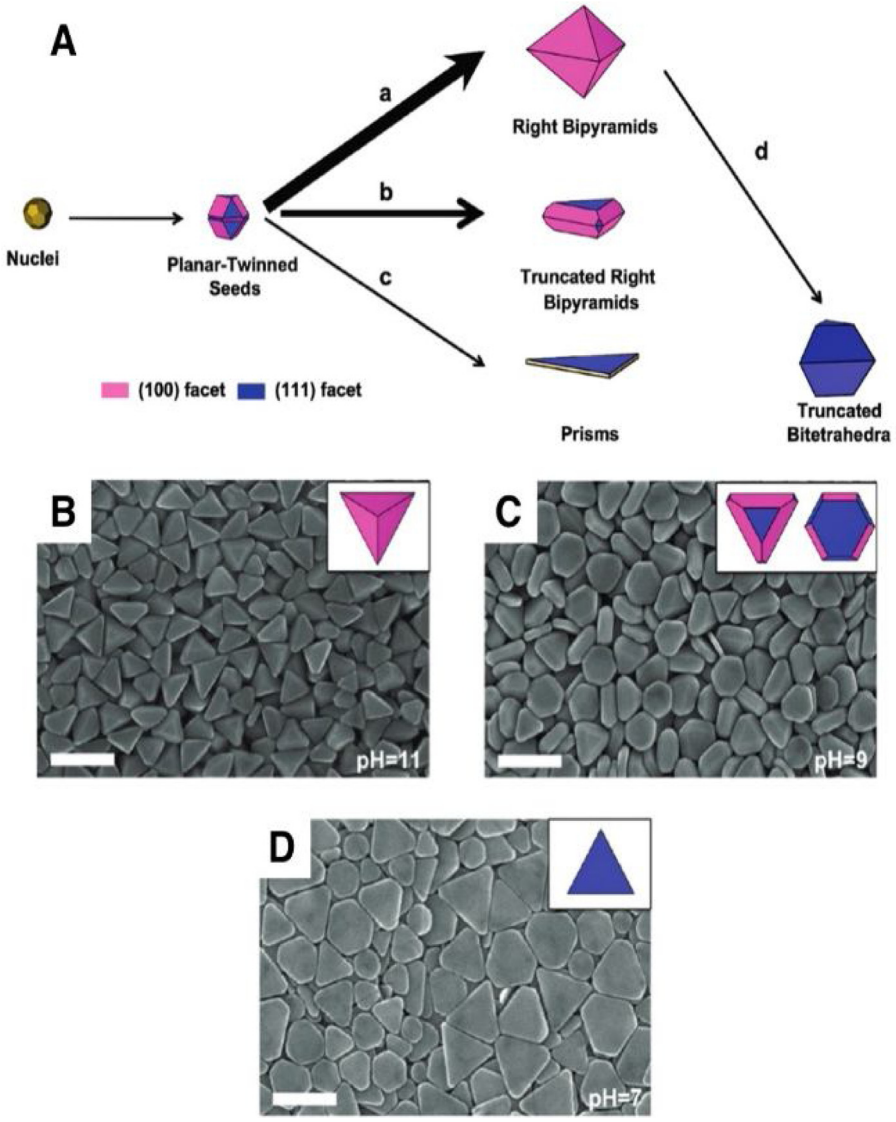

Fig. 6. (A) Mechanistic scheme summarizing different pathways to four different shapes, each time starting from planar twinned seeds of silver nanoparticles. The use of light enables shape control forming either triangular prisms, truncated right bipyramids, right bipyramids or truncated bitetrahedra. (B–D) STEM micrographs of the different shapes obtained for silver nanoparticles.

Adapted with permission from Ref. [84] Copyright (2010) American Chemical Society.

of these post-treatment processes, the final shape of the segregated particles will depend on the surface energies between the two materials as well as their relative amounts and the reaction conditions (surfactants, temperature).

Compositional control

Multi-component materials, both at the bulk and nanoscale, often boast properties that are superior to either individual component. Naturally, alloyed nanomaterials (or nanoalloys) have found an important place in catalysis as well, due to promising activity, selectivity, and stability properties. Nanoalloys offer many exciting possibilities: nanoalloys exist in a variety of different customizable atomic arrangements (i.e. random alloys, intermetallics, core-shell structures), they include some alloy combinations which might not stably exist as a bulk alloys [97]. However, in traditional synthetic approaches, a fundamental understanding of multimetallic catalysts is often frustrated by a lack of control over multimetallic nanostructures, making it difficult to correlate alloyed structure to any beneficial catalytic properties. Colloidal synthesis plays an increasingly valuable role in synthesizing multimetallic materials with well-defined atomic arrangements in order to probe catalytic properties of alloys. However, although there are a number of rigorous studies regarding the nucleation and growth kinetics of monometallic nanomaterials [35], such dynamics become more complicated with the controlled incorporation of multiple metals into a single nanocrystal. Understanding the growth mechanisms of multimetallic nanocrystals allows access to a host of interesting nanostructures [35]. For these reasons, many different colloidal approaches have been used to target controlled nanoalloy materials for catalytic applications.

One-pot reduction/thermal decomposition

Bimetallic nanocrystals can most simply be synthesized through a one-pot reaction of metalorganic precursors that each undergo reduction or thermal decomposition in the same reaction flask. Such one-step syntheses often involve reduction of acetylacetonate precursors or thermal decomposition of carbonyl precursors; they are generally quicker, and produce alloyed or intermetallic nanocrystals [98]. As mentioned before a pioneering work

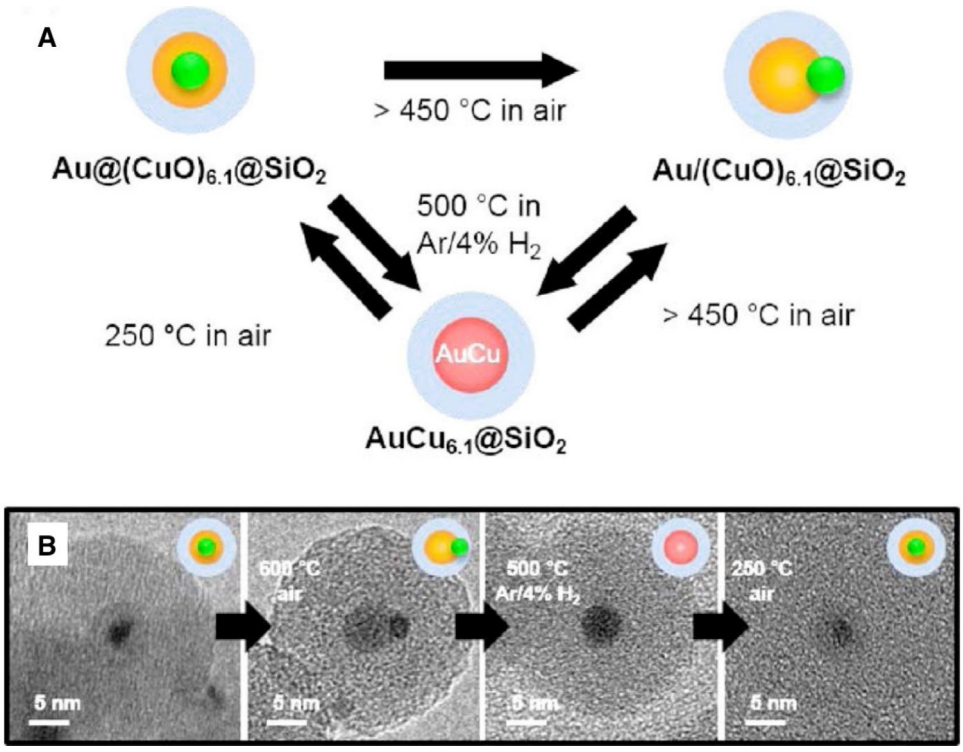

Fig. 7. Sequential formation of AuCu-alloy nanoparticles starting from a core shell structure. Reprinted with permission from Ref. [94]. Copyright (2017) American Chemical Society.

of Sun et al. reported the size controlled synthesis of FePt-particles from $Fe(CO)_5$ and $Pt(acac)_2$ [32]. From this method, the FePt particles with controlled composition showed the tunable size from 3- to 10-nanometer diameter with a standard deviation of less than 5%. The nanocrystals demonstrated remarkable uniformity and large area self-assembled superlattices were grown. The researchers further utilize thermal annealing to convert between ordered and disordered alloy phases, which led to tunable magnetic properties, and highlights the versatility of structure and property of bimetallic nanocrystals. Several other works used this method to prepare a variety of bimetallic nanocrystals, including metal oxide and mixed-metal oxide nanocrystals [99].

Building on these previous approaches, we recently have reported a versatile one-pot co-reduction method of multiple metal acetylacetonate precursors, targeting Pd and Pt alloyed nanocrystals [100,101]. Excitingly, we have identified an approach to alloy a range of cheap base metals with Pd in a variety of compositions and sizes (base metals including V, Mn, Fe, Co, Ni, Zn, Sn) (Fig. 8) [100].

These materials provide a complete library to understand how substituting a cheaper second metal for Pd may affect the catalytic activity of Pd nanocrystals, with the goal of targeting emissions control catalysts with less precious metals. These materials are created using a one-pot in-situ seed-mediated approach. Using conditions developed to synthesize nanometer-precise Pd nanoparticles, base-metal precursors were added into the reaction mixture alongside Pd precursors, and produced alloyed nanomaterials with nanometer precision. Mechanistically, Pd seeds nucleate and grow independently of the base-metal precursor. However, after Pd nucleation and growth, at temperatures higher than those required for Pd nucleation, the second base metal could heterogeneously nucleate onto the Pd seeds. This method allows for independent tuning of size (Pd seeds) and composition (amount of base-metal precursor).

Seed-mediated approaches

Seed-mediated approaches are particularly useful in the synthesis of bimetallic nanocrystals, and often provide finer control of overall bimetallic size, composition, and nanostructure. Here, we identify seed-mediated approaches as those involving the isolation of precursor nanoparticles, followed by a separate reaction step to decompose a second metal onto the colloidal seeds. This second step can involve a reductive deposition, thermal decomposition, or galvanic exchange of the second metal onto the precursor seeds. Seed-mediated approaches are versatile and may generate core-shell and heterostructures at lower temperatures, or random alloys and intermetallic nanocrystals at higher temperatures, depending on atomic diffusion rates and atomic mobility. The case of Au alloys is particularly useful to discuss because Au has a relatively low melting point and it is expected that low-temperature diffusional processes could facilitate the formation of alloyed materials. Indeed, a few years ago several Au-based alloy nanocrystals have been reported using Au seeds, followed by reduction of a second metal in solution, forming alloys such as Au/Cu [102], Au/Cd [103], and Au/Ag [104]. A general synthesis protocol was described more recently to access several bimetallic systems (Ag, Pt, Hg, Sn, Cd) starting from monodisperse Au seeds [105]. The nanocrystals were larger than the starting seeds after alloying, indicating that the reaction was a reduction/deposition, not galvanic replacement. The composition of the bimetallic crystals was heavily dependent on the metallic precursor and reducing agent used, but a good correlation between precursor utilized and final metal incorporation was found. The diffusion of the second metal within the Au nanocrystal lattice could have been facilitated by the presence of defects and grain boundaries in the seed particles. It is worth mentioning that the use of these materials as model catalysts requires in-situ or operando observation of the working catalyst or at least post-catalysis structural analyses, as it has been shown that these materials may change spontaneously even at room temperature or under reaction conditions [106,107].

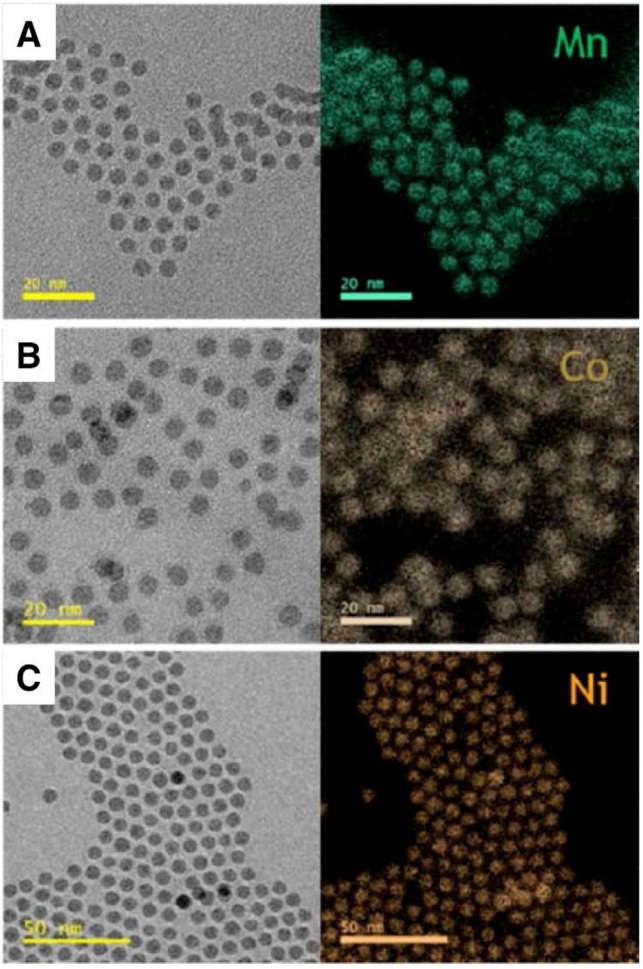

Fig. 8. One-pot co-reduction method for synthesis of several Pd-based alloyed nanocrystals. TEM images and corresponding energy-filtered TEM images of (A) PdMn, (B) PdCo and (C) PdNi bimetallic nanocrystals demonstrating the homogeneous co-localization of the two elements within each nanocrystal.

Reprinted with permission from Ref. [100]. Copyright (2017) American Chemical Society.

In addition to approaches involving the addition of a second component to a nanocrystal seed, galvanic replacement is an incredibly versatile tool to make a host of bimetallic materials, ranging from alloys in the diluted regime (also known as single atom alloys, SAA) [108], to metal heterostructures [109], to hollow and porous bimetallic structures [110,111]. In this technique, one component in a low oxidation state (usually a metal) in a preformed nanocrystal is replaced by a second component through the spontaneous oxidation and dissolution of the first component, which drives the reduction of the second because of their redox potentials [112]. Such a technique can be utilized on a variety of substrates and nanocrystal shapes, mostly on metals but even on metal oxide nanocrystals [111]. The technique is particularly useful to deposit controlled, limited amounts of a material on a nanocrystal host, as for example in the case of Pd/Cu nanoparticles with very low amounts of Pd (0.18 atomic% in the initial Pd/Cu nanocrystals), which is a very useful architecture to better utilize precious, expensive metals [113].

Template-directed compositional control

Hard templates can also be used to prepare materials with compositional control, especially when target materials possess a high melting point or are refractory. The strategy is to use hard templates to confine the precursor reactivity within a small volume, and then remove the template through some process that would selectively etch the outer (template) material and liberate the target core component. In addition to compositional control, templating methods can lead to increased stability in both synthesis and crystal structure. A common templating material that is often used is silica because of its resistance to high temperature and its easy dissolution in either diluted HF or base. Metals can be reduced inside silica structures, including ordered mesoporous silicas, followed by dissolution of the shell in the presence of ligands to recover monodisperse metal nanocrystals [114]. More recently, this method was extended to refractory materials in an elegant approach by the Román-Leshkov group to create tungsten carbide nanoparticles with a thin platinum shell (Fig. 9) [115]. This approach can be generalized to produce core-shell structures with very low precious metal loadings [116]. In the first particular example, tungsten and platinum precursors were loaded inside silica shells to maintain tungsten and platinum precursors within a template space throughout conditions for the formation of tungsten carbide. This process was run by carbonization at very high temperatures (900 °C). If the template approach had not been used, unprotected precursors would randomly agglomerate. During the carbonization process, the Pt component segregated to the outer part of the core volume, thus creating small Pt particles on top of a tungsten carbide core. The final silica dissolution provided nanocrystal precursors that could be deposited on arbitrary substrates and used for catalysis.

In a similar way, SiO_2 shells were also employed for creating platinum-tin intermetallic compounds within a porous “ship in a bottle” synthesis strategy [117]. In this case, the authors used protected platinum seeds and relied on diffusion of alternate metal precursors into the platinum-rich silica center (Fig. 9). The high thermodynamic stability of the intermetallics made their formation possible only under extreme conditions consisting of high temperatures and pressures. This “ship in a bottle” synthesis strategy is promising in both replacing cores of valuable noble metal particles with less expensive ones, and for creating thermodynamically favorable intermetallic structures of many types.

Nanocrystal-based composites

Colloidal nanocrystals can be used as starting building blocks to create more complex architectures in composite materials. In addition to depositing the nanocrystals onto high surface area supports for the preparation of active catalysts, these materials represent the starting point to form inorganic or hybrid organic-inorganic materials via the controlled embedding of particles into porous matrices. This process allows the precise study of metal-support interactions by changing the nature of the support while keeping the exact same nanocrystal cores. Composites are often more stable due to a reduction in sintering and ripening mechanisms resulting from the hybrid structure.

Inorganic hybrids

The first designs of encapsulated nanocrystals in amorphous porous supports were aimed at sinter-resistant catalysts. Modifications of the classic process developed by Stöber to form silica nanospheres enabled the design of nanocrystal core-silica shell materials [118]. An important advantage of this concept as opposed to depositing particles in porous supports is that in the latter case the pore diameter limits the use of particle sizes, whereas in the first case a porous silica shell can cover nanoparticles independent of size post-synthetically.

With this so-called Stöber process, the preparation of well-defined core–shell structures is possible if a homogenous distribution of the colloids could be guaranteed. Silica shells have been successfully grown onto gold nanoparticles from the 1990s

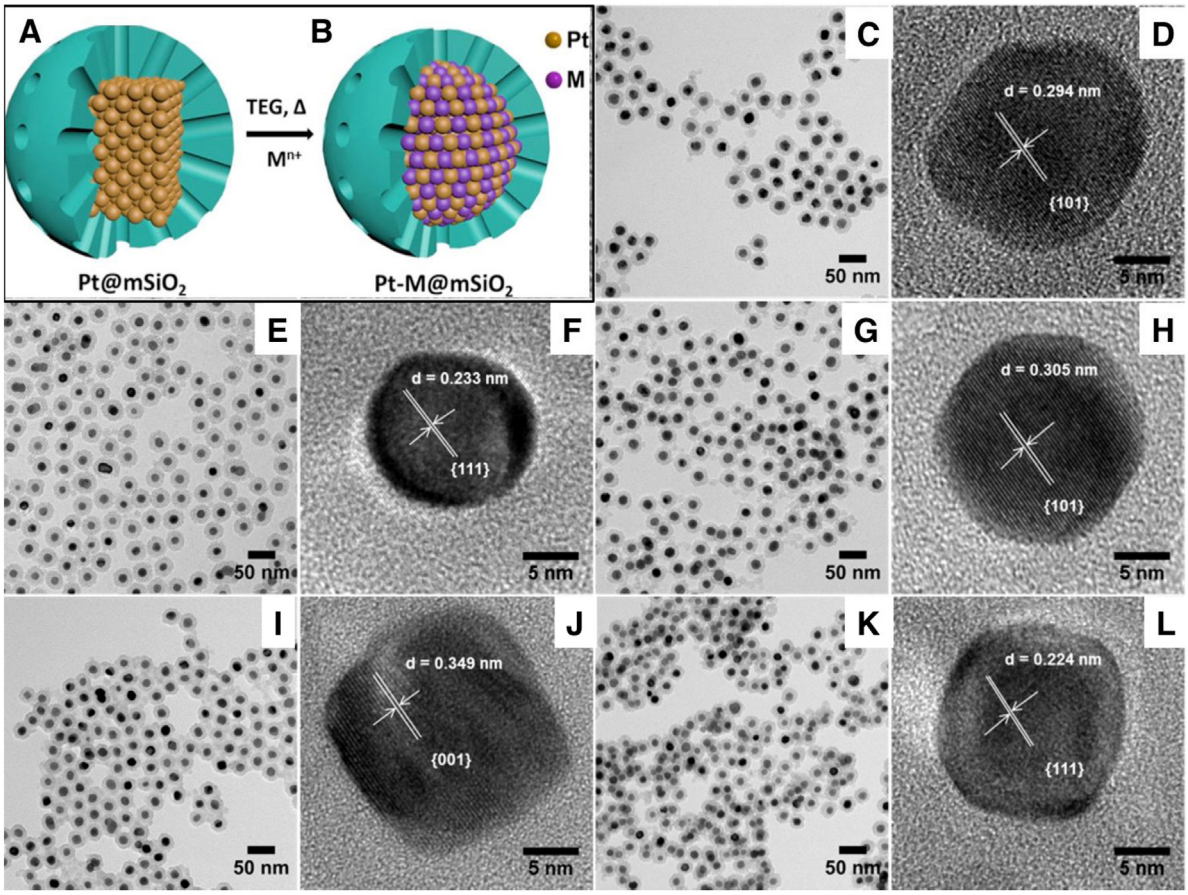

Fig. 9. Schematic of a "ship in a bottle technique" (A, B), $Pt@mSiO_2$ is alloyed to other metals (M) while overall particle sizes are maintained. TEM and HRTEM images of intermetallic $Pt_xM@mSiO_2$-nanoparticles (C – L) for (C, D) PtSn; (E, F) Pt_3Sn; (G, H) PtPb; (I, J) PtZn; and (K, L) Pt_3Zn. Lattice spacings calculated from the HRTEM images are indicated.

Reprinted with permission from Ref. [117] Copyright (2016) American Chemical Society.

onwards. Liz-Marzan et al. were among the first researchers to recognize and describe the difficulties in covering gold particles with silica [119]. In their study, they were relating this difficulty to the chemical differences between the two materials, they were describing surface interactions that prompted the use of the term *vitreophobicity*. This property originates first in the poor affinity of metallic gold to silica, because it does not form an oxide film on its surface, and secondly in the presence of ligands or surfactants on the gold surface stabilizing the particles against coagulation. Their solution to overcome this limitation was to perform a ligand exchange adding a surface primer (e.g. (3-Aminopropyl)trimethoxysilane (APS), onto the gold nanoparticles rendering them vitreophilic, i.e. increasing their affinity towards silica precursors such as tetraethoxysilane [120,121]. This method allowed the generation of a single silica layer around nanoparticles, which could then be transferred into other solvents and the shells could be grown to different thicknesses in a controlled way. One downside of this technique, especially regarding an eventual catalytic application, is that the silica shells are a priori impermeable to molecular transfer. Therefore, various approaches have emerged to tackle this limitation. As depicted in Fig. 10A–C the group of F. Schüth realized a successive overgrowth on a first nonporous silica shell [122], with a second mesoporous zirconia shell. Upon dissolution of the silica shell in alkaline medium, ZrO_2-hollow spheres are obtained, which have been shown to hinder gold nanoparticles from sintering at temperatures as high as 800 °C.

An alternative strategy that has been successfully explored by multiple groups, which consists in growing silica shells around partially vitreophilic nanoparticles. One approach used colloidal gold or palladium nanoparticles capped with a mixture of a vitreophobic ligand (1-dodecanethiol) and a vitreophilic one (3-mercaptopropyltrimethoxysilane), whereby a partial overgrowth was guaranteed and a mesoporous silica shell eventually encapsulated the nanoparticles [124,125]. Another approach consists of first colloidally synthesizing platinum nanoparticles covered with tetradecyltrimethyammonium (TTA) bromide. These particles were then encaged by a silica shell in alkaline medium (typically pH must be adjusted to 10–11 to allow silica growth). Herein the increased affinity towards silica monomers stems from exposed ammonium centers at the TTA-bilayer on the Pt-particles. After calcining the template materials, this method yields mesoporous (ø = 2 nm) silica shells with good access to Pt-surface atoms [126].

Thanks to a physical barrier in such core-shell hybrid materials, sinter-resistant catalysts can be designed and realized [127]. This embedding technique is particularly attractive since the nature of the metal nanoparticles, as well as of the shell, may be varied. For instance, instead of using "inert" silica shells, more active materials for catalysis can be employed. Ceria is a known example of an oxygen-active support and several embedding strategies based on it have been developed [128]. This method inspired multiple other approaches, including microemulsions, where palladium nanoparticles were first synthesized in the water pockets of reverse micelles using hydrazine as a reducing agent, and later ceric tetrakis(octyloxide) was added to the same mixture to form the ceria shell [129]. More recently, borrowing from the previous literature, a way to synthesize soluble $Pd@CeO_2$ colloidal

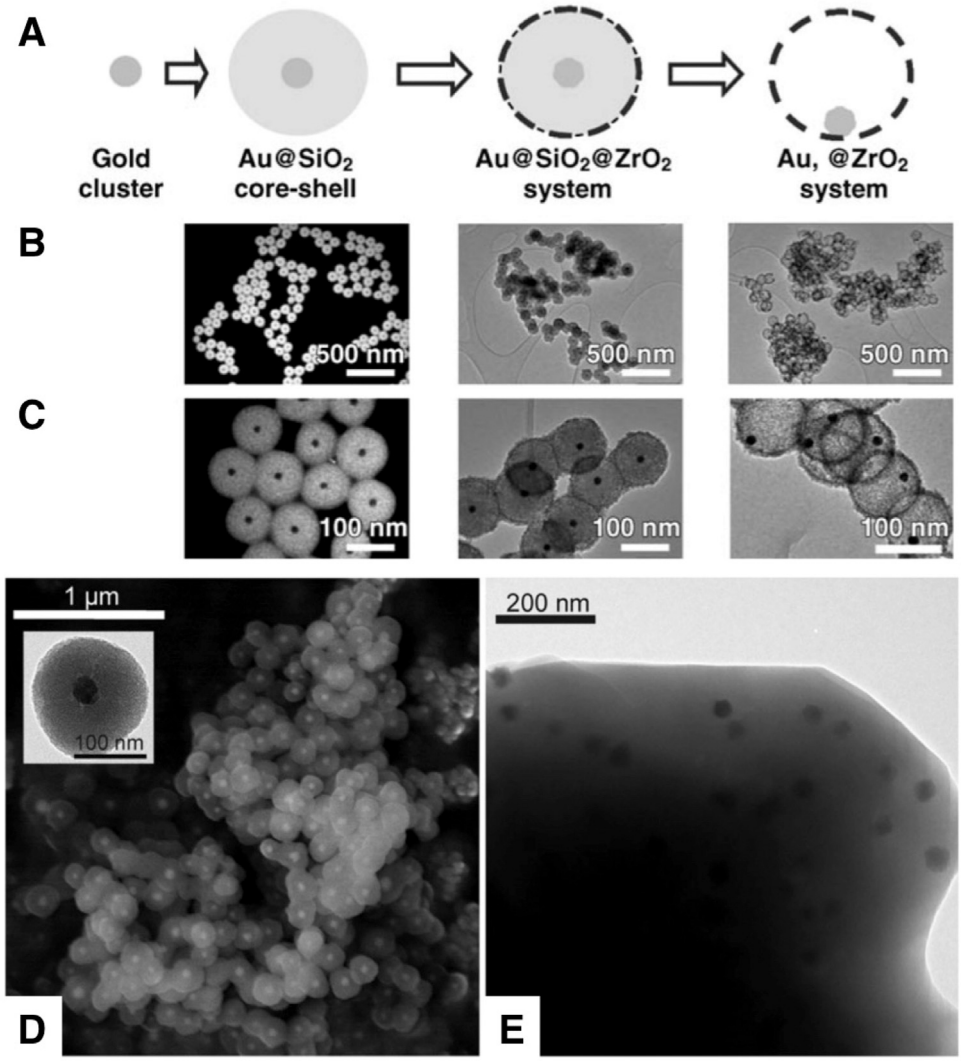

Fig. 10. (A) The controlled encapsulation of metal-nanoparticles in SiO_2-shells was demonstrated the 1990s and enabled to overgrow silica shells with other active support materials in order to obtain hollow ZrO_2-spheres that encapsulate metal nanoparticles after the leaching of the silica layer. (B, C) TEM micrographs for the sequence $Au@SiO_2$, $Au@SiO_2@ZrO_2$ and $Au@ZrO_2$ from left to right at different magnifications Reproduced with permission from Ref. [122] Copyright 2006 Wiley-VCH. (D, E) The transformation of CoO_x nanoparticles@SiO_2 shells into CoO_x-nanoparticles entrapped in microporous crystalline zeolite ZSM-5. Reproduced with permission from Ref. [123] © 2015 WILEY-VCH.

particles was described starting from 11-mercaptoundecanoic acid-functionalized Pd nanocrystals, used to anchor a Ce(IV) alkoxide that was then hydrolyzed to obtain a ceria shell [130].

Along all these advantages of the core-shell configuration, one downside of this approach is the loss of active noble metal surface area due to the coverage with inorganic shells. Habibi et al. indeed reported that the encapsulation of Pd nanoparticles with porous silica shells led to a blocking of the noble metal surface [131]. This study concluded that in some cases up to two-thirds of the Pd surface atoms of 8 nm particles are actually not accessible during catalysis, even with the addition of porogen compounds that can drastically increase the surface area of the catalysts.

Rather than amorphous spherical shells, metal nanoparticles can also be embedded in crystalline, ordered supports, leading to highly engineered composites. This approach permits the study and rational improvement of many catalytic properties such as the selectivity via shape selective diffusion of substrates and products, heat transfer via engineering thermal conductivity, the sinter-resistance, or the metal-support interaction. Microporous zeolites are among the most attractive supports in this respect since their porosity allows for the preparation of shape-selective hybrids. A myriad of studies reported the preparation of small particles embedded in zeolites by incorporation of metal salts via wetness impregnation or ion exchange and subsequent reduction [132]. These studies however are not to be considered part of the building block approach benefitting of preformed colloidal nanoparticles, the focus of this review. In contrast, there exist approaches that are aimed at incorporating pre-formed colloidal nanoparticles in microporous shape-selective aluminosilicates. An interesting and versatile strategy has been recently reported for the embedding of gold nanoparticles in silicalite-1 (MFI) [133]. Gold nanoparticles were deposited onto amorphous silica using a linker silane ((3-Mercaptopropyl)trimethoxysilane, MPTS) and a supplementary silica source (tetraethyl orthosilicate, TEOS) was used to coat them with further amorphous silica. This material was subjected to a hydrothermal synthesis to convert the silica into silicalite-1. It is, however, important to note that the quality of the as-made zeolite crystals was affected by the presence of the gold nanoparticles during the synthesis. Moreover, the gold nanoparticles did not result as being particularly uniform and controlled in size and shape, nor were they quantitatively incorporated within the microporous framework. Despite these issues, the method inspired multiple

other approaches, including a recent one using pre-formed Co_3O_4 nanoparticles that were then covered by a non-porous silica shell using the Stöber process [123]. The authors of this study managed to convert the silica shell into H-ZSM-5 zeolite via dissolution-recrystallization, while the nanoparticles became encapsulated in the microporous crystal (Fig. 10D, E). It is noteworthy that these microporous aluminosilicate would normally not accommodate nanoparticles of the size used in the study (40 nm). This strategy is especially promising since it allows for the synthesis of hybrid materials bringing together engineered metal nanoparticle activity and microporous shape selectivity. Along the same lines, G. Prieto et al. used a similar approach but through a different synthetic route to first synthesize CoO_x nanoclusters with a microemulsion technique, while in parallel a MWW zeolite was delaminated and silanized forming hydrophobic zeolite nanosheets [43]. These nanosheets were added to the former microemulsion and the as-formed hybrid cobalt/MWW nanosheets were calcined to yield the final embedded Co(10 wt.%)/MWW composite. It is worth mentioning that the authors were able to tune the size of the incorporated Co_3O_4 particles between 6 and 12 nm.

In addition to the strategies of bringing nanoparticles in close contact with zeolite materials, substantial progress in introducing metal nanoparticles into mesoporous SBA-15 silica as well as a variety of ordered nanocasted mesoporous metal oxides has been made and reported by Somorjai's group [134]. In particular the use of metal oxides is attractive considering the potential application of these materials for the study of metal-support interactions [135]. Such metal nanoparticles are not easily impregnated into mesopores, considering that the ligand and solvation shells contribute to drastically increase the hydrodynamic radius of a colloidal nanoparticle that may become too large for a given mesopore diameter. Therefore, these studies showed that controlled deposition of particles into the mesoporous supports was achieved by using prolonged sonication treatments, up to three hours at room temperature, producing controlled materials where colloidal nanocrystals were uniformly distributed within the ordered mesoporous channels. Conventional impregnation processes would hardly achieve this level of control, highlighting the benefits of using colloidal nanocrystals as catalyst precursors. In a similar approach as described above concerning the crystallization of a microporous material around preformed microporous materials, Konya et al. reported the successful growth of SBA-15 mesoporous silica around Pt and Au nanoparticles [136]. It is important to repeat in this case that if such a route is planned, it has to be ascertained that the preformed nanoparticles are stable under the synthesis conditions of the mesoporous materials which regularly involve acidic medium.

Organic-inorganic hybrids

While inorganic supports present clear advantages in stability and durability, embedding colloidal nanocrystals inside organic matrices can leverage the large space in chemical functionality that can be introduced by using organic synthesis. Similar to the silica shells via the Stöber process, it is possible to encapsulate colloidal nanoparticles in amorphous organic porous supports that are polymeric in nature. These structures can be formed by two-step approaches where colloidal nanocrystals are prepared first, and then embedded through a polymerization reaction to create polymer microspheres [137]. This approach allows for control of the polymer particle size by varying the ratio of monomer and surfactants, and the thickness of the polymer layer around metal or oxide nanoparticles. Consecutive carbonization of the material leads to porous active catalysts composed of metal oxide nanoparticles coated by a porous carbonaceous shell.

It has also been proven possible to encapsulate self-assembled superstructures of colloidal nanocrystals without the use of polymeric materials. In this elegant approach, Fe_3O_4 superlattices are created first from monodisperse nanocrystals [139]. The nanocrystal ligands are then pyrolized into a porous superlattice template. Similar to molding, or nanocasting, the authors use the fcc template left from dissolving the nanoparticles out of the superlattice as a way to make another superlattice from alternate metal precursor addition via wetness impregnation into the pores of the resultant carbon matrix. This allows for a way to make superlattices without needing to remove the ligands, as the authors demonstrate with a Sb lithium battery electrode.

While the above mentioned carbonized superlattices constitute mesoporous ordered supports, the embedding of metal nanoparticles in microporous ordered partially organic supports is also a quickly expanding field. As opposed to zeolites, MOFs (metal organic frameworks) and COFs (covalent organic frameworks) have much larger potential for adaptability to desired needs. As already briefly mentioned before, MOFs are coordination crystalline frameworks of organic bridging ligands with metal atoms, while covalently bonded crystalline frameworks with or without metallic centers are usually referred to as COFs. It is imaginable to introduce secondary active sites into such hybrid nanoparticle@M/COF catalysts (e.g. Lewis or Brønsted acidic or basic, or metal ions or clusters). Embedding particles within ordered organic structures also poses several advantages in general degree of control over material properties. This can be achieved through a variety of synthetic approaches.

First, physically trapping metal or metal oxide colloidal nanoparticles has the advantage of being insensitive to chemical composition of the colloidal particle relative to the support. For example, Lu et al. demonstrate a controlled encapsulation strategy of any PVP coated nanostructure into MOFs [138]. Noble metals, metal oxides, and semiconductors are all reported. They used ZIF-8 as the MOF-support and varied the sequence of particle introduction in a MOF synthesis to control MOF overlayer thickness (Fig. 11). In a similar process, Rodriguez-San-Miguel et al. demonstrate encapsulation of colloidal nanoparticles into an amorphous polymer by introduction into a continuous polymerization process where the particles are mechanically trapped in a polymer matrix as it forms at room temperature [140]. This process can be more general in the nanoparticle type encapsulated given the mechanical nature of the encapsulation process. The same authors also show that the precursor of the amorphous polymer can be converted into a covalent organic framework (COF) when refluxed in acetic acid. Despite the harsh condition required for the COF conversion, metal (oxide) nanoparticles (e.g. Au, Pd, Fe_3O_4) even maintain catalytic activity towards reduction of nitrophenol [141]. The same process was also used by the Wang group, which further extended it to encapsulate iron oxide nanoparticles in ordered frameworks [142].

Chemical embedding compared to physical embedding uses the chemical nature of the support material, which allows for precise colocalization of metal nanoparticles and ordered materials. As an example, Yang et al. use sacrificial templates of metal oxide materials to grow MOF supports, then support metal nanoparticles on the surface of the template. The metal oxide materials etching rate is controlled with the amount of added MOF precursor ligands. The ligand concentration determines which mechanism of oxide dissolution the support undergoes, which consequently varies the placement of the nanoparticles relative to the oxide support. With high ligand concentration, the nanoparticles are essentially stuck to the support with the dissolution-precipitation mechanism, whereas with low support concentration, the particles are carried to the edges of the composite in the localized conversion mechanism. These two mechanisms give rise to regimes of growth, which allow precise control over particle location when creating nanoparticle@MOF hybrids [143]. It is worth mentioning that their synthesis method was inspired by what has been described by J.

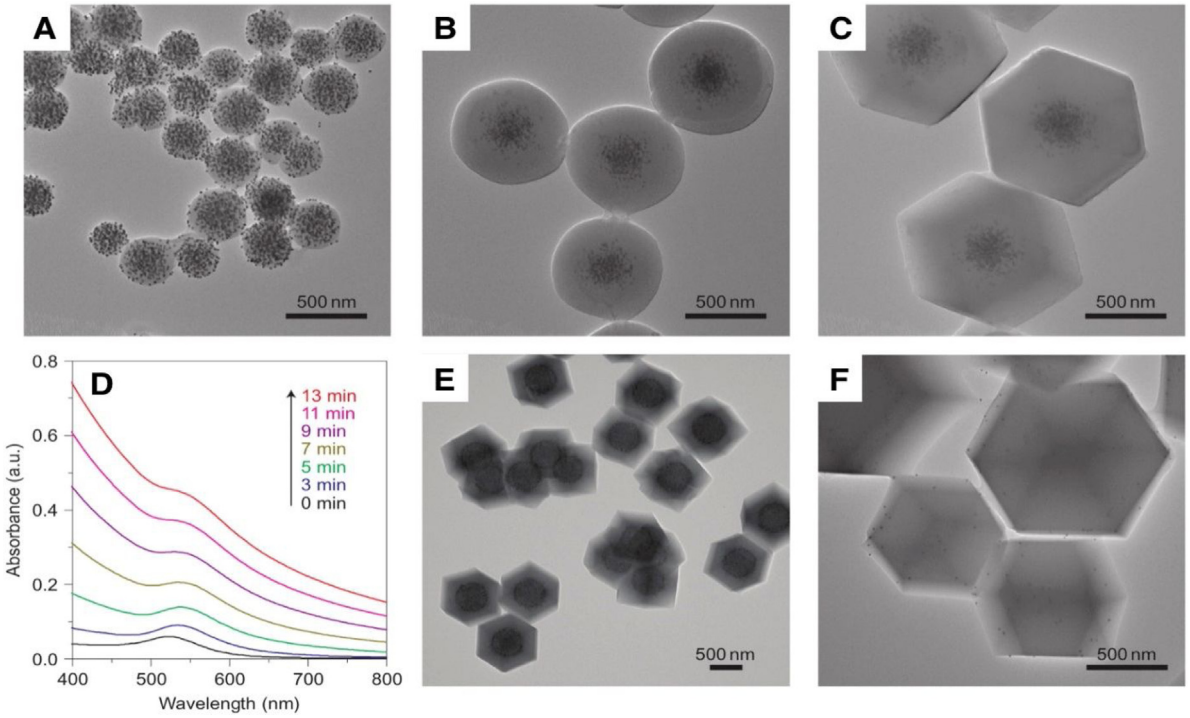

Fig. 11. Monitoring the nucleation and crystallization of ZIF-8 around gold nanoparticles forming Au nanoparticle/ZIF-8 hybrid crystals. Ex-situ TEM micrographs are shown for samples collected after (A) six minutes, (B) 30 min and (C) three hours of reaction. (D) UV–vis absorption spectra of the reaction solution recorded in the initial 13 min. (E) TEM image of hybrid crystals obtained when Au nanoparticles were introduced 15 min after the initiation of the reaction, and (F) TEM image of product obtained when excess free PVP was present in the reaction.

Reproduced with permission from Ref. [138] Copyright 2012, Springer Nature.

Reboul et al. before [144]. This in turn is a very similar strategy to what has been dubbed ñanocastingin synthesizing mesoporous inorganic supports. Though the latter is based on the formation of negative replica, the former is a direct morphological replication [144].

In both the organic and inorganic worlds of tailored support fabrication, there is a plethora of methods to embed or encapsulate nanoparticles for further use as hybrid heterogeneous catalysts. The above cited examples do not constitute an exhaustive list of all the possible strategies, but we rather intended to give an idea of the vast maneuverability that inorganic and organic porous supports offer to the field of designing novel hybrid heterogeneous catalysts.

Preparation of colloidal heterogeneous catalysts: deposition, removal of capping agents, activation

The preparation of colloidal nanocrystals with a high degree of control over size, shape and composition is only the first step in the preparation of uniform colloidal heterogeneous catalysts. In order to obtain catalytically active materials, it is necessary to deposit the colloidal nanocrystals onto appropriate substrates for catalysis (most often high surface area materials), and subsequently remove organic ligands in a controlled way to clean nanocrystal surfaces from synthesis debris. While recent research has shown that in some cases, the presence of specific ligands can be beneficial to drive the selectivity for certain reactions [145,146], we will not extensively discuss this interesting area of research herein. One such representative study evidenced that carbon residues do not necessarily need to be completely removed in order to still observe reactivity of supported nanocrystals: [147] in Au colloids prepared with PVP, the deposition on titania causes the support to be also covered by PVP ligands, and mild thermal treatments that remove the polymer from the Au nanocrystals (but not the support) are sufficient to allow the catalysts to show activity for oxidation reactions.

After the synthesis of size, shape and composition controlled nanocrystals it is important to consider that their deposition onto supports can be a first challenging step. The group of Krijn de Jong investigated several methods to obtain well-defined catalysts for Fisher-Tropsch synthesis by deposition of nanocrystals of Fe and Co of controlled size onto carbon nanotube supports [148]. Iron oxide nanocrystals, because of magnetic interactions, tend to agglomerate and poorly disperse onto the supports. However, careful control of deposition conditions, such as increasing the temperature during the deposition process, can allow for better dispersion of the particles and, thus, improved catalytic properties. More recently, the same group demonstrated that the oxidation state of the particles (in the case Co) is also a crucial parameter that affects the deposition: mild oxidation of Co nanocrystals in solution leads to better dispersion [149]. The question of the ligand support interaction, respectively affinity allows also some possibilities to tune this interaction after a colloidal synthesis of NCs. If for instance, metal nanoparticles with a shell of oleylamine ligands are produced, the hydrophobic particles may have weak interactions with a polar oxide support containing hydroxyl groups. If that is the case, a ligand exchange towards more polar polyvinylpirrolidone (PVP) ligand might help to overcome such limitation. Even the choice among various types of PVP ligand can be crucial: if the aim is to introduce particles into small mesopores with comparable size, cross-linked PVP, which results in a smaller overall metal-ligand particle size, are more promising (Fig. 12A–C) [146,150]. On the other hand, if a controlled interparticle distance on a flat support surface is aimed for, as briefly introduced in previous sections, linear PVP-ligands with varying lengths can be a more appealing route. It has been shown that it is possible to deposit nanocrystals onto flat supports with a certain control of interparticle distances. The latter

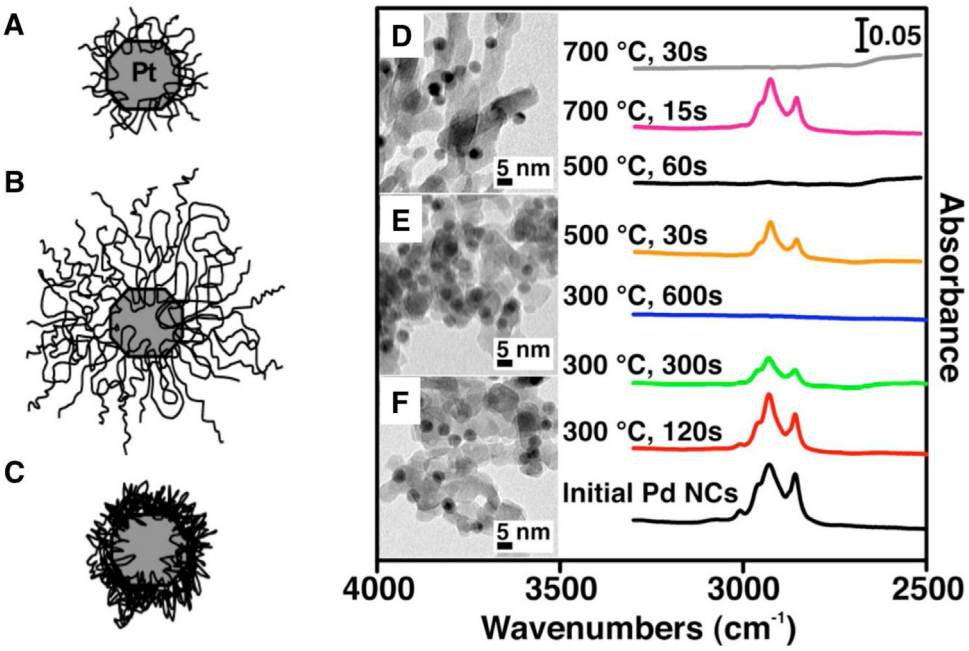

Fig. 12. Schematic illustration of PVP/Pt nanoparticles with different structure (morphology) of capping polymeric macroligand: (A) low molecular weight PVP, (B) high molecular weight PVP, and (C) dense, cross-linked PVP. Adapted from Ref. [150] Copyright (2006) American Chemical Society. (D–F) Optimized short-term high temperature treatment leading to successful removal of organic ligands, which absorbing in the 3000 cm^{-1}-range whose signal is disappearing at a 30 s treatment at 700 °C. Reprinted with permission from Ref. [151] Copyright (2015) American Chemical Society.

is guaranteed by the 2D-supramolecular ordering of PVP-coated particles [42].

The removal of ligands from supported nanocrystals can be performed using three general strategies: washing with solvents, low temperature oxidation treatment, and high temperature oxidation treatment, in order of increasing harshness of the treatment [152].

First, the most intuitive approach constitutes a washing step. The removal of ligands with solvents has the advantage that it is a very mild treatment and will not alter the particle morphology or size distribution. Another benefit of this technique relies in the possibility of selectively tuning the polarity of the solvents to the ligands that need to be removed. Considering Ostwald's dilution law, it is intuitive that a multistep washing process is preferred over a single washing step. For example 13 nm ruthenium-nanoparticles have been effectively deposited onto alumina, resulting in a performant catalyst for ammonia synthesis. In their report Miyazaki et al. achieved the removal of ethylene glycol by diluting ten times with an aqueous 0.3 M $NaNO_3$ solution [153]. The solid was collected by filtration (as opposed to frequently used centrifugation), and then dried in air. A further interesting example is washing with hot water to remove capping agents and surfactants from gold and palladium gold nanoparticles by the Hutchings group to create powerful CO oxidation catalysts [154]. Despite all the above-mentioned advantages, it needs to be noted that a washing step can be insufficient to fully remove organics. Several spectroscopic techniques as amongst which IR (presented in Fig. 12), can be used to determine if the ligands have been quantitatively removed.

The second approach for ligand removal relies in low temperature oxidizing treatments, which usually involve the use of reactive gases to chemically remove the ligands without affecting the supported nanocrystals. A classical example is the use of UV/ozone to treat supported nanocrystals, which removes ligands without affecting particle morphology. The Somorjai group investigated the ligand removal process with several techniques, including sum frequency generation vibrational spectroscopy (SFGVS), to demonstrate the full removal of the organics from the particle surfaces [155]. The same group also compared solvent washing with UV/ozone treatment, showing that the former is less effective than the latter in removing PVP molecules but that the consequence is also a lower stability of fully cleaned nanocrystals under reaction conditions [156]. More in-depth studies on UV/ozone processes also showed that this method may lead to reconstruction [157]. D. Li compared cleaning with UV/ozone, to thermal annealing and washing with acetic acid [158]. They found that another promising and comparably low temperature treatment is thermal annealing in air at temperatures below 185 °C. They reported that this treatment did not affect the nanoparticle shape nor size. Spatz et al. instead used oxygen plasma as an oxidizing agent while remaining at low temperatures to remove PVP ligands from metal nanoparticles deposited onto supports [41]. In their procedure oxygen plasma was generated and contacted with a monolayered material that was prepared by dip-coating. During the 10 min treatment the temperature does not exceed 100 °C.

Instead of low temperature, long duration calcination treatments, it is also possible to use very short treatments at high temperatures to induce combustion of ligands while impeding the rearrangement of nanocrystals on the support surface. This fast treatment method was shown to activate catalysts while maintaining size, shape and size distributions of the supported nanocrystals (Fig. 12D–F) [151]. More classic long duration, high temperature treatments have nonetheless been successfully applied to various supports over the last decades. For example, a report by Prieto et al. describes the removal of surfactants from the surface of cobalt metal nanoparticles using a very slow heating rate (1 °C min^{-1}) up to 500 °C. In this first step of their treatment, metallic cobalt is recrystallized into Co-oxide in diluted 10% O_2 in N_2, while once at 500 °C they switched to 20% O_2 in N_2 for further 3 h to remove the surfactants [43]. Even for high temperature calcinations, one potential issue is to demonstrate that carbon is really removed. Recent spectroscopic work shows that although calcination processes in air would intuitively remove any carbon, this fact may not necessarily be the case even at very high temperatures (800 °C) because of the kinetics of carbon removal from surfaces as identified in samples made of thick layers of nanocrystals [159]. This final

step requires appropriate characterization. Two deleterious phenomena can occur at this stage of the catalyst synthesis: metallic particles may sinter, and the may end up covered by a carbonaceous layer due to unburnt surfactant. The first phenomenon can be ruled out by structural analysis such as electron microscopy and X-ray diffraction. In order to address the second potential problem in the last stage of catalyst preparation, spectroscopic and sorption techniques are used to characterize the exposed active surfaces. Carbon remains are detected by IR, Raman and NMR (Fig. 12). In addition, chemisorption techniques with probe molecules prove very useful to ascertain and titrate the accessible active surface. While the adsorption guarantees a satisfying titration of accessible sites, temperature programmed desorption (TPD) allows the discrimination between different accessible active sites. Despite the largely established use of CO, NO, CO_2 etc. as probe molecules, care must be taken when choosing the probe molecule depending on the metal surface. Besides these classical characterization methods, the activity and selectivity of a catalyst also reveals information about its shape, size and composition if reference data are available in the literature. In addition to these means of characterization the following section will expose emerging advanced tools for characterization.

The final step in obtaining an active catalyst from the building block approach, the removal of the ligand shell offers hence a vast pool of possible treatments. It remains nevertheless a delicate choice rather guided by trial and error and necessitating an additional characterization step of the material prior its use in catalysis.

Advanced tools for characterization

To keep pace with the continuous innovation in synthesis and development of catalytic materials, there is a need for the development of new characterization techniques to access mechanistic information at both supramolecular and molecular levels during nanocrystals formation. This information is vital to designing better synthesis processes to precisely and scalably prepare controlled nanocrystals [9]. New tools are being developed to characterize the underlying supramolecular and molecular processes. A gradual move from rather ex-situ to in-situ characterization techniques can be noted, but is also required to truly understand the mechanisms of ongoing crystal growth processes.

While XPS and FTIR are good methods to acquire information at the surfactant-metal nanoparticle interface [160], various other advanced tools for characterization of the processes involved in the formation of nanocrystals are emerging. One example is free electron laser X-ray scattering that was used for the direct observation of Au-Au bond formation [161]. The technique enabled the controlled bond formation via photoexcitation of a gold complex aggregate and the observation of these dynamics at very high temporal resolution (fs - ps). Another work using synchrotron radiation studied the growth of Pd nanocrystals by in-situ small and wide angle X-ray scattering (SAXS and WAXS). Here the authors, besides describing in detail the mechanism of formation of the nanocrystals as related to reaction conditions (precursor concentration, ligand nature, temperature, time [35], found that Pd nanocrystals can spontaneously self-assemble into superlattices at high temperatures and in few seconds [162]. Interestingly, after formation of such superlattices the nanocrystals continued to grow. These observations were possible thanks to the use of in-situ techniques during nanocrystal growth. More recently, techniques to watch nanocrystals grow within TEM environments have also been developed, especially in conjunction with specially designed cells that allow the observation of events occurring inside the high vacuum of the TEM instrument [163–166]. Silicon nitride cells for example are popular and allow the observation of nanocrystal growth while introducing external stimuli, such as light in the plasmon-mediated nanocrystal synthesis [83]. Cryo electron microscopy, where samples are frozen in liquid ethane before analysis, also allows gathering snapshots of the formation of nanoparticles, although in an ex-situ mode [167].

Apart from advanced tools for in-situ characterizations, the exponential growth of in-silico methods is another avenue to gain further understanding on fundamental processes of nanocrystal growth. In particular, the increasing power of modern computational methods makes simulations of very large systems more accessible (e.g. thousands of metal atoms and millions of ligand atoms as well as billions of solvent molecules). Density functional theory (DFT), and (ab initio) molecular dynamics (AI)MD are two sets of tools that are emerging in response to these needs, which are very much felt in the community [7].

It appears that, in order to fully understand processes occurring during colloidal NC synthesis techniques collaborative efforts between synthetic chemists, nanotechnology to move from ex-situ to in-situ techniques and computer scientists allowing correct in-silico predictions are already undertaken, but also further required.

Applications of colloidal materials in catalysis

The present review will expose various aspects and lessons learnt in heterogeneous catalysis when colloidal nanocrystals were employed as building blocks for catalysts. The focus will be steered on the three guiding selection criteria for heterogeneous catalysts; i.e. *activity, selectivity* and *stability*. The following sections will highlight studies that evidence effects of nanocrystal size, shape and composition on the final catalytic properties of these uniform materials. The selected examples come from the quickly expanding fields of thermal catalysis, electrocatalysis and photocatalysis.

Impact of particle size

Particle size effects in thermal catalysis

Colloidally synthesized nanocrystals of uniform size can help elucidate the important role of the nanocrystal-support interface in catalytic reactions. Using nanoparticle catalysts, one may synthesize materials with well-defined surfaces and interfaces. Utilizing size-selected Ni, Pd, and Pt nanocrystal catalysts, different reaction mechanisms were observed for the CO oxidation reaction on Al_2O_3- vs CeO_2-supported catalysts [168]. While Al_2O_3-supported materials show a CO oxidation activity proportional to the total exposed nanoparticle surface area, CeO_2-supported materials show activity exclusively dictated by the length of the nanocrystal-support interface (Fig. 13A–D). This pattern, pinpointing the reaction active site at the nanocrystal-CeO_2 interface, was demonstrated across nine different nanocrystal catalysts. The study helped demonstrate that CO oxidation activity increased at decreasing particle size for metals supported onto reducible materials, with the limit of single-atom catalysts being highly efficient for the reaction as demonstrated in other works [20,169–173].

A similar size effect was also found for Pd/Al_2O_3 catalysts for methane steam reforming [151]. Selectivity differences were evidenced in this reaction where multiple pathways are possible and different types of sites present at different particle sizes can influence the overall reactivity. This was the case when Pd particles of sizes varying from 2.3 to 7.7 nm were supported on either CeO_2 or Al_2O_3. On CeO_2, nanocrystals of all diameters produced exclusively CO_2 during methane steam reforming under differential conditions (<10% conversion); however, Pd/Al_2O_3 catalysts showed a clear trend in selectivity towards CO, with smaller particles resulting in about 30% CO selectivity, whereas larger particles produced CO almost exclusively. Through studies of the water-gas shift (WGS) reaction on the size-controlled samples, it was shown that small particles delivered high rates for the reaction, thus causing the CO

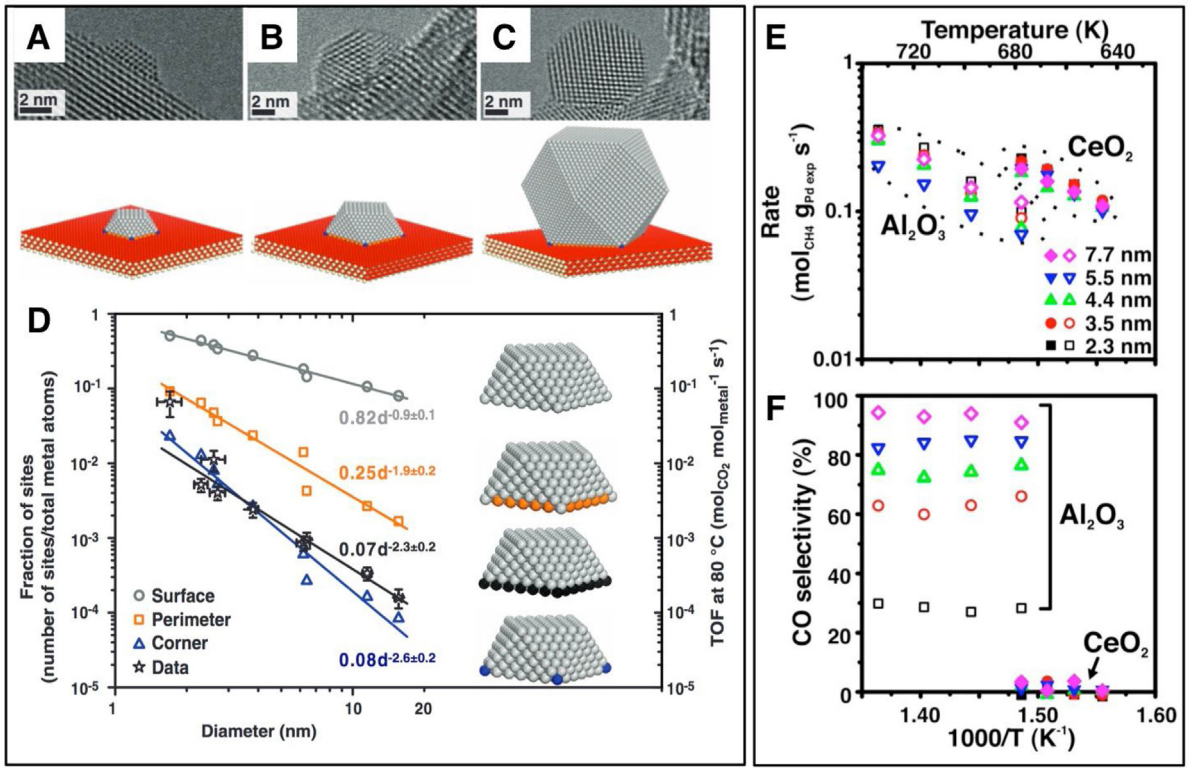

Fig. 13. (A–C) Different geometric models demonstrating how different nanocrystal sizes have varied, but well-defined interfaces and facets. (D) Scaling of different geometric features (i.e. surface, perimeter, corners) with nanoparticle sizes, given the model. Black trace indicates observed reactivity, held in comparison to the scaling of other geometrical features. Reproduced with permission from Ref. [168] Copyright (2013) American Association for the Advancement of Science. (E) and (F) Graphs for methane steam reforming reaction on size-selected Pd NCs on alumina (empty symbols) and ceria (filled symbols). Reproduced with permission from Ref [151]. Copyright (2015) American Chemical Society.

formed by the reforming reaction to quickly react with water and bring WGS to equilibrium; however, large particles were slower in WGS, thus causing the observation of mostly CO at the reactor outlet. Because Pd/ceria is a very good WGS catalyst [174], these samples would all show equilibrated WGS and therefore only CO_2 as reaction product (Fig. 13E and F).

Although higher catalytic performance is usually associated with reduced particle size, there are exceptions. Cobalt-based Fischer-Tropsch catalysts are one example, where improved catalytic activity is obtained at particle sizes of about 10 nm [175]. The better performance of larger nanocrystals was ascribed to the structure sensitivity of the reaction in addition to CO restructuring under reaction conditions. Somorjai et al. showed that a similar trend holds for CO_2 hydrogenation reactions on colloidal Co nanocrystals [176]. In this case, the authors also found that the synthesis method, with the use of trioctylphosphine oxide, resulted in catalysts with poor or no catalytic activity, whereas removing phosphorus from the synthesis conditions allowed them to obtain materials that were active and showed that particles of 10 nm had larger rates than those of 3 or 7 nm. Particle size was controlled by tuning the temperature of the solution when $Co_2(CO)_8$ was injected to initiate the nanocrystal formation.

A recent study in our group demonstrated that intermediate Pd sizes around 4.3 nm, rather than smaller or larger particles, were most intrinsically active (i.e. highest turnover per number of accessible active sites and time) for the methane combustion reaction due to different crystal structures exposed on the surface of the nanoparticles [36]. It is also possible that differences in the oxidation state of smaller particles, and in particular the strong binding of oxygen on undercoordinated Pd sites, is the cause for the decreased activity of smaller nanocrystal phases. Nanometer size-control of supported Pd catalysts (2.5–8.2 nm) was crucial to identify this effect. In another study, colloidally synthesized Pt nanoparticles of size 2, 4, and 6 nm were used to study the size-dependent kinetics of ethanol oxidation [177]. Interestingly, researchers used the same material to study this reaction in the gas and liquid phases. In both systems, larger particles are shown to have a higher intrinsic activity for this reaction. However, an explanation for this effect was not provided.

Much work has also been done demonstrating size-dependent selectivity using controlled colloidal catalysts. For example, Wang et al. studied the size-dependant activity and selectivity of Pt nanoparticles for the selective oxidation of methanol to formaldehyde [178]. As Pt nanoparticles approached one nanometer in size, a dramatic shift towards higher selectivity for formaldehyde was observed. Using XPS and DRIFTS, the researchers found smaller Pt nanocrystals to be more oxidized and less crystalline than particles of two nanometers and above. It was posited that more oxidized, less crystalline Pt nanoparticles might decrease binding strength to methanol intermediates, or present less reactive oxygen than metallic Pt nanoparticles with chemisorbed oxygen adatoms. Similar strategies were employed by the same group to identify pronounced size effects on selectivity of Pt catalysts both for pyrrole and furfural hydrogenation [179,180], invoking electronic changes due to particle size effects for the selectivity differences observed in their studies.

A more recent emerging application of colloidally synthesized materials with size control is in understanding sintering and deactivation mechanisms in heterogeneous catalysts, a crucial first step for the rational design of stable catalysts [180]. Nanocrystal size is a critically important parameter for stability, as smaller particles have a larger thermodynamic driving force to change towards bulk, sintered aggregates because of their higher surface energy. Colloidal nanocrystal approaches allow for precisely defined powder

catalysts, with programmable nanoparticle size distributions. However, unlike other mass-selected methods, colloidal catalysts can be synthesized on the gram scale, and allow for direct study of catalytic stability under realistic conditions. In an example, Zhang et al. synthesized Pt/Al_2O_3 catalysts with either unimodal (nanocrystals of either 2.2 nm or 4.4 nm) or "artificially" bimodal (by combining 2.2 and 4.4 nm nanocrystals on the same alumina support) size distributions and analyzed the changes occurring to the materials in-situ using an atmospheric pressure TEM cell [181]. The use of monomodal catalysts allowed one to discern the contribution of particle migration and coalescence to the sintering process, because small particles migrate faster on the support than larger particles. In this system, larger particles were found to be essentially immobile under the conditions studied (800 °C in H_2/N_2). However, when bimodal samples were imaged, ripening processes started to occur at lower temperatures because of the driving force provided by the difference in surface energy between smaller and larger nanocrystals. It was therefore hypothesized that monomodal 4.4 nm samples would not aggregate because ripening, although active, would not cause a dramatic change in particle size distributions, similarly to previous studies on size-selected clusters supported on alumina [182]. Such studies not only elucidate atomistic mechanisms of the atomic ripening processes, but also present a promising approach to mitigate such parasitic ripening processes through uniform materials.

Another important area, where size plays a key role in catalysis, is for porous materials. Namely, microporous crystals such as MOFs, COFs and zeolites exhibit significant differences in catalytic performance as a function of crystallite size. In this case however, differently from the above described metal (oxide) nanoparticles, the predominant molecular phenomena relate rather to intracrystalline mass transfer, than to nanoparticle surface energetics. E.W. Thiele described critical crystal sizes for pore diffusion limited reactions already in 1939 and triggered the emergence of descriptors such as the effectiveness factor (η), which describes the ratio between reaction rate to diffusion rate [183,184]. Effectiveness factors have for instance been evaluated for n-hexane cracking over H-ZSM-5 crystals in a size-dependence study, where the authors concluded that crystal sizes <100 nm are required to avoid reactions governed by diffusion rate [185]. In a similar study, the hydrocracking reaction on Pt/Beta-zeolite/alumina has been analyzed as a function of zeolite crystal size [186]. An optimal crystallite size <50 nm was found instead. These examples by no means constitute an exhaustive list, but it is important to point out that controlling the size of porous crystals is central to the respective scientific communities of zeolites, MOFs, COFs and POFs altogether. Finally, the crystal size control via colloidal syntheses represents an attractive solution to the problem of synthesizing porous catalyst crystallites without diffusion limitations.

Particle size effects in electrocatalysis

In addition to thermal catalytic applications, size controlled colloidal particles can reveal activity trends in electrochemistry, as well as create materials that are highly active on a per mass basis. A dendrimer-based synthesis resulted in very small (12–60 atom) platinum clusters that were intrinsically very active for the oxygen reduction reaction [187]. The authors created the clusters using phenylazomethine dendrimer cages that absorbed a specific amount of platinum precursor (platinum chloride), providing the needed synthetic control. While these particles had excellent surface area to mass ratios and were active, some authors have reported that the breakdown of bulk electronic structure at such small sizes is detrimental for another electrocatalytic reaction, hydrogen oxidation [188]. This latter study, however, showed that even very small clusters were still active, suggesting that any changes in electronic properties do not preclude activity and that very small clusters are a viable way to reduce noble metal loading in fuel cells. Strong effects on and of electronic structure were further demonstrated in electrochemical CO oxidation on gold using colloidally synthesized materials [42]. Here, the authors investigated the electronic properties of the particles by measuring the gold Au 4f binding energy of different size (1.5, 4, 6 nm) particles on different supports and correlated this parameter with the CO oxidation after depositing them on indium tin oxide (ITO). The authors found that smaller clusters had a higher percentage of Au^{3+}, which correlated to higher catalytic activity.

Recently, we have used nickel nanoparticles deposited on molybdenum foils to explore the effect of particle size on hydrogen evolution activity [189]. This revealed a surprising result where larger particles are more active on a mass basis than smaller particles, suggesting that the synergy arises from an electronic interaction, and not just an interface. This is perhaps a counter-intuitive result, and is not always the case. For example, enhanced oxygen reduction reaction (ORR) activity for the smaller CoO particles on carbon can be attributed to the enlarged interface between CoO and carbon [190].

Along similar lines, colloidal synthesis can also be used to directly explore the active catalyst for CO_2 reduction reaction (CO_2RR) [191]. In this work, the authors synthesized spherical copper nanoparticles with sizes down to 1.9 nm (Fig. 14). Smaller particles demonstrated higher selectivity towards hydrogen than carbon dioxide. This effect was attributed to more under-coordinated sites. The authors were also able to correlate this effect to a geometrical model of the exposed sites based on particle size. Studies like these will increase the ability to compare experiments directly to calculated electronic properties.

Another interesting application that uses size control to investigate not only facet dependence but also exploit the high surface area-to-volume ratio is presented in a work where the authors explored the correlation between bulk electronic descriptors and the oxygen reduction reaction activity [192]. By looking at small enough particles, the authors demonstrated that the bulk electronic descriptors could not work anymore at small particle sizes and that the surface states became more important.

Particle size effects in photocatalysis

An early report on how monodisperse, colloidal nanocrystals can be used to elucidate factors influencing activity in photocatalysts was contributed by Kamat and co-workers in 2004 [193]. Three sizes of gold NPs (3, 5 and 8 nm) were colloidally synthesized. The gold NPs were then combined with 15 nm sized TiO_2 particles. By carefully studying the decay of charge carriers in TiO_2 by UV-VIS and transient absorption spectroscopies, it was shown that photogenerated electrons transferred to the gold particles. Moreover, the Fermi level after charge equilibration in the Au-TiO_2 system was assessed by equilibration with the C60/C60- redox couple. It was shown that after charge transfer from TiO_2 to Au, the Fermi level in the Au-TiO_2 system was dictated by the size of the Au particle, where smaller particles gave rise to more negative Fermi levels. The Fermi level in turn dictates the reductive potential of electrons in the co-catalyst and is therefore an important parameter to account for when designing an active photocatalyst system (where a more negative reduction potential gives a more active system, other things equal). Thus, Kamat's early study showed how precise control over NP size via colloidal synthesis could reveal relevant fundamental physical characteristics of a photocatalytic system.

Alivisatos and co-workers have used colloidal synthesis of CdSe seeded CdS rods, tipped with Pt NPs to demonstrate how precise size control (via colloidal synthesis) over both seed size and rod length can be used to optimize photocatalytic efficiency [194]. It was shown that smaller seeds gave better charge separation and therefore a higher quantum efficiency (QE). Moreover, separation

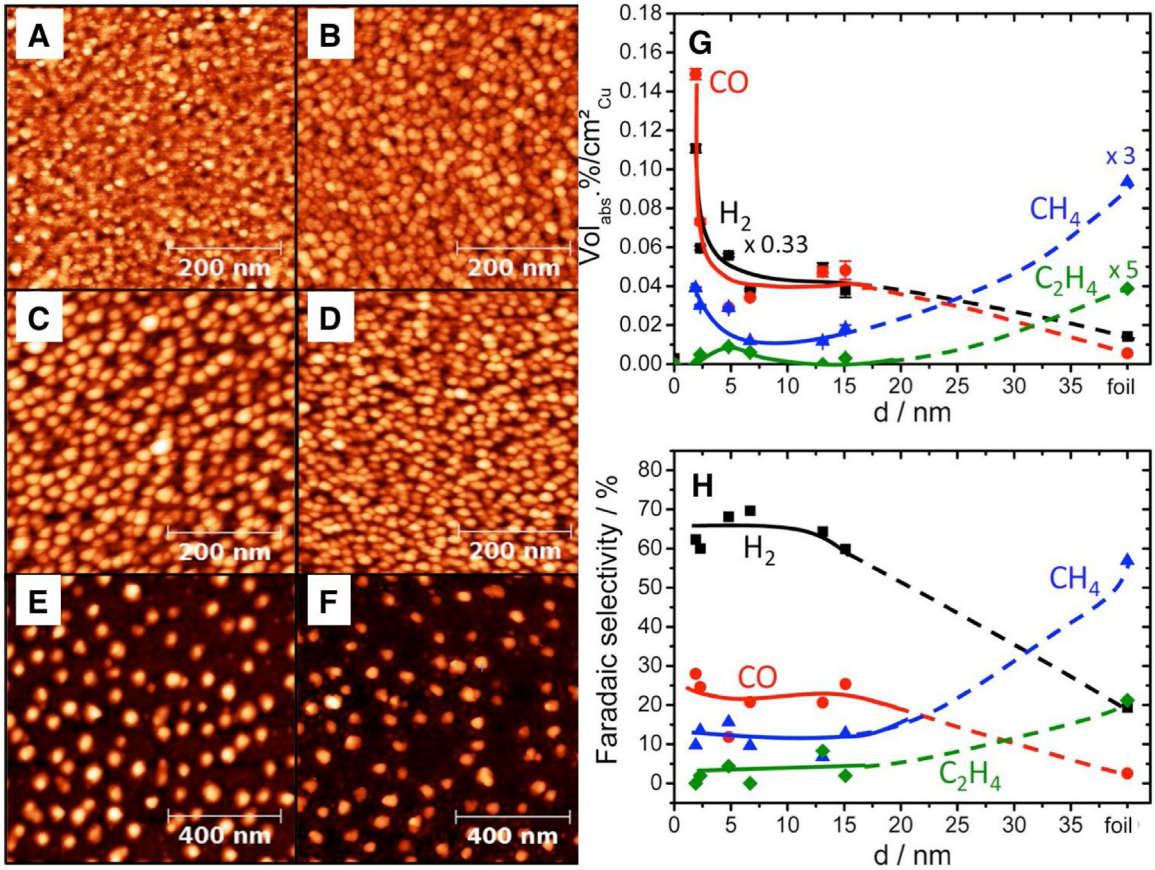

Fig. 14. Tapping-mode AFM images of micellar Cu NPs with average particle heights of (A) 1.9 ± 0.7, (B) 2.3 ± 0.8, (C) 4.8 ± 1.4, (D) 6.7 ± 1.8, (E) 13.1 ± 3.5, and (F) 15.1 ± 5.2; and particle size dependence of the gas product composition during the electrocatalytic CO_2RR over (G) the same Cu NP samples, and (H) corresponding faradic selectivity of reaction products.

Reproduced with permission from Ref. [191] Copyright (2014) American Chemical Society.

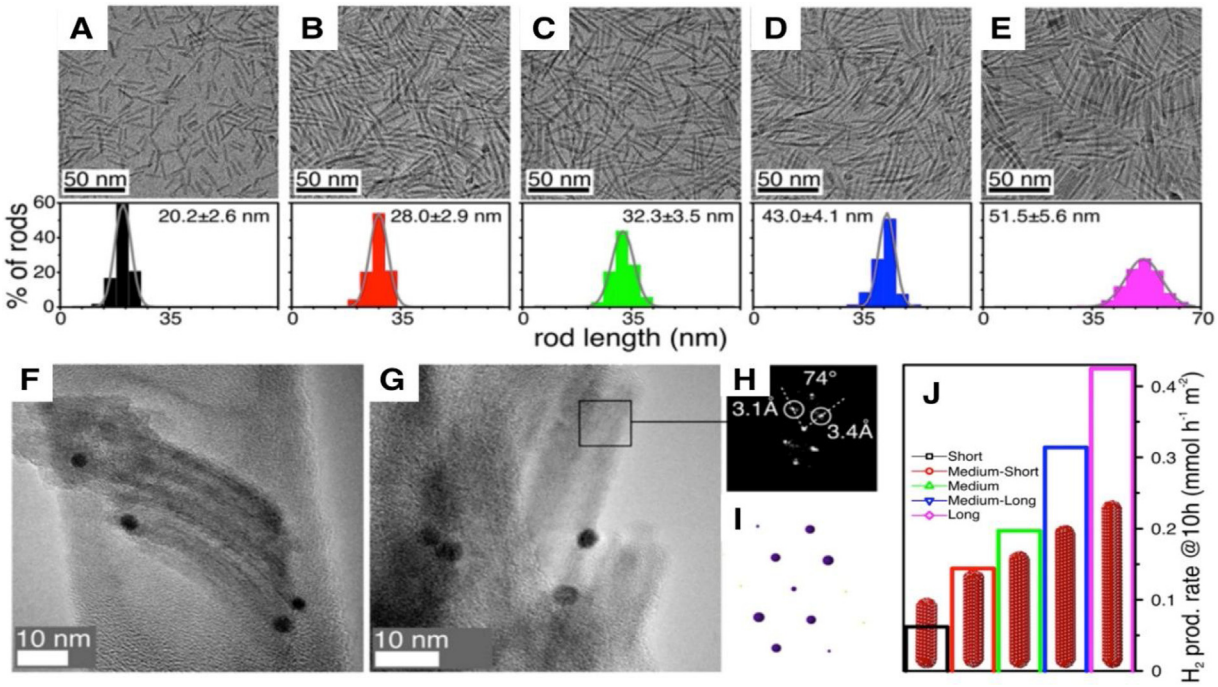

Fig. 15. (A–E) TEM images of short, short-medium, medium, medium-long and long brookite rods synthesized by a seed-mediated approach, with associated histograms of length distributions (bottom). (F, G) High-resolution TEM characterization of long nanorods after photocatalytic activity. Representative high-resolution (HR) TEM images. Black particles are Pt nanocrystals. (H) Digital diffraction pattern of a selected area, showing distances and angles for specific planes. (I) Simulated diffraction pattern for brookite phase viewed along the [213] zone axis, and (J) Rates after 10 h under illumination normalized by surface area of the photocatalysts.

Reproduced with permission from Ref [74]. Copyright 2016 National Academy of Sciences.

of reduction (Pt NPs) and oxidation sites (CdSe seeds) was tuned by changing CdS rod length, and it was shown that larger separation gave higher activity. It was not specifically mentioned in the work but postulated that holes would migrate to the surface to react with methanol. It was argued that the higher activity of longer rods was due to increased spatial separation of reduction and oxidation sites, which suppressed back-reactions between reactive chemical intermediates on the photocatalyst surface. Recently, this same system was optimized to give record QEs approaching 100% [195]. In the same vein, further demonstrating the power of size control via colloidal synthesis, Murray and co-workers synthesized monodisperse TiO_2 brookite rods modified with monodisperse Pt NPs, which showed very high quantum efficiency for ethanol reforming (65% at 365 nm) [74]. Rods of lengths between 20.2 and 51.5 nm (Fig. 15A–E) were co-deposited with 1 wt% of monodisperse (4.5 nm +/- 0.4 nm) Pt NPs in thin films, and it was shown that the photocatalytic activity was highly dependent on rod length, with longer rods being more active when the activity was normalized per exposed titania surface area (Fig. 15J). These rods were active for days, and TEM characterization before and after reaction confirmed that the size and shape of both the brookite rods and Pt NPs were maintained after lengthy photocatalytic reaction (Fig. 15F–I). The works by Alivisatos and Murray clearly show that precise engineering of particle size (in these cases rod lengths) of semiconductor NPs for photocatalysis is critical to optimize photocatalytic activity.

Optimization of the photoabsorber NP size is critical, as demonstrated by optimizing rod lengths in brookite TiO_2 and CdS systems (see above). However, the work by Kamat, which showed the influence of cocatalyst NP size on the Fermi level of irradiated photocatalysts, suggests that the size of co-catalysts should also be tightly controlled in optimal photocatalysts. Banin and co-workers synthesized Au-tipped CdS rods by a colloidal route and showed that an optimal size existed for the Au co-catalyst in photocatalytic H_2 production from aqueous suspensions in the presence of Na_2S and Na_2SO_3 as hole scavengers [196]. The authors investigated Au NPs in the size range 1.6 nm – 6.2 nm and found that the optimal particle size in their system was 3.0 nm. Similarly, Amirav and co-workers investigated the influence of Ni NP tip size on photocatalytic activity of Ni tipped, CdSe seeded CdS rods towards hydrogen production from isopropanol-water suspensions [197]. The CdSe seeded CdS rods (length $\tilde{5}$0 nm) were colloidally synthesized and then Ni tips of different sizes (2.3 nm–10.1 nm) were colloidally grown in-situ onto the pre-formed rods. It was found that 5.2 nm was the optimal size of the Ni co-catalyst in their system. For the CdS-Au system studied by Banin, it was argued that photocatalytic activity was limited for small tip sizes by rate of electron injection from rod to tip (decreasing with decreasing tip size). For large tip sizes, it was argued that the activity was limited by increasing rate of hole injection from rod to tip, which competes with water reduction on the tip. In contrast, Amirav argued that in their CdSe/CdS-Ni system, Coulomb blockade charging in small co-catalyst NPs was limiting rod-tip electron transfer, while a Schottky barrier was limiting rod-tip electron transfer for large cocatalyst NPs. [197] As can be inferred from the different mechanisms proposed, discussion regarding the factors underlying dependence of photocatalytic activity on co-catalyst NP size is not settled, and mechanisms may also substantially vary between semiconductor/metal combinations. However, irrespective of underlying mechanisms, the pioneering works by Amirav and Banin establish that there exists a dependence of activity on co-catalyst size [196,197]. The dependence appears strong and as an example, Amirav reported a decrease in QE (at 450 nm) from 23.4% to 1.2% upon changing the Ni co-catalyst size from 5.2 nm to 10.1 nm (i.e yielding a surprisingly high $\tilde{2}$0-fold decrease in activity upon doubling the co-catalyst NP size).

Given the strong activity-size correlation both for photoabsorbers and co-catalysts, it appears plausible that in the polydisperse photocatalysts (with respect to both photoabsorber and cocatalyst) typically reported in the literature, only a small subset of the particle population will contribute significantly to photocatalytic activity. Because inactive particles nonetheless absorb light, inactive particles with the "wrong size" will substantially reduce the obtainable QEs from such polydisperse samples. As demonstrated by the work discussed in this section, colloidal synthesis provides a unique means of controlling size within sufficiently close ranges for fundamental studies into size effects. Moreover, as the studies into size effects begin to show, it appears crucial to tightly control NP size distribution (possible through colloidal synthesis) of photocatalyst components to obtain systems with high activity.

Impact of nanocrystal shape

Particle shape effects in thermal catalysis

Due to the possibility of high-temperature morphological reconstruction, the majority of shape-dependant reactivity studies is performed under relatively mild conditions, and involves reactions such as low temperature oxidations or reductions. Most studies involve either precious metals (Pt, Pd, Ag) or metal oxides (CeO_x, CoO_x, TiO_x), due to their industrial importance, and the hard-earned ability of researchers to sculpt nano-shapes of these metals (i.e. Pd) [67]. Noble metals Pt and Pd have been found to display unique shape-dependent selectivity for hydrogenation reactions, depending on exposed crystal planes and the corresponding densities of specifically-coordinated sites. In one of the first shape-dependant gas-phase studies, Pt nanocrystals with different exposed facets were shown to display shape-dependent catalytic activity for isomerization of olefins [198]. It was found that at low temperatures, tetrahedral Pt nanocrystals exhibited higher catalytic selectivity for isomerization of trans-2-butene to its cis isomer than the opposite cis-to-trans reaction. In contrast to tetrahedral Pt nanocrystals, nanocrystals with cubic shape displayed comparable catalytic activity in both reactions. The shape-dependent catalytic selectivity was due to the fact that the isomerization of trans olefins to cis counterparts is promoted by the (111) facets found only on the platinum tetrahedral particles.

In another early demonstration of how colloidal nanocrystals bridge the gap between ultrahigh vacuum studies and realistic reaction conditions, Bratlie et al. studied benzene hydrogenation over shape-selected Pt nanocrystals [199]. Interestingly, different nanocrystal shapes display different hydrogenation selectivity, where cuboctahedral nanocrystals showed the formation of both fully and partially hydrogenated products, but cubic nanocrystals had high selectivity only for the fully hydrogenated product. This study is notable as the shape-dependent catalysis agrees well with single-crystalline studies on Pt(100) and Pt(111) single crystals, where the facets reproduced in colloidal nanocrystals exhibited the same selectivity as the corresponding single-crystal surfaces.

Perhaps due to increased stability, many examples exist of shape-selective catalysis in the liquid phase. Crespo-Quesada et al. studied selective alkyne reduction over cubic, octahedral, and cuboctahedral Pd nanocrystals of different sizes (Fig. 16A–D) [200]. Using well-defined nanocrystal geometries, the researchers could provide quantitative statistics of the relative population of (100), (111), and edge surface atoms (Fig. 16E). By correlating the relative populations of these sites with the product distribution, the group found that semi-hydrogenation was facilitated by (100) and (111) planes, while over-hydrogenation was associated with nanocrystal edge sites. This statistical model also allowed to plot turnover frequencies, taking into account the modelled active site populations, as a function of nanocrystal size. Cuboctahedra are slightly disfa-

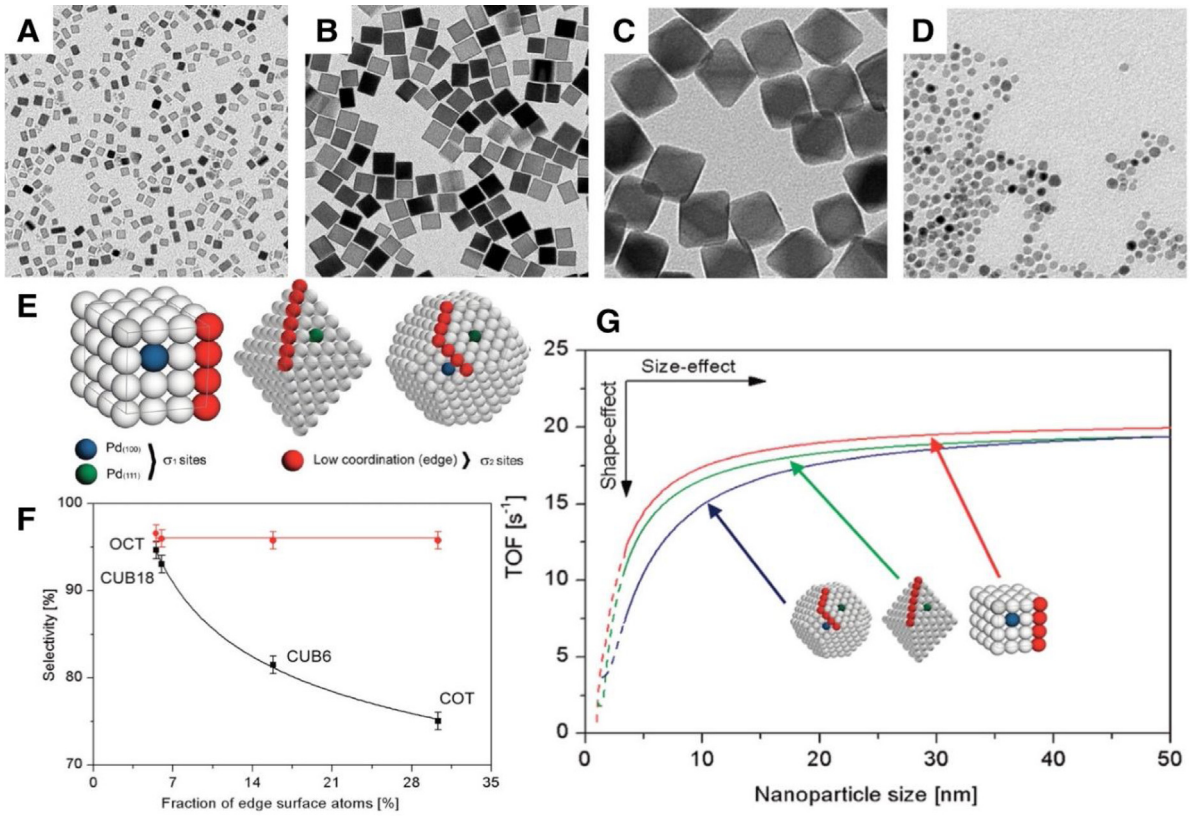

Fig. 16. TEM images of colloidally synthesized Pd nanoparticles in various shapes: (A) small cubes, (B) large cubes, (C) octahedra, (D) cuboctahedra. (E) Schematic illustrations of different types of active sites in the hydrogenation of 2-methyl-3-buten-2-ol. (F) The overall catalytic selectivity towards the target semihydrogenated product 2-methyl-3-buten-2-ol, and (G) Graph depicts turnover frequencies with respect to different active site populations as a function of nanocrystal size.
Reproduced with permission from Ref. [200] Copyright (2011) American Chemical Society.

vored due to the larger fraction of edge sites, which are considerably less active in the semihydrogenation of 2-methyl-3-buten-2-ol relative to plane sites. The most significant size effect is observed in the 3–20 nm range, after which the reaction becomes size and shape independent with respect to turnover frequency (TOF). Nanocrystals smaller than 3 nm in size start to lose their bulk properties, and, consequently, the catalytic behavior may not follow the prediction. Therefore, this region is depicted with dotted lines (Fig. 16G).

Metal oxides with different shapes have been widely studied in oxidation catalysis. Oxygen vacancies present in mixed valent oxides are often catalytic active sites, because they can promote the adsorption and dissociation of oxygen molecules. Both experimental studies and DFT calculations demonstrate that oxygen vacancies on surfaces are caused by electron localization [201], indicating that the density of oxygen vacancies could be manipulated by "defect engineering" through controlling the different exposed metal oxides facets and the nanocrystal size [71,202]. It has been reported that CO oxidation activity on CeO_2 nanoparticles strongly depend on the concentration of oxygen vacancies on the surfaces [203]. For this reason, CeO_2 nanoparticles with {100} and {110} planes showed higher CO oxidation activity and oxygen storage capability than those with {111} planes [71,203]. The improved catalytic activity in the oxidation of CO over CeO_2 {100} and {110} planes is attributed to the higher concentration of oxygen vacancies on these two surfaces than on (111) surface [204,205]. In addition to CeO_2, Co_3O_4 nanomaterials have also attracted considerable attention for oxidation catalysis. Shen et al. developed a hydrothermal method using cobalt acetate as a precursor and subsequent direct thermal decomposition to obtain Co_3O_4 nanorods [206]. In contrast to other planes containing both Co(III) and Co(II) cations (e.g. {001} and {111}), the {110} plane exposes mainly Co(III) cations. The Co_3O_4 nanorods with predominantly exposed their {110} planes showed better catalytic properties than Co_3O_4 nanoparticles for CO oxidation at temperatures as low as −77 °C. The kinetic study revealed that both Co_3O_4 nanorods and nanoparticles had the same apparent activation energy of 22 kJ mol^{-1}, indicating that active sites in both materials are identical. Those active sites are reported to be Co(III) sites. However, the reaction rate on Co_3O_4 nanorods is 10 times higher than the corresponding value for the nanoparticles. The high activity was probably due to the surface richness of active Co(III) sites on the {110} surfaces that can interact preferably with CO. The surface oxygen coordinated with three Co(III) cations then reacts with CO to form CO_2. Dissociating a gas-phase oxygen molecule then fills the formed oxygen vacancy with a neighbouring partially reduced cobalt site. In addition to this study, other works proposed the higher activity of Co(III) cations in certain coordination environments. Li et al. performed CO oxidation on Co_3O_4 nanobelts and nanocubes, which have a predominance of exposed {011} and {001} planes, respectively [207]. It was shown that the Co_3O_4 nanobelts were more active than Co_3O_4 nanocubes in CO oxidation, which originated from the higher turnover frequency of Co^{3+} sites of {011} planes than that of {001} planes. These findings revealed that the exposed crystal planes of Co_3O_4 could be tailored during synthesis so as to control the amount of surface Co(III) sites and concentration of oxygen vacancies, which influences the catalytic activity behavior for Co_3O_4 nanomaterials synthesized.

These few examples highlight the richness of studies that demonstrated the improved activity of specific facets in thermal catalysis. The study of well-defined nanocrystalline materials for this purpose has only merely begun, and a number of important discoveries are expected in this area of catalytic science.

Particle shape effects in electrocatalysis

Colloidal nanoparticles are also useful for studying electrochemical reactions with facet or shape dependence, like the oxygen reduction reaction (ORR) and carbon dioxide reduction reaction (CO_2RR).

Platinum is known to have facet dependent ORR activity from single-crystal studies [208]. In a seminal study on Pt single crystal facets under ultra-high vacuum Stamenkovic et al. report a 10 fold activity of a Pt(111) facets compared to commercial Pt catalyst [209]. Building on these studies, Sun and co-workers added small amounts of iron carbonyl to the synthesis of platinum particles to tune their shape, preparing monodisperse Pt polyhedron (3 nm), truncated cubes (5 nm) and cubes (7 nm) [210]. The samples exhibited different ORR activity, with cubic particles being the most active owing to their higher fraction of (100) facets. It is noteworthy that compared to the mentioned UHV study, these tests were carried out with an H_2SO_4 electrolyte instead of $HClO_4$, which may also lead to different specific activities. These materials were also high performing. Their specific activity was twice that of commercial platinum catalysts [211]. Many more examples followed in this same area, helping to bridge studies from single-crystals and high surface area materials. In particular, a common metric for ORR fuel cell catalysts is the amount of platinum or platinum-group metals needed to achieve a certain current density, as the usage of this element maps to the eventual cost of the catalyst in an automobile [121]. Colloidal techniques can be used to make nanostructures with very high platinum utilization. Two such examples in which shape control is beneficial are multimetallic nanoframes and hollow platinum cubes [90,212]. In both cases, the materials showed similar activity to a Pt/carbon black catalyst on an electrochemically active surface area basis, but much higher activity on a per-platinum mass basis, as would be anticipated. Colloidal systems have also been used to produce hollow nanocages and similar structures for other reactions [90,91,213,214]. This elegant strategy shows the great promise that colloidal synthesis has for electrocatalysis. Given the large body of synthetic literature, many possible structures can be made. As the number of techniques to characterize electrocatalysis in-situ increase, these improvements will lead to enable the extraction of powerful structure-property relations.

CO_2RR on copper has shown a rich dependence on morphology, with many studies focusing on different facets and defects [215–217]. The development in this field has been recently comprehensively reviewed [218], and herein we highlight the fact that colloidal nanoparticles offer an excellent platform to study these effects. It has been established from single crystalline surface studies that the electrochemical activity on cubic {100} planes exceed the one of {111} planes. It has also been shown that the product distribution was greatly dependent on the amount of {111} and {110} steps on the {100} terraces. More C—C coupling products (higher C_nH_m/CH_4 ratio, with $n > 1$) were observed when more such steps were present [219]. From these surface studies it emerged that copper nanocrystals can yield catalysts active for CO_2RR to higher products (C_{2+}) by controlling their properties [220]. In another recent example, it has been found that colloidal nanocrystals act as a pre-catalyst for the final active structure, which was found to be mostly cubic agglomerates [221]. Interestingly, copper cubes directly synthesized do not show the same high selectivity for higher (C_{2+}) products, pointing to some unique active sites created by the sintering copper particles.

Particle shape effects in photocatalysis

As described earlier, the size of both photoabsorber and co-catalyst have profound effects on photocatalytic activity and the same is true regarding the shape of nanocrystals for photocatalysis. Unfortunately, using conventional techniques such as hydrothermal synthesis, it is difficult to simultaneously control both size and shape of nanocrystals and in reported systems, it can often be difficult to deconvolute the influence of size from the influence of shape on photocatalytic activity. In contrast, colloidal synthesis methods give excellent and simultaneous control over both shape and size of nanocrystals. Consequently, colloidally synthesized nanocrystals have been successfully used to elucidate the influence of shape in photocatalysis. As an illustrative example, monodisperse anatase TiO_2 nanocrystals with truncated tetragonal bipyramidal geometry and tunable fractions of the {001} and {101} facets exposed were used to elucidate which facet is more active for hydrogen production via methanol reforming (Fig. 17) [61]. Thanks to the precise control over both faceting and size it could be shown that the {101} facet of anatase is substantially more active for photo-reforming of methanol than the {001} facet (Fig. 17). Because fluorine was used during the synthesis to shape the nanocrystals, evaluation of the photocatalytic activity after fluoride removal by way of a diluted sodium hydroxide solution was also performed. The results showed an increase in the activity of the sample with more {101} facets, a decrease in activity for the sample with mostly {001} facets, and basically no change for a sample having both facets. This observation strongly favored the ranking of the facet activity.

Impact of nanocrystal composition

Particle composition effects in thermal catalysis

As described in previous sections, colloidal synthesis offers a level of control over catalyst composition unmatched by other catalyst synthesis techniques. It not only allows for the control over the ratios of catalyst components, but more importantly can be used to ensure the mixture and geometry of the resulting multimetallic catalyst. These advantages allow for true testing and determination of the impact of each metal in a multimetallic system. In the case of randomly alloyed bimetallic particles, colloidal synthesis ensures that particles are mixtures of metals with the desired composition, rather than two populations of particles of different metals. Such synthetic control sets colloidal synthesis apart from co-impregnation in the preparation of bimetallic systems. The formation of pre-formed bimetallic colloidal nanocrystals has been used with many combinations of metals including Pd/Au [101,222–224]. Precise control over catalyst composition allows researchers to better understand bimetallic catalysis.

In thermal catalysis, bimetallic catalysts are used to take advantage of changes in the local electronic structure at the nanoparticle surface due to the presence of a different atom. Controlling the surface composition is therefore crucial. An example from our group examined mixed Pd/Pt particles (Fig. 18). Colloidal nanocrystals with compositions from pure Pd to pure Pt with many mixtures in between were synthesized to test the effect of varying composition [101]. For all samples the nanoparticle size was maintained at 2–3 nm to avoid size effects on catalysis. This set of catalysts allowed for the determination of why Pd/Pt systems performed better than their respective components in methane combustion in the presence of water. Many previous studies had given conflicting results but were based on catalyst synthesis procedures that deposited metals using wet impregnation methods. These conventional approaches resulted in catalysts containing a broad range of pure Pd, pure Pt and Pd/Pt alloy particles in one sample, thus making finding consistent trends difficult. With the colloidal nanocrystals it was determined that the addition of even a small amount of Pt to Pd phase caused the activity for methane combustion to drop by three orders of magnitude. This decrease in activity was due to the stabilization of metallic Pd when Pt was added, reducing the coverage of the highly active PdO phase. However, studying the materials under wet conditions showed that Pt-based bimetallics

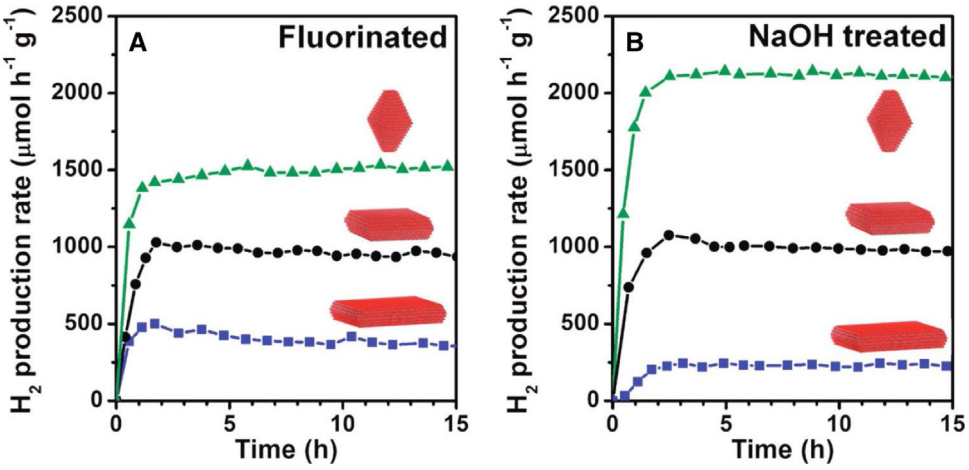

Fig. 17. Hydrogen production rates in μmol(H_2-evolved).(g.h)$^{-1}$ from 1 wt% Pt-loaded samples of ligand exchanged, (A) fluorinated and (B) NaOH-treated TiO_2-nanocrystals under solar illumination in 1:1 mixtures of MeOH/H_2O.

Reproduced with permission from Ref. [61] Copyright (2012) American Chemical Society.

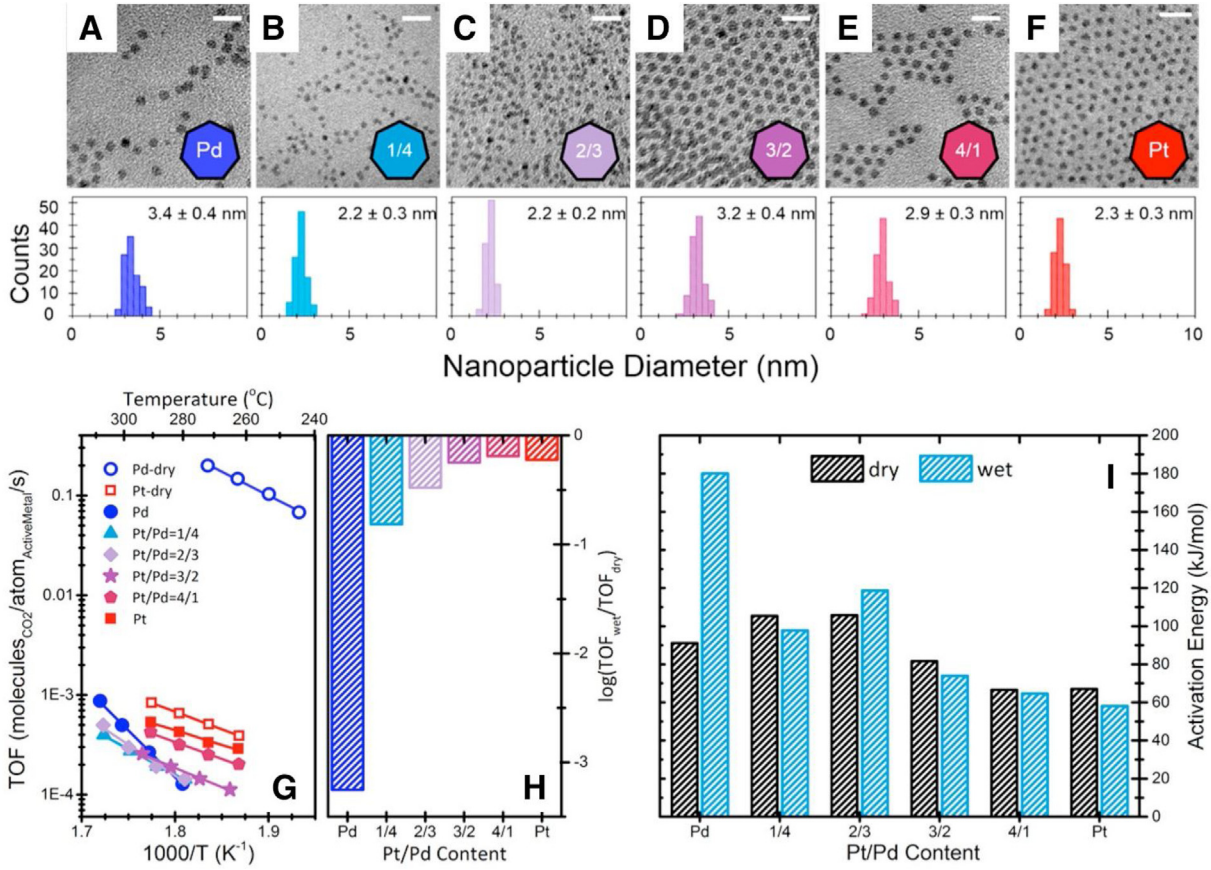

Fig. 18. The use of composition-controlled bimetallic Pd/Pt nanocrystals, (A–F) TEM micrographs and particle size distributions to demonstrate the effect of adding Pt to Pd for methane combustion. (G) In the presence of water (steam) added to the feed, the catalytic activity of pure Pd is highly affected, whereas Pt-based nanocrystals are more stable (bottom left). (H) The inhibiting effect of water is represented in a plot of log(TOF_{wet}.TOF_{dry}^{-1}) as a function of Pt-content, and (I) Graph depicts the respective apparent activation energies extracted from Arrhenius plots for the different materials in wet (blue) and dry (black) conditions.

Reproduced with permission from Ref. [101] Copyright (2017) American Chemical Society.

retained their activity, whereas Pd catalyst severely deactivated thus providing lower rates compared to a 1/1 Pd/Pt alloy material.

Another example where the secondary metal atoms are present as isolated features on the nanoparticle surface are dilute or single atom alloys (SAA) [108]. The isolated metals are often Pd or Pt metal, which are rare, expensive materials with high activity and poor selectivity. The combination of the platinum group atoms with a less active, more selective, and cheaper coinage metal nanoparticle (e.g., Au, Ag, Cu) offers a potential avenue for tuning product selectivity while achieving high activity. There have been several works detailing the application of SAAs to thermal hydrogenation. One example showed that isolated Pd atoms are capable of splitting

hydrogen molecules, resulting in adsorbed H atoms that spillover onto the bulk nanoparticle surface (Ag) for subsequent reaction [225]. Similar results have been found for several combinations of platinum group metals with coinage metals where single atoms of Pt or Pd lead to the highest activity and selectivity for hydrogenation reactions [225]. This result is due to the ability of single Pd or Pt atoms to split hydrogen and spill it over to the coinage metal, which is more selective for hydrogenation. The construction of such catalysts and the determination of these trends from them would not be possible without the fine control over catalyst construction provided by colloidal methods.

Single atoms can also offer catalytic improvements as a result of different surface electronic properties. This change is leveraged in a Pt/Cu SAA system where a change in electronic structure reduced Pt poisoning by CO. Due to the lack of adjacent Pt atoms, CO is forced to bind linearly to the single Pt atoms rather than binding more strongly at bridged sites [222]. As a result, the catalyst remains active in the presence of CO. This result demonstrates the promise of SAAs for developing stable, effective catalytic materials without requiring extensive treatment of the feed to remove contaminants that would poison the catalyst.

In addition to ensuring close mixing between metals, colloidal methods can also be used to increase the amount of interface between metal nanocrystals and metal oxides. For many reactions the metal oxide support is not inert but plays an important role either stabilizing reaction intermediates or providing reactants to the catalytic metals. The techniques to create several metal/metal geometries were described in the synthesis section of this review. In one catalytic example from our group, Pd nanocrystals were combined with islands of a variety of different metal oxides (V, Mn, Fe, Co, Ni, Zn, Sn) to determine the best promoter for methane combustion [100]. Several of the metal oxide phases strongly affected the activity of the PdO phase, with NiO-promoted materials delivering turnover frequencies three times higher than a Pd/Al_2O_3 catalyst. In another example, SnO_2 islands were added to Pd particles and changed the binding energies of intermediates enough to increase the reaction rate and selectivity for several hydrogenation reactions [226]. This technique has also been utilized many times to increase the metal-metal oxide interfacial area. For example, colloidally synthesized Pd and CeO_2 nanoparticles were combined to give increased interfacial area. This in turn gave an increased activity for methane combustion [227]. Through colloidal methods many aspects of catalysts can be precisely controlled which can help give new understanding of thermal catalytic systems.

Particle composition effects in electrocatalysis and photocatalysis

Similar benefits can be extended to electrocatalysis. The ability to replace expensive elements is particularly attractive. In electrocatalysis, this frequently means replacing Pt or Au with non-noble metal materials like MoP [228]. The Sun group used colloidal particles to explore iron-metal oxides as catalysts for the oxygen reduction reaction [229]. The composition was controlled by varying the amount of metal precursor, acetylacetonate salts in all cases. Optimizing the second metal and the composition of the mixed oxides, the authors found that $MnFe_2O_4$ was the most active material. At relevant mass loadings on carbon support ($\tilde{2}0\%$) this catalyst was as active, and more stable, than commercial platinum catalysts. This result shows that the compositional control afforded by colloidal methods can be used to efficiently sweep out variable space to optimize catalytic design.

Colloidal techniques can also be used to make sophisticated core-shell structures, once again with the goal of minimizing precious metal usage. As mentioned before, palladium can be used to create core-shell structures with platinum shells, increasing activity per platinum mass. However, palladium is still a valuable and rare metal. Another approach is to use carbides as the core, which have electronic properties similar to noble metals [230,231]. Using reverse microemulsion synthesis, Hunt et. al. exploited the thermodynamic stability of noble metal overlayers on tungsten carbide to make highly active and stable electrocatalysts for the methanol oxidation reaction [115].

Noble metal overlayers can also be made by surface enrichment of alloyed nanoparticles. For example, tuning the parameters of the colloidal synthesis of gold-copper nanoparticles can control how ordered the particles are on an atomic basis and introduce a gold overlayer that shows CO_2RR activity comparable to pure gold [115,232]. The series of compared particles are exposed to various thermal treatments. With increasing harshness, longer exposition times, or higher temperature treatments particles become more ordered and a gold overlayer emerges. Due to compressive strain, this layer is more active than pure gold nanoparticles. Interestingly, disordered nanocrystals mostly provided H_2 under CO_2RR conditions; instead, ordered alloys produced CO (Fig. 19). The results, corroborated by DFT analysis, clearly show the power of colloidal nanocrystals not only in providing useful fundamental information about catalytic reactions, but also in drastically tuning the activity and selectivity of catalytic transformations.

Many studies have explored the impact of nanoparticle composition on photocatalysis, for example by engineering the band gap of the photo-absorber via doping or by using solid solutions [234]. Efficient co-catalysts have also been fabricated by using bi-metallics or by using core-shell structures [235]. However, few studies have combined optimized compositional control with precise size and shape control to deconvolute the impact of composition from the influence of size and shape, in particular using colloidal methods. Thus, combining the existing and ample knowledge regarding optimal photo-absorber and co-catalyst composition with the excellent size and shape control offered by colloidal synthesis methods may prove a fruitful future research direction.

Impact of nanocrystal-based composite structure

In addition to the control over size, shape and composition, uniform colloidal materials can also be used to extend the control beyond the single nanocrystal level in composites. These hybrid materials are attractive due to the possibility of systematically improving catalytic systems in terms of selectivity (e.g. pore sizes can be tuned.), activity (e.g. particle support interactions can be adapted, using for example acidic/basic or redox active/inactive supports), and stability (e.g. the design of embedded particles has allowed the synthesis of sinter-resistant catalysts).

The possibility to study the discrete effects of supports and interfaces in thermal, photo-, and electro-catalytic transformations serves as principal motivation for the development of nanoparticle composite materials. While depositing nanoparticles on supports already allows for the study of metal support interactions, a more complete way is to embed the nanocrystals inside support materials to form well-defined 3D nanocrystal-support composite materials.

An et al. report an example of depositing platinum nanoparticles into ordered mesoporous oxide supports [135]. By using different reducing and non-reducing mesoporous structured supports, the group evidenced the ability to tune electronic interactions between oxide materials and colloidal Pt-nanoparticles. With these materials, the authors identified the interface of cobalt oxide with platinum nanoparticles to be most active for CO oxidation.

Beyond the support interface, ligand interactions with colloidal particles present another means of control over catalytic properties. The electronic structure of the surface of rhodium particles supported on mesoporous silica, for instance, is demonstrably affected by the presence of ligands, which influence the binding of CO to the metallic surface. Intrinsic activity of CO Oxidation is increased as a

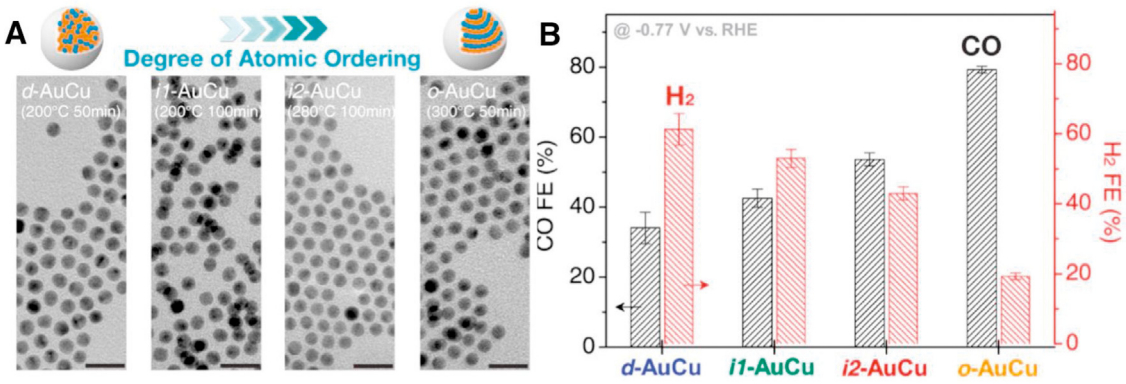

Fig. 19. (A) TEM images of AuCu bimetallic NPs synthesized at various conditions allowing for systematic tuning of the degree of ordering. Scale bar, 20 nm, and (B) Electrochemical CO_2 reduction activities of AuCu bimetallic NPs evaluated by faradaic efficiencies of CO and H_2.
Adapted with permission from Ref. [233] Copyright (2017) American Chemical Society.

result. A systematic kinetic evaluation of the catalytic system before and after removal of PVP-ligands deposited in SBA-15 mesoporous silica has proven that the presence of unaltered ligands favored the reaction occurring on rhodium bridging sites. The higher activity has been ascribed to these bridge sites of the Rh particle [237].

A common problem of many metal nanoparticle catalysts is sintering under reaction conditions. The previously described strategy of growing silica shells around metal nanoparticles that enabled synthesizing porous hollow spheres encapsulating noble metal nanoparticles has proven to be a versatile technique in imparting sinter-resistance. The use of both ligands that make particles at least partially vitreophilic and mesopore-directing ligands permitted syntheses of mesoporous silica shells encapsulating for example Au-nanoparticles. This composite material has been demonstrated as a powerful and sinter-resistant CO oxidation catalyst which is promising as Gold nanoparticles are highly sensitive towards sintering under reaction conditions [124]. Alternatively, the use of tetradecyltrimethylammonium (TTA) bromide yields mesoporous (ø = 2 nm) silica shells with a preserved good accessibility of Pt-surface atoms. The Pt-particles have shown to be promising non-sintering catalysts at high reaction temperatures up to 750 °C for the hydrogenation of ethylene and oxidation of CO [126]. Creating single Ni-nanoparticles with protective silicon dioxide shells also worked as a stabilizing strategy forming so-called "yolk-shell" catalysts [238]. These composite materials were tested in the methane steam reforming (MSR) reaction for which Ni is the industrially applied metal, and compared to which improved lifetimes were reported.

Instead of using "inert" silica shells, more active support materials for catalysis can be employed to prevent sintering, and to modulate the activity of the particles. Porous ZrO_2 hollow spheres have been shown to hinder gold nanoparticles from sintering during CO oxidation at temperatures as high as 800 °C. Arnal et al. also elegantly proved that crushing the hollow ZrO_2-spheres in a ball mill restored the expected sintering behavior of gold nanoparticles [122]. Ceria, as a reducible support has also been used in several attempts to embed metal nanoparticles for making use of strong metal support interactions (SMSI). These interactions are generally reported for metal-ceria systems and more specifically affect metal ceria interfaces. Metal particles on non-ordered, low surface area ceria logically exhibit only a limited number of such interfacial sites. Encapsulating metal nanoparticles in ceria instead increases the fraction of interfacial sites with respect to the total number of surface atoms, while also enabling the synthesis of sinter resistant catalysts. In the following, we expose a few works that were based on such hypotheses. Yeung et al. described a Pt/CeO_2 system produced using a microemulsion that exhibited superior water gas shift (WGS) activity compared to classic Pt/CeO_2 systems [128]. The authors were able to cover the metal nanoparticles with a thin ceria layer and to harness strong metal support interactions. In contrast, a comparable work focused on producing Pd-nanoparticles covered with CeO_2-layers of various thicknesses. Though the authors report an improved stability during the WGS reaction, they also conclude that a critical thickness of the ceria layers is required to prevent Pd-particles from sintering [129]. It is particularly noteworthy that it has been possible to tune such $Pd@CeO_2$ encapsulated catalysts to form core shell supramolecular units. The latter could be deposited on hydrophobized alumina supports and used as catalytic composite materials for the complete catalytic combustion of methane. Cargnello et al. showed that their catalytic system was benefitting, not only from beneficial metal support interactions promoting intrinsic PdO-activity, but also the reducibility of the ceria shell that efficiently wraps the particles [227]. Both effects were tuned while also leading to a sinter-resistant catalyst that was stable even after treatments at temperatures as high as 850 °C.

The possible synergies between supports and metal nanoparticles for stability and activity are well known in electrochemistry as well [239,240], but have not been heavily explored using colloidal nanoparticles so far. Nonetheless, given the challenges of in-situ analysis in electrochemistry, we believe that the use of well-defined colloidal nanoparticles as starting materials offers a way to reach fundamental understanding on topics such as the active site geometry.

Similarly, we also believe colloidal synthesis techniques may be promising to clearly deconvolute effects of redox site separation from size, shape or compositional effects in photocatalytic applications. For example, engineering the mesoscale organization of photocatalytic building blocks (photoabsorbers and co-catalysts) can increase diffusion lengths between reactive intermediates, thereby preventing back-reactions and thus increasing the photocatalytic activity [241–243]. However, hierarchical mesoscale organization of photocatalytic building blocks is a still novel and emerging research direction and such hierarchical organization has not yet been employed with nanocrystals of well controlled sizes and shapes.

A great deal of research is also focusing on the design of tandem catalysts by following two main strategies: (i) encapsulate or deposit different types of metal nanoparticles into, and therefore separated by, the same inert support. In general terms, the totality of the previously described embedding techniques can be applied to reach this goal. (ii) Use encapsulating supports that possess intrinsic catalytic activity. Attractive avenues that are explored in order to address this challenge are microporous solids such as

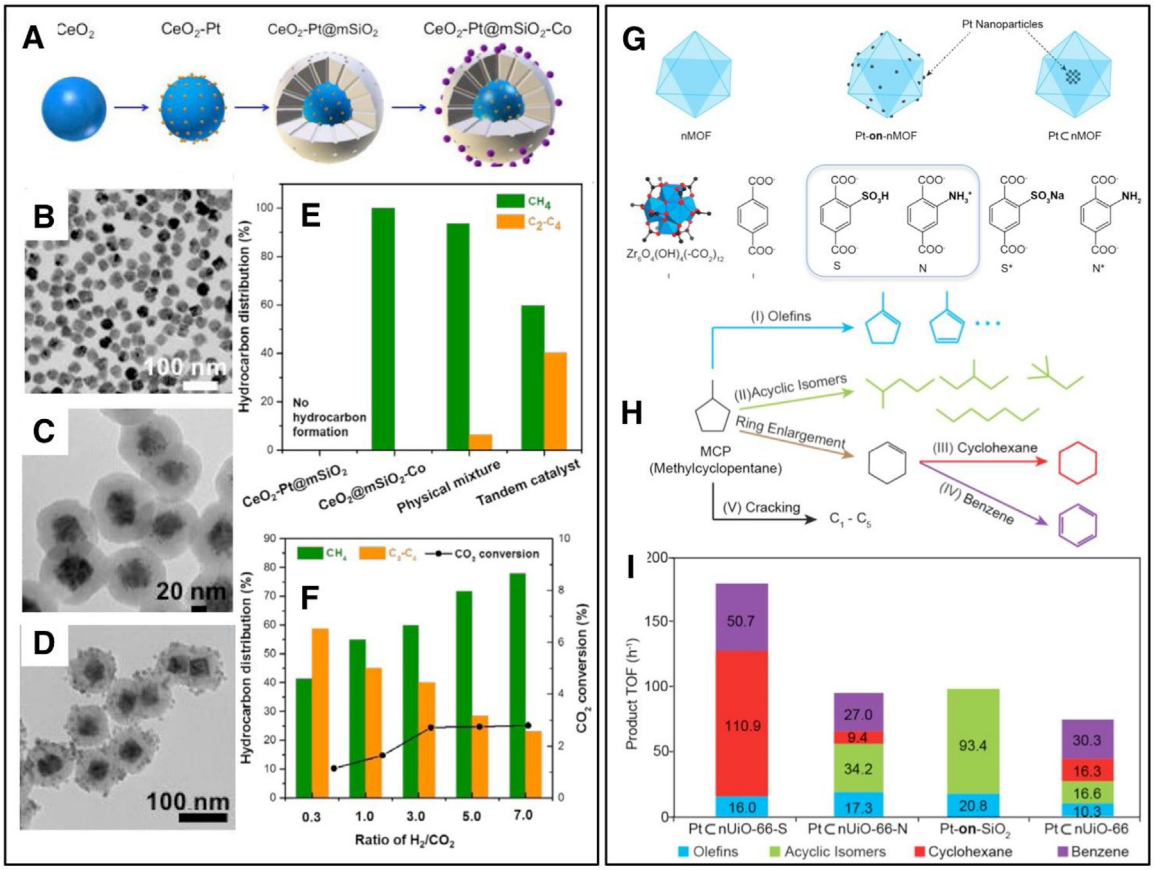

Fig. 20. (A) Schematic representation of the design of a multilayered CeO_2-Pt@$mSiO_2$-CoO_x catalyst for tandem catalysis. (B–D) TEM micrographs of the correspondingly sequentially synthesized materials. (E) Multilayer catalyst compared to the respective components and a physical mixture of the latter. A higher share of C—C coupling products can be observed for the multilayer catalyst. Adapted with permission from Ref. [236] Copyright (2017) American Chemical Society, and (G–I) Figures represent the efforts undertaken to control the intrinsic activity of functionalized MOF, UIO-66 that encapsulates Pt-nanoparticles. Their performance was evaluated by applying them in a reaction network of methylcyclopentene (MCP) isomerization, where product distributions differed as a function of the composites. It is concluded that acidic MOF favors the reaction pathway of first a MCP-ring expansion and then its hydrogenation to cyclohexane. Adapted with permission from Ref [236]. Copyright (2015) American Chemical Society.

zeolites metal organic frameworks (MOFs) and covalent organic frameworks (COFs).

A representative example for the first strategy has been reported by Xie et al., who designed a multilayered catalyst with a Pt/CeO_2 core enveloped by a CoO_x/SiO_2 shell [236]. This hybrid catalyst was studied in the reduction of CO_2. The cascade reaction was envisaged as first the reverse water gas shift reaction occurring at the core of the catalyst particles, followed by Fischer Tropsch (FT) type hydrocarbons production at the CoO_x/SiO_2-shell. Most notably, this specific layered design significantly outperformed a physical mixture of the same materials in terms of selectivity towards hydrocarbons. The improved selectivity was tentatively explained by locally higher CO partial pressures, as produced CO has to stream past CoO_x particles in this specific tandem catalyst. A comparable strategy was employed by Li et al. who designed a "yolk-satellite-shell" structured Ni-yolk@Ni@SiO_2 nanocomposite for the dry reforming of CO_2 with methane (DRM) [244,245]. Their investigation focussed on varying the shell thickness of Ni@SiO_2 core shell nanoparticles. They were able to evidence that compared with Ni@SiO_2, their composite Ni-yolk@Ni@SiO_2 with an 11.2 nm silica shell thickness was stable quasi-equilibrium conversion for CH_4 and CO_2 for 90 h at 800 °C with negligible carbon deposition, which is a limitation for the DRM-reaction.

Another example for the first strategy used MOF-chemistry to influence catalytic activity by embedding colloidal nanoparticles within structured supports, and varying both steric and electronic effects. Precise control of pore size and overlayer thickness of a MOF framework allowed Lu et. al. to determine that a coating layer of MOF has imparted steric selectivity in alkene hydrogenation over platinum nanoparticles due to steric hindrance of binding of larger molecules [138]. The authors synthesized a Pt@ZIF-8 composite that exhibits substrate shape selectivity, where hex-1-ene was hydrogenated, while bulkier cyclooctene was not. Furthermore, this system permitted regioselective conversion of only primary alkenes over trans secondary olefins. On the other hand, altering the electronic structure of the catalytic interface with the embedding support can also influence selectivity. The versatile functionality within organic frameworks has also proven to impact selectivity during catalysis. For instance, Zhao et al developed a MIL-101@Pt@MIL-101 hybrid catalyst for which the interaction of the substrate with the framework metal ions and the interface of platinum nanoparticles imparted higher selectivity of C=O bond hydrogenation over the more thermodynamically favorable C=C bond in alpha-beta unsaturated aldehydes [246].

The second strategy, intrinsically active supports to encapsulate active nanoparticles is elegantly used by Kruse et al. who used a sequential transformation of initially embedded CoO_x@SiO_2 composites to CoO_x-particles embedded in ZSM-5 zeolite [123]. This composite material was proven to be active in the tandem Fischer Tropsch (FT) and hydroprocessing (HP) reaction, evidenced by a shift from waxy (long chain alkanes > C_{15}) to liquid products (shorter alkanes) as it is depicted in the Anderson-Schulz-Flory

(ASF) plot. Adapting chemical functionality to tandem catalysis is also possible given the many reported porous organic frameworks materials. In these systems, the combination of organic functional groups and inorganic components provides additional knobs for tuning the catalyst performance. A landmark study following these hypotheses has been published by Choi et al. [247] The authors were able to prepare colloids of Pt nanoparticles incorporated into MOFs with tailorable chemistry where the MOF chemistry consequently changed the product distribution of methylcyclopentane (MCP) isomerization. As shown in Fig. 20G–I, MCP isomerization consists of a reaction network that can lead to a variety of products. For the Brønsted acid containing MOF it appears that the Pt-nanoparticle catalyzed hydrogenation occurs only after an acid catalyzed ring expansion leading to a high selectivity toward cyclohexane and proving the cascade type reactivity. A concept that is currently being explored is substrate channeling, in other words controlling molecular transport using pores for catalysis as a biomimetic approach towards cascade reactions [248]. Indeed, similarities between tailored porous multifunctional catalysts and enzymes are emerging.

Conclusions and outlook

In this review, we highlighted how colloidal synthesis can be used to prepare, understand, and design new and improved heterogeneous catalysts. An advantage of this approach is its versatility: colloidal catalysts can be used to explore a variety of reaction systems within heterogeneous catalysis including gas-phase catalysis, electrochemical reactions and photochemical processes. The complex interplay between particle size and shape (sites with different coordination numbers/geometries can lead to different reactivity), and their composition (multimetallic particles are tuned in various ways to obtain for instance core-shell, alloyed or single atom alloy particles, influencing thereby their electronic properties), has been shown to be crucial in optimizing and discovering new catalysts. An additional advantage is the potential of uniform colloidal catalysts to be used as model systems. Already such systems have allowed for increased understanding of a large number of heterogeneously catalyzed reactions.

However, certain current limitations, which motivate future work in the field, need to be considered. While nanostructured catalysts do not pose much of a specific health concern during operation, nanoparticle toxicity is an increasingly debated topic. The catalyst manufacturer exposes scientists and factory workers during the loading of large scale reactors to free airborne particles, of whose toxicological effect is poorly documented. Furthermore, at the end of their use these materials are deactivated and therefore need to be reactivated, disposed of or recycled. In these cases, humans could potentially come in contact with nanoparticles. The toxicity issue has already been addressed mainly by an increasing number of detailed studies on the multitude of emerging new materials [249–251]. However a few more aspects need to be considered. Even though many more such studies are on their way, long term exposure effects cannot yet be estimated and it is simply impossible to perform clinical toxicological trials with the plethora of different emerging nanoparticle sizes, shapes and compositions, all of which may have very different health effects. The quickly developing fields of "big data, artificial intelligence and machine learning" might be potential avenues for dealing with this issue if some of the properties can be predicted in-silico through accumulated data.

Another current limitation, and probably the biggest, for the large scale application of colloidal nanoparticles in industrial catalysis is the scale at which they are currently produced. Scale up for nanoparticle synthesis is limited by the necessity for precise control over synthesis conditions. To give a hypothetical example: considering a large scale batch reactor with mechanical stirring, the temperature might not be increased fast enough to guarantee the same control over particle nucleation and growth; hot injection may not be performed quickly enough; turbulences in the stirred tank reactor might lead to local concentration gradients, and more. Furthermore, purification is also problematic as centrifugation at large scale is extremely costly, and therefore better methods for purifying colloidal nanocrystals with lower cost must be developed [252], for example by electropurification [253]. Various interesting attempts have been made over the last 10 years to overcome the cost limitation and to eventually allow large-scale production of catalytically active colloidal materials.

Various methods for continuously synthesizing colloidal nanoparticles have been reported, such as the use of systems where the synthesis occurs in micelles within oil carrier phases [254,255]. Another interesting approach is the move towards nanoparticle bio-factories. As T.J. Park et al. state in their study, "Microbes can be employed as a factory for metal-NP synthesis!" [255,256] Scale-up trials are being undertaken, bioreactors with volumes of up to 50 L were producing up to 120 g of bio-magnetite (ø = 10–15 nm) [257].

In summary, a glimpse at the standards used nowadays in colloidal catalyst synthesis and utilization was given. This work tried to decipher and expose the untackled challenges in the still young, yet promising field of using colloidal nanocrystals in heterogeneous catalysis. Finally, current research in the design of heterogeneous catalysts with colloidal nanocrystals is at the verge of creating a toolbox of nearly infinite possible combinations of support properties such as vast number of supplementary functionalities, or pore sizes, as well as the incredible numbers of possible metal nanoparticle sizes, shapes and compositions. As the number of different metal nanoparticles used with different supports can also be, in principle, adapted at will, it appears that the number of possible catalysts, resulting from the herein presented building block approach, must be truly gargantuan.

Acknowledgements

We acknowledge the kind support of several agencies and foundations that allow us to pursue our efforts in the area of colloidal catalysts: the U.S. Department of Energy, Chemical Sciences, Geosciences, and Biosciences (CSGB) Division of the Office of Basic Energy Sciences, via Grant DE-AC02-76SF00515 to the SUNCAT Center for Interface Science and Catalysis; NYSEARCH/Northeast Gas Association; the Natural Gas Initiative at Stanford University; the TomKat Center for Sustainable Energy at Stanford University; the Villum Foundation to the Villum Center for the Science of Sustainable Fuels and Chemicals; the Alfred P. Sloan Foundation; the Hellman Foundation; and the Packard Foundation. Furthermore, P. L. acknowledges support from the Fulbright Scholar Program. E. G. and A. R. R. thank the support of the National Science Foundation through Graduate Research Fellowships; M. C. acknowledges the support from the School of Engineering at Stanford University and a Terman Faculty Fellowship.

References

[1] A.T. Bell, Science 299 (2003) 1688–1691.
[2] P. Munnik, P.E. de Jongh, K.P. de Jong, Chem. Rev. 115 (2015) 6687–6718.
[3] K. Na, Q. Zhang, G.A. Somorjai, J. Clust. Sci. 25 (2014) 83–114.
[4] S. Cao, F.(Feng) Tao, Y. Tang, Y. Li, J. Yu, Chem. Soc. Rev. 45 (2016) 4747–4765.
[5] B. Wu, N. Zheng, Nano Today 8 (2013) 168–197.
[6] B. Roldan Cuenya, F. Behafarid, Surf. Sci. Rep. 70 (2015) 135–187.
[7] R. Jin, C. Zeng, M. Zhou, Y. Chen, Chem. Rev. 116 (2016) 10346–10413.
[8] C.-J. Jia, F. Schüth, Phys. Chem. Chem. Phys. 13 (2011) 2457.
[9] C.J. Murphy, J.M. Buriak, Chem. Mater. 27 (2015) 4911–4913.
[10] H. Bönnemann, W. Brijoux, R. Brinkmann, T. Joußen, B. Korall, E. Dinjus, Angew. Chemie Int. Ed. 30 (1991) 1312–1314.

[11] P.T. Witte, P.H. Berben, S. Boland, E.H. Boymans, D. Vogt, J.W. Geus, J.G. Donkervoort, Top. Catal. 55 (2012) 505–511.
[12] J. Gu, Y.-W. Zhang, F.(Feng) Tao, Chem. Soc. Rev. 41 (2012) 8050.
[13] K. Zhou, Y. Li, Angew. Chemie Int. Ed. 51 (2012) 602–613.
[14] H. Yoshida, Y. Kuwauchi, J.R. Jinschek, K. Sun, S. Tanaka, M. Kohyama, S. Shimada, M. Haruta, S. Takeda, Science 335 (2012) 317–319.
[15] M. Cargnello, P. Fornasiero, R.J. Gorte, ChemPhysChem 14 (2013) 3869–3877.
[16] Brian L. Cushing, Vladimir L. Kolesnichenko, C.J. O'Connor, Chem. Rev. 104 (2004) 3893–3946.
[17] C.B. Murray, D.J. Norris, M.G. Bawendi, J. Am. Chem. Soc. 115 (1993) 8706–8715.
[18] S. Sun, C.B. Murray, J. Appl. Phys. 85 (1999) 4325.
[19] J. van Embden, A.S.R. Chesman, J.J. Jasieniak, Chem. Mater. 27 (2015) 2246–2285.
[20] J. Jones, H. Xiong, A.T. DeLaRiva, E.J. Peterson, H. Pham, S.R. Challa, G. Qi, S. Oh, M.H. Wiebenga, X.I. Pereira Hernández, Y. Wang, A.K. Datye, Science 353 (2016) 150–154.
[21] R. Lanza, S.G. Järås, P. Canu, Appl. Catal. A Gen. 325 (2007) 57–67.
[22] M. Faraday, Philos. Trans. R. Soc. London 147 (1857) 145–181.
[23] J. Turkevich, P.C. Stevenson, J. Hillier, Discuss. Faraday Soc. 11 (1951) 55.
[24] J. Turkevich, G. Kim, Science 169 (1970), 873–839.
[25] X. Ji, X. Song, J. Li, Y. Bai, W. Yang, X. Peng, J. Am. Chem. Soc. 129 (2007) 13939–13948.
[26] J. Piella, N.G. Bastús, V. Puntes, Chem. Mater. 28 (2016) 1066–1075.
[27] N.G. Bastu's, J. Comenge, V. Puntes, Langmuir 27 (2011) 11098–11105.
[28] N.G. Bastús, F. Merkoçi, J. Piella, V. Puntes, Chem. Mater. 26 (2014) 2836–2846.
[29] C.B. Murray, S. Sun, H. Doyle, T. Betley, MRS Bull. 26 (2001) 985–991.
[30] J.V.I. Timonen, E.T. Seppälä, O. Ikkala, R.H.A. Ras, Angew. Chemie Int. Ed. 50 (2011) 2080–2084.
[31] D. Ito, S. Yokoyama, T. Zaikova, K. Masuko, J.E. Hutchison, ACS Nano 8 (2014) 64–75.
[32] S. Sun, C.B. Murray, D. Weller, L. Folks, A. Moser, Science 287 (2000) 1989–1992.
[33] J. Park, K. An, Y. Hwang, J.-G. Park, H.-J. Noh, J.-Y. Kim, J.-H. Park, N.-M. Hwang, T. Hyeon, Nat. Mater. 3 (2004) 891–895.
[34] M. Cargnello, V.V.T. Doan-Nguyen, C.B. Murray, AIChE J. 62 (2016) 392–398.
[35] L. Wu, H. Lian, J.J. Willis, E.D. Goodman, I.S. McKay, J. Qin, C.J. Tassone, M. Cargnello, Chem. Mater. 30 (2018) 1127–1135.
[36] J.J. Willis, A. Gallo, D. Sokaras, H. Aljama, S.H. Nowak, E.D. Goodman, L. Wu, C.J. Tassone, T.F. Jaramillo, F. Abild-Pedersen, M. Cargnello, ACS Catal. 7 (2017) 7810–7821.
[37] M. Antonietti, E. Wenz, L. Bronstein, M. Seregina, Adv. Mater. 7 (1995) 1000–1005.
[38] A.K. Ganguli, A. Ganguly, S. Vaidya, Chem. Soc. Rev. 39 (2010) 474–485.
[39] M. Boutonnet, M. Sanchez-Dominguez, Catal. Today 285 (2017) 89–103.
[40] M. Boutonnet, J. Kizling, P. Stenius, G. Maire, Colloids Surf. 5 (1982) 209–225.
[41] J.P. Spatz, S. Mössmer, C. Hartmann, M. Möller, T. Herzog, M. Krieger, H. Boyen, P. Ziemann, B. Kabius, Langmuir 16 (1999) 407–415.
[42] B.R. Cuenya, S.-H. Baeck, T.F. Jaramillo, E.W. McFarland, B. Roldan Cuenya, Sung-Hyeon Baeck, A.Thomas F. Jaramillo, E.W. McFarland, J. Am. Chem. Soc. 125 (2003) 12928–12934.
[43] G. Prieto, A. Martínez, P. Concepción, R. Moreno-Tost, J. Catal. 266 (2009) 129–144.
[44] A. Martínez, G. Prieto, Catal. Commun. 8 (2007) 1479–1486.
[45] M.A. Michaels, S. Sherwood, M. Kidwell, M.J. Allsbrook, S.A. Morrison, S.C. Rutan, E.E. Carpenter, J. Colloid Interface Sci. 311 (2007) 70–76.
[46] K. Na, C. Jo, J. Kim, K. Cho, J. Jung, Y. Seo, R.J. Messinger, B.F. Chmelka, R. Ryoo, Science 333 (2011) 328–332.
[47] J. Kim, W. Park, R. Ryoo, ACS Catal. 1 (2011) 337–341.
[48] K. Na, M. Choi, W. Park, Y. Sakamoto, O. Terasaki, R. Ryoo, J. Am. Chem. Soc. 132 (2010) 4169–4177.
[49] M. Castro, P. Losch, W. Park, M. Haouas, F. Taulelle, C. Loerbroks, G. Brabants, E. Breynaert, C.E.A. Kirschhock, R. Ryoo, W. Schmidt, Chem. Mater. 30 (2018) 2676–2686.
[50] B.J. Smith, L.R. Parent, A.C. Overholts, P.A. Beaucage, R.P. Bisbey, A.D. Chavez, N. Hwang, C. Park, A.M. Evans, N.C. Gianneschi, W.R. Dichtel, ACS Cent. Sci. 3 (2017) 58–65.
[51] M. Sindoro, N. Yanai, A.-Y. Jee, S. Granick, Acc. Chem. Res. 47 (2014) 459–469.
[52] N.V. Krstajić, V.D. Jović, L. Gajić-Krstajić, B.M. Jović, A.L. Antozzi, G.N. Martelli, Int. J. Hydrogen Energy 33 (2008) 3676–3687.
[53] J.R. McKone, E.L. Warren, M.J. Bierman, S.W. Boettcher, B.S. Brunschwig, N.S. Lewis, H.B. Gray, Energy Environ. Sci. 4 (2011) 3573.
[54] D.K. Oppedisano, L.A. Jones, T. Junk, S.K. Bhargava,J. Electrochem. Soc. 161 (2014), D489–D494.
[55] M.T. Reetz, W. Helbig, J. Am. Chem. Soc. 116 (1994) 7401–7402.
[56] M.T. Reetz, S.A. Quaiser, Angew. Chemie Int. Ed. 34 (1995) 2240–2241.
[57] L. Durán Pachón, M.B. Thathagar, F. Hartl, G. Rothenberg, Phys. Chem. Chem. Phys. 8 (2006) 151–157.
[58] M.T. Reetz, W. Helbig, S.A. Quaiser, Chem. Mater. 7 (1995) 2227–2228.
[59] E.M. Abdelkader, P.A. Jelliss, S.W. Buckner, Inorg. Chem. 54 (2015) 5897–5906.
[60] H.G. Yang, C.H. Sun, S.Z. Qiao, J. Zou, G. Liu, S.C. Smith, H.M. Cheng, G.Q. Lu, Nature. 453 (2008) 638–641.
[61] T.R. Gordon, M. Cargnello, T. Paik, F. Mangolini, R.T. Weber, P. Fornasiero, C.B. Murray, J. Am. Chem. Soc. 134 (2012) 6751–6761.
[62] G. Ertl, Angew. Chemie Int. Ed. 47 (2008) 3524–3535.
[63] G.A. Somorjai, R.L. York, D. Butcher, J.Y. Park, Phys. Chem. Chem. Phys. 9 (2007) 3500–3513.
[64] G.A. Somorjai, H. Frei, J.Y. Park, J. Am. Chem. Soc. 131 (2009) 16589–16605.
[65] Y. Xiong, Y. Xia, Adv. Mater. 19 (2007) 3385–3391.
[66] X. Huang, Y. Li, Y. Li, H. Zhou, X. Duan, Y. Huang, Nano Lett. 12 (2012) 4265–4270.
[67] H. Zhang, M. Jin, Y. Xiong, B. Lim, Y. Xia, Acc. Chem. Res. 46 (2013) 1783–1794.
[68] Y. Kang, X. Ye, C.B. Murray, Angew. Chemie Int. Ed. 49 (2010) 6156–6159.
[69] Y. Kang, C.B. Murray, J. Am. Chem. Soc. 132 (2010) 7568–7569.
[70] Y. Xia, Y. Xiong, B. Lim, S.E. Skrabalak, Angew. Chemie Int. Ed. 48 (2009) 60–103.
[71] H.-X. Mai, L.-D. Sun, Y.-W. Zhang, R. Si, W. Feng, H.-P. Zhang, H.-C. Liu, C.-H. Yan, J. Phys. Chem. B 109 (2005).
[72] N.R. Jana, L. Gearheart, C.J. Murphy, J. Phys. Chem. B 105 (2001) 4065–4067.
[73] R. Buonsanti, V. Grillo, E. Carlino, C. Giannini, T. Kipp, R. Cingolani, P.D. Cozzoli, J. Am. Chem. Soc. 130 (2008) 11223–11233.
[74] M. Cargnello, T. Montini, S.Y. Smolin, J.B. Priebe, J.J. Delgado Jaén, V.V.T. Doan-Nguyen, I.S. McKay, J.A. Schwalbe, M.-M. Pohl, T.R. Gordon, Y. Lu, J.B. Baxter, A. Brückner, P. Fornasiero, C.B. Murray, Proc. Natl. Acad. Sci. 113 (2016), 3966–3671.
[75] T.K. Sau, C.J. Murphy, J. Am. Chem. Soc. 126 (2004) 8648–8649.
[76] T. Lv, X. Yang, Y. Zheng, H. Huang, L. Zhang, J. Tao, L. Pan, Y. Xia, J. Phys. Chem. C. 120 (2016) 20768–20774.
[77] L. Carbone, P.D. Cozzoli, Nano Today 5 (2010) 449–493.
[78] C.-L. Lu, K.S. Prasad, H.-L. Wu, J.A. Ho, M.H. Huang, J. Am. Chem. Soc. 132 (2010) 14546–14553.
[79] Y. Xia, X. Xia, H.-C. Peng, J. Am. Chem. Soc. 137 (2015) 7947–7966.
[80] R. Jin, Y. Cao, C.A. Mirkin, K.L. Kelly, G.C. Schatz, J.G. Zheng, Science 294 (2001) 1901–1903.
[81] R. Jin, Y. Charles Cao, E. Hao, G.S. Métraux, G.C. Schatz, C.A. Mirkin, Nature. 425 (2003) 487–490.
[82] A. Callegari, D. Tonti, M. Chergui, Nano Lett. 3 (2003) 1565–1568.
[83] P. Sutter, Y. Li, C. Argyropoulos, E. Sutter, J. Am. Chem. Soc. 139 (2017) 6771–6776.
[84] J. Zhang, M.R. Langille, C.A. Mirkin, J. Am. Chem. Soc. 132 (2010) 12502–12510.
[85] J. Zhang, S. Li, J. Wu, G.C. Schatz, C.A. Mirkin, Angew. Chemie Int. Ed. 48 (2009) 7787–7791.
[86] J. Zhang, M.R. Langille, C.A. Mirkin, Nano Lett. 11 (2011) 2495–2498.
[87] Y. Zhai, J.S. DuChene, Y.-C. Wang, J. Qiu, A.C. Johnston-Peck, B. You, W. Guo, B. DiCiaccio, K. Qian, E.W. Zhao, F. Ooi, D. Hu, D. Su, E.A. Stach, Z. Zhu, W.D. Wei, Nat. Mater. 15 (2016) 889–895.
[88] S. Schultz, D.R. Smith, J.J. Mock, D.A. Schultz, Proc. Natl. Acad. Sci. 97 (2000) 996–1001.
[89] Y. Yin, R.M. Rioux, C.K. Erdonmez, S. Hughes, G.A. Somorjai, A.P. Alivisatos, Science 304 (2004) 711–714.
[90] C. Chen, Y. Kang, Z. Huo, Z. Zhu, W. Huang, H.L. Xin, J.D. Snyder, D. Li, J.A. Herron, M. Mavrikakis, M. Chi, K.L. More, Y. Li, N.M. Markovic, G.A. Somorjai, P. Yang, V.R. Stamenkovic, Science 343 (2014) 1339–1343.
[91] Z. Niu, N. Becknell, Y. Yu, D. Kim, C. Chen, N. Kornienko, G.A. Somorjai, P. Yang, Nat. Mater. 15 (2016) 1188–1194.
[92] H. Zhu, A. Sigdel, S. Zhang, D. Su, Z. Xi, Q. Li, S. Sun, Angew. Chem. 126 (2014) 12716–12720.
[93] S. Zhou, H. Yin, V. Schwartz, Z. Wu, D. Mullins, B. Eichhorn, S.H. Overbury, S. Dai, ChemPhysChem 9 (2008) 2475–2479.
[94] K.-W. Jeon, D.-G. Lee, Y.K. Kim, K. Baek, K. Kim, T. Jin, J.H. Shim, J.Y. Park, I.S. Lee, Chem. Mater. 29 (2017) 1788–1795.
[95] N.E. Motl, J.F. Bondi, R.E. Schaak, Chem. Mater. 24 (2012) 1552–1554.
[96] Y. Wang, D. Wan, S. Xie, X. Xia, C.Z. Huang, Y. Xia, ACS Nano 7 (2013) 4586–4594.
[97] R. Ferrando, J. Jellinek, R.L. Johnston, Chem. Rev. 108 (2008) 845–910.
[98] D. Wang, Y. Li, Adv. Mater. 23 (2011) 1044–1060.
[99] S. Sun, H. Zeng, D.B. Robinson, S. Raoux, P.M. Rice, S.X. Wang, G. Li, J. Am. Chem. Soc. 126 (2004) 273–279.
[100] J.J. Willis, E.D. Goodman, L. Wu, A.R. Riscoe, P. Martins, C.J. Tassone, M. Cargnello, J. Am. Chem. Soc. 139 (2017) 11989–11997.
[101] E.D. Goodman, S. Dai, A.-C. Yang, C.J. Wrasman, A. Gallo, S.R. Bare, A.S. Hoffman, T.F. Jaramillo, G.W. Graham, X. Pan, M. Cargnello, ACS Catal. 7 (2017) 4372–4380.
[102] W. Chen, R. Yu, L. Li, A. Wang, Q. Peng, Y. Li, Angew. Chemie Int. Ed. 49 (2010) 2917–2921.
[103] P. Guardia, K. Korobchevskaya, A. Casu, A. Genovese, L. Manna, A. Comin, ACS Nano 7 (2013) 1045–1053.
[104] M.S. Shore, J. Wang, A.C. Johnston-Peck, A.L. Oldenburg, J.B. Tracy, Small 7 (2011) 230–234.
[105] M. Cargnello, R. Agarwal, D.R. Klein, B.T. Diroll, R. Agarwal, C.B. Murray, Chem. Mater. 27 (2015) 5833–5838.
[106] T. Shibata, B.A. Bunker, Z. Zhang, D. Meisel, C.F. Vardeman II, J.D. Gezelter, J. Am. Chem. Soc. 124 (2002) 11989–11996.
[107] F. Tao, M.E. Grass, Y. Zhang, D.R. Butcher, J.R. Renzas, Z. Liu, J.Y. Chung, B.S. Mun, M. Salmeron, G.A. Somorjai, Science 322 (2008) 932–934.
[108] G. Kyriakou, M.B. Boucher, A.D. Jewell, E.A. Lewis, T.J. Lawton, A.E. Baber, H.L. Tierney, M. Flytzani-Stephanopoulos, E.C.H. Sykes, Science 335 (2012) 1209–1212.

[109] Y. Yu, Q. Zhang, Q. Yao, J. Xie, J.Y. Lee, Chem. Mater. 25 (2013) 4746–4756.
[110] A.G.M. da Silva, T.S. Rodrigues, S.J. Haigh, P.H.C. Camargo, Chem. Commun. 53 (2017) 7135–7148.
[111] M.H. Oh, T. Yu, S.-H. Yu, B. Lim, K.-T. Ko, M.-G. Willinger, D.-H. Seo, B.H. Kim, M.G. Cho, J.-H. Park, K. Kang, Y.-E. Sung, N. Pinna, T. Hyeon, G.A. Somorjai, P. Yang, V.R. Stamenkovic, Science 340 (2013) 964–968.
[112] X. Xia, Y. Wang, A. Ruditskiy, Y. Xia, Adv. Mater. 25 (2013) 6313–6333.
[113] M.B. Boucher, B. Zugic, G. Cladaras, J. Kammert, M.D. Marcinkowski, T.J. Lawton, E.C.H. Sykes, M. Flytzani-Stephanopoulos, Phys. Chem. Chem. Phys. 15 (2013) 12187.
[114] A. Fukuoka, H. Araki, Y. Sakamoto, N. Sugimoto, H. Tsukada, Y. Kumai, Y. Akimoto, M. Ichikawa, Nano Lett. 2 (2002) 793–795.
[115] S.T. Hunt, M. Milina, A.C. Alba-Rubio, C.H. Hendon, J.A. Dumesic, Y. Román-Leshkov, Science 352 (2016) 974–978.
[116] S.T. Hunt, Y. Román-Leshkov, Acc. Chem. Res. 51 (2018) 1054–1062.
[117] R.V. Maligal-Ganesh, C. Xiao, T.W. Goh, L.-L. Wang, J. Gustafson, Y. Pei, Z. Qi, D.D. Johnson, S. Zhang, F.(Feng) Tao, W. Huang, ACS Catal. 6 (2016) 1754–1763.
[118] W. Stöber, A. Fink, E. Bohn, J. Colloid Interface Sci. 26 (1968) 62–69.
[119] L.M. Liz-Marzán, A.P. Philipse, J. Colloid Interface Sci. 176 (1995) 459–466.
[120] L.M. Liz-Marzán, M. Giersig, P. Mulvaney, Langmuir 12 (1996) 4329–4335.
[121] DOE, https://www.energy.gov/Sites/Prod/Files/2014/02/F8/Fctt_roadmap_june2013.pdf. (2013).
[122] P.M. Arnal, M. Comotti, F. Schüth, Angew. Chemie Int. Ed. 45 (2006) 8224–8227.
[123] N. Kruse, A.G. Machoke, W. Schwieger, R. Güttel, ChemCatChem 7 (2015) 1018–1022.
[124] G. Budroni, A. Corma, Angew. Chemie Int. Ed. 45 (2006) 3328–3331.
[125] G. Budroni, A. Corma, H. García, A. Primo, J. Catal. 251 (2007) 345–353.
[126] S.H. Joo, J.Y. Park, C.-K. Tsung, Y. Yamada, P. Yang, G.A. Somorjai, Nat. Mater. 8 (2009) 126–131.
[127] L. De Rogatis, M. Cargnello, V. Gombac, B. Lorenzut, T. Montini, P. Fornasiero, ChemSusChem 3 (2010) 24–42.
[128] C.M.Y. Yeung, K.M.K. Yu, Q.J. Fu, D. Thompsett, M.I. Petch, S.C. Tsang, J. Am. Chem. Soc. 127 (2005) 18010–18011.
[129] M. Cargnello, T. Montini, S. Polizzi, N.L. Wieder, R.J. Gorte, M. Graziani, P. Fornasiero, Dalton Trans. 39 (2010) 2122–2127.
[130] M. Cargnello, N.L. Wieder, T. Montini, R.J. Gorte, P. Fornasiero, J. Am. Chem. Soc. 132 (2010) 1402–1409.
[131] A.H. Habibi, R.E. Hayes, N. Semagina, Catal. Sci. Technol. 8 (2018) 798–805.
[132] W.M.H. Sachtler, Catal. Today 15 (1992) 419–429.
[133] A.B. Laursen, K.T. Højholt, L.F. Lundegaard, S.B. Simonsen, S. Helveg, F. Schüth, M. Paul, J.-D. Grunwaldt, S. Kegnaes, C.H. Christensen, K. Egeblad, Angew. Chemie. 122 (2010) 3582–3585.
[134] R.M. Rioux, H. Song, J.D. Hoefelmeyer, P. Yang, G.A. Somorjai, J. Phys. Chem. B 109 (2004) 2192–2202.
[135] K. An, S. Alayoglu, N. Musselwhite, S. Plamthottam, G. Melaet, A.E. Lindeman, G.A. Somorjai, J. Am. Chem. Soc. 135 (2013) 16689–16696.
[136] Z. Kónya, V.F. Puntes, I. Kiricsi, Ji Zhu, A.A. Paul Alivisatos, G.A. Somorjai, Nano Lett. 2 (2002) 907–910.
[137] T. Wang, P. Zhang, Y. Sun, B. Liu, Y. Liu, Z.-A. Qiao, Q. Huo, S. Dai, Chem. Mater. 29 (2017) 4044–4051.
[138] G. Lu, S. Li, Z. Guo, O.K. Farha, B.G. Hauser, X. Qi, Y. Wang, X. Wang, S. Han, X. Liu, J.S. DuChene, H. Zhang, Q. Zhang, X. Chen, J. Ma, S.C.J. Loo, W.D. Wei, Y. Yang, J.T. Hupp, F. Huo, Nat. Chem. 4 (2012) 310–316.
[139] Y. Jiao, D. Han, Y. Ding, X. Zhang, G. Guo, J. Hu, D. Yang, A. Dong, Nat. Commun. 6 (2015) 6420.
[140] I. Imaz, J. Hernando, D. Ruiz-Molina, D. Maspoch, Angew. Chem. Int. Ed. 48 (2009) 2325–2329.
[141] D. Rodríguez-San-Miguel, A. Yazdi, V. Guillerm, J. Pérez-Carvajal, V. Puntes, D. Maspoch, F. Zamora, Chem. - A Eur. J. 23 (2017) 8623–8627.
[142] J. Tan, S. Namuangruk, W. Kong, N. Kungwan, J. Guo, C. Wang, Angew. Chem. Int. Ed. 55 (2016) 13979–13984.
[143] Q. Yang, W. Liu, B. Wang, W. Zhang, X. Zeng, C. Zhang, Y. Qin, X. Sun, T. Wu, J. Liu, F. Huo, J. Lu, Nat. Commun. 8 (2017) 14429.
[144] J. Reboul, S. Furukawa, N. Horike, M. Tsotsalas, K. Hirai, H. Uehara, M. Kondo, N. Louvain, O. Sakata, S. Kitagawa, Nat. Mater. 11 (2012) 717–723.
[145] S.T. Marshall, M. O'Brien, B. Oetter, A. Corpuz, R.M. Richards, D.K. Schwartz, J.W. Medlin, Nat. Mater. 9 (2010) 853–858.
[146] Z. Niu, Y. Li, Chem. Mater. 26 (2014) 72–83.
[147] B. Donoeva, P.E. de Jongh, ChemCatChem 10 (2018) 989–997.
[148] M. Casavola, J. Hermannsdörfer, N. de Jonge, A.I. Dugulan, K.P. de Jong, Adv. Funct. Mater. 25 (2015) 5309–5319.
[149] T.W. van Deelen, H. Su, N.A.J.M. Sommerdijk, K.P. de Jong, Chem. Commun. 54 (2018) 2530–2533.
[150] Y. Borodko, S.E. Habas, M. Koebel, P. Yang, H. Frei, G.A. Somorjai, J. Phys. Chem. B 110 (2006) 23052–23059.
[151] M. Cargnello, C. Chen, B.T. Diroll, V.V.T. Doan-Nguyen, R.J. Gorte, C.B. Murray, J. Am. Chem. Soc. 137 (2015) 6906–6911.
[152] W. Huang, Q. Hua, T. Cao, Catal. Lett. 144 (2014) 1355–1369.
[153] A. Miyazaki, I. Balint, K. Aika, Y. Nakano, J. Catal. 204 (2001) 364–371.
[154] J.A. Lopez-Sanchez, N. Dimitratos, C. Hammond, G.L. Brett, L. Kesavan, S. White, P. Miedziak, R. Tiruvalam, R.L. Jenkins, A.F. Carley, D. Knight, C.J. Kiely, G.J. Hutchings, Nat. Chem. 3 (2011) 551–556.
[155] C. Aliaga, J.Y. Park, Y. Yamada, H.S. Lee, C.-K. Tsung, P. Yang, G.A. Somorjai, J. Phys. Chem. C 113 (2009) 6150–6155.
[156] J.M. Krier, W.D. Michalak, L.R. Baker, K. An, K. Komvopoulos, G.A. Somorjai, J. Phys. Chem. C 116 (2012) 17540–17546.
[157] M. Crespo-Quesada, J.-M. Andanson, A. Yarulin, B. Lim, Y. Xia, L. Kiwi-Minsker, Langmuir 27 (2011) 7909–7916.
[158] D. Li, C. Wang, D. Tripkovic, S. Sun, N.M. Markovic, V.R. Stamenkovic, ACS Catal. 2 (2012) 1358–1362.
[159] P. Mohapatra, S. Shaw, D. Mendivelso-Perez, J.M. Bobbitt, T.F. Silva, F. Naab, B. Yuan, X. Tian, E.A. Smith, L. Cademartiri, Nat. Commun. 8 (2017) 2038.
[160] D.R. Baer, D.J. Gaspar, P. Nachimuthu, S.D. Techane, D.G. Castner, Anal. Bioanal. Chem. 396 (2010) 983–1002.
[161] K.H. Kim, J.G. Kim, S. Nozawa, T. Sato, K.Y. Oang, T.W. Kim, H. Ki, J. Jo, S. Park, C. Song, T. Sato, K. Ogawa, T. Togashi, K. Tono, M. Yabashi, T. Ishikawa, J. Kim, R. Ryoo, J. Kim, H. Ihee, S. Adachi, Nature 518 (2015) 385–389.
[162] L. Wu, J.J. Willis, I.S. McKay, B.T. Diroll, J. Qin, M. Cargnello, C.J. Tassone, Nature 548 (2017) 197.
[163] C.B. Murray, Science 324 (2009) 1276–1277.
[164] J.M. Yuk, J. Park, P. Ercius, K. Kim, D.J. Hellebusch, M.F. Crommie, J.Y. Lee, A. Zettl, A.P. Alivisatos, Science 336 (2012) 61–64.
[165] H. Zheng, R.K. Smith, Y.-W. Jun, C. Kisielowski, U. Dahmen, A.P. Alivisatos, Science 324 (2009) 1309–1312.
[166] X. Ye, M.R. Jones, L.B. Frechette, Q. Chen, A.S. Powers, P. Ercius, G. Dunn, G.M. Rotskoff, S.C. Nguyen, V.P. Adiga, A. Zettl, E. Rabani, P.L. Geissler, A.P. Alivisatos, Science 354 (2016) 874–877.
[167] M. Castro, M. Haouas, I. Lim, H.J. Bongard, F. Schüth, F. Taulelle, G. Karlsson, V. Alfredsson, E. Breyneart, C.E.A. Kirschhock, W. Schmidt, Chem. - A Eur. J. 22 (2016) 15307–15319.
[168] M. Cargnello, V.V.T. Doan-Nguyen, T.R. Gordon, R.E. Diaz, E.A. Stach, R.J. Gorte, P. Fornasiero, C.B. Murray, Science 341 (2013) 771–773.
[169] B. Qiao, A. Wang, X. Yang, L.F. Allard, Z. Jiang, Y. Cui, J. Liu, J. Li, T. Zhang, Nat. Chem. 3 (2011) 634–641.
[170] L. DeRita, S. Dai, K. Lopez-Zepeda, N. Pham, G.W. Graham, X. Pan, P. Christopher, J. Am. Chem. Soc. 139 (2017) 14150–14165.
[171] L. Nie, D. Mei, H. Xiong, B. Peng, Z. Ren, X.I.P. Hernandez, A. DeLaRiva, M. Wang, M.H. Engelhard, L. Kovarik, A.K. Datye, Y. Wang, Science 358 (2017) 1419–1423.
[172] Y. Tang, Y. Li, V. Fung, D. Jiang, W. Huang, S. Zhang, Y. Iwasawa, T. Sakata, L. Nguyen, X. Zhang, A.I. Frenkel, F. Tao, Nat. Commun. 9 (2018) 1231.
[173] W. Huang, S. Zhang, Y. Tang, Y. Li, L. Nguyen, Y. Li, J. Shan, D. Xiao, R. Gagne, A.I. Frenkel, F.F. Tao, Angew. Chem. 128 (2016) 13639–13643.
[174] T. Bunluesin, R.J. Gorte, G.W. Graham, Appl. Catal. B Environ. 15 (1998) 107–114.
[175] G.L. Bezemer, J.H. Bitter, H.P.C.E. Kuipers, H. Oosterbeek, J.E. Holewijn, X. Xu, F. Kapteijn, A.J. van Dillen, K.P. de Jong, J. Am. Chem. Soc. 128 (2006) 3956–3964.
[176] V. Iablokov, S.K. Beaumont, S. Alayoglu, V.V. Pushkarev, C. Specht, J. Gao, A.P. Alivisatos, N. Kruse, G.A. Somorjai, Nano Lett. 12 (2012) 3091–3096.
[177] A. Sapi, F. Liu, X. Cai, C.M. Thompson, H. Wang, K. An, J.M. Krier, G.A. Somorjai, Nano Lett. 14 (2014) 6727–6730.
[178] H. Wang, Y. Wang, Z. Zhu, A. Sapi, K. An, G. Kennedy, W.D. Michalak, G.A. Somorjai, Nano Lett. 13 (2013) 2976–2979.
[179] J.N. Kuhn, W. Huang, C.-K. Tsung, Y. Zhang, G.A. Somorjai, J. Am. Chem. Soc. 130 (2008) 14026–14027.
[180] V.V. Pushkarev, N. Musselwhite, K. An, S. Alayoglu, G.A. Somorjai, Nano Lett. 12 (2012) 5196–5201.
[181] S. Zhang, M. Cargnello, W. Cai, C.B. Murray, G.W. Graham, X. Pan, J. Catal. 337 (2016) 240–247.
[182] P. Tabib Zadeh Adibi, F. Mazzotta, T.J. Antosiewicz, M. Skoglundh, H. Grönbeck, C. Langhammer, ACS Catal. 5 (2015) 426–432.
[183] E.W. Thiele, Ind. Eng. Chem. 31 (1939) 916–920.
[184] P.B. Weisz, J.S. Hicks, Chem. Eng. Sci. 17 (1962) 265–275.
[185] H. Konno, T. Okamura, T. Kawahara, Y. Nakasaka, T. Tago, T. Masuda, Chem. Eng. J. 207–208 (2012) 490–496.
[186] M.V. Landau, L. Vradman, V. Valtchev, J. Lezervant, E. Liubich, M. Talianker, Ind. Eng. Chem. Res. 42 (2003) 2773–2782.
[187] K. Yamamoto, T. Imaoka, W.-J. Chun, O. Enoki, H. Katoh, M. Takenaga, A. Sonoi, Nat. Chem. 1 (2009) 397–402.
[188] Y. Sun, L. Zhuang, J. Lu, X. Hong, P. Liu, J. Am. Chem. Soc. 129 (2007) 15465–15467.
[189] I.S. McKay, J.A. Schwalbe, E.D. Goodman, J.J. Willis, A. Majumdar, M. Cargnello, MRS Commun. 6 (2016) 241–246.
[190] J. Liu, L. Jiang, B. Zhang, J. Jin, D.S. Su, S. Wang, G. Sun, ACS Catal. 4 (2014) 2998–3001.
[191] R. Reske, H. Mistry, F. Behafarid, B. Roldan Cuenya, P. Strasser, J. Am. Chem. Soc. 136 (2014) 6978–6986.
[192] Y. Zhou, S. Xi, J. Wang, S. Sun, C. Wei, Z. Feng, Y. Du, Z.J. Xu, ACS Catal. 8 (2018) 673–677.
[193] V. Subramanian, E.E. Wolf, P.V. Kamat, J. Am. Chem. Soc. 126 (2004) 4943–4950.
[194] L. Amirav, A.P. Alivisatos, J. Phys. Chem. Lett. 1 (2010) 1051–1054.
[195] P. Kalisman, Y. Nakibli, L. Amirav, Nano Lett. 16 (2016) 1776–1781.
[196] Y. Ben-Shahar, F. Scotognella, I. Kriegel, L. Moretti, G. Cerullo, E. Rabani, U. Banin, Nat. Commun. 7 (2016) 10413.
[197] Y. Nakibli, Y. Mazal, Y. Dubi, M. Wächtler, L. Amirav, Nano Lett. 18 (2018) 357–364.
[198] I. Lee, R. Morales, M.A. Albiter, F. Zaera, Proc. Natl. Acad. Sci. 105 (2008) 15241–15246.

[199] K.M. Bratlie, H. Lee, K. Komvopoulos, P. Yang, G.A. Somorjai, Nano Lett. 7 (2007) 3097–3101.
[200] M. Crespo-Quesada, A. Yarulin, M. Jin, Y. Xia, L. Kiwi-Minsker, J. Am. Chem. Soc. 133 (2011) 12787–12794.
[201] F. Esch, S. Fabris, L. Zhou, T. Montini, C. Africh, P. Fornasiero, G. Comelli, R. Rosei, Science 309 (2005) 752–755.
[202] A. Migani, G.N. Vayssilov, S.T. Bromley, F. Illas, K.M. Neyman, Chem. Commun. 46 (2010) 5936.
[203] X. Liu, K. Zhou, L. Wang, B. Wang, Y. Li, J. Am. Chem. Soc. 131 (2009) 3140–3141.
[204] T.X.T. Sayle, S.C. Parker, C.R.A. Catlow, Surf. Sci. 316 (1994) 329–336.
[205] J. Conesa, Surf. Sci. 339 (1995) 337–352.
[206] X. Xie, Y. Li, Z.-Q. Liu, M. Haruta, W. Shen, Nature. 458 (2009) 746–749.
[207] L. Hu, K. Sun, Q. Peng, B. Xu, Y. Li, Nano Res. 3 (2010) 363–368.
[208] N.M. Markovic, H.A. Gasteiger, P.N. Ross, J. Phys. Chem. 99 (1995) 3411–3415.
[209] V.R. Stamenkovic, B. Fowler, B.S. Mun, G. Wang, P.N. Ross, C.A. Lucas, N.M. Marković, Science. 315 (2007) 493–497.
[210] C. Wang, H. Daimon, T. Onodera, T. Koda, S. Sun, Angew. Chem. Int. Ed. 47 (2008) 3588–3591.
[211] C. Wang, H. Daimon, Y. Lee, J. Kim, S. Sun, J. Am. Chem. Soc. 129 (2007) 6974–6975.
[212] L. Zhang, L.T. Roling, X. Wang, M. Vara, M. Chi, J. Liu, S.-I. Choi, J. Park, J.A. Herron, Z. Xie, M. Mavrikakis, Y. Xia, Science 349 (2015) 412–416.
[213] M.A. Mahmoud, F. Saira, M.A. El-Sayed, Nano Lett. 10 (2010) 3764–3769.
[214] B.Y. Xia, H. Bin Wu, X. Wang, X.W. (David) Lou, J. Am. Chem. Soc. 134 (2012) 13934–13937.
[215] C.W. Li, M.W. Kanan, J. Am. Chem. Soc. 134 (2012) 7231–7234.
[216] C.W. Li, J. Ciston, M.W. Kanan, Nature 508 (2014) 504–507.
[217] C. Hahn, T. Hatsukade, Y.-G. Kim, A. Vailionis, J.H. Baricuatro, D.C. Higgins, S.A. Nitopi, M.P. Soriaga, T.F. Jaramillo, Proc. Natl. Acad. Sci. 114 (2017) 5918–5923.
[218] H. Xie, T. Wang, J. Liang, Q. Li, S. Sun, Nano Today 21 (2018) 41–54.
[219] Y. Hori, I. Takahashi, O. Koga, N. Hoshi, J. Mol. Catal. A Chem. 199 (2003) 39–47.
[220] D. Gao, I. Zegkinoglou, N.J. Divins, F. Scholten, I. Sinev, P. Grosse, B. Roldan Cuenya, ACS Nano 11 (2017) 4825–4831.
[221] D. Kim, C.S. Kley, Y. Li, P. Yang, Proc. Natl. Acad. Sci. 114 (2017) 10560–10565.
[222] H. Miura, K. Endo, R. Ogawa, T. Shishido, ACS Catal. 7 (2017) 1543–1553.
[223] N.M. Wilson, P. Priyadarshini, S. Kunz, D.W. Flaherty, J. Catal. 357 (2018) 163–175.
[224] H. Zhang, T. Watanabe, M. Okumura, M. Haruta, N. Toshima, Nat. Mater. 11 (2012) 49–52.
[225] P. Aich, H. Wei, B. Basan, A.J. Kropf, N.M. Schweitzer, C.L. Marshall, J.T. Miller, R. Meyer, J. Phys. Chem. C 119 (2015) 18140–18148.
[226] M. Liu, W. Tang, Z. Xie, H. Yu, H. Yin, Y. Xu, S. Zhao, S. Zhou, ACS Catal. 7 (2017) 1583–1591.
[227] M. Cargnello, J.J. Delgado Jaén, J.C. Hernández Garrido, K. Bakhmutsky, T. Montini, J.J. Calvino Gámez, R.J. Gorte, P. Fornasiero, Science 337 (2012) 713–717.
[228] J.W.D. Ng, T.R. Hellstern, J. Kibsgaard, A.C. Hinckley, J.D. Benck, T.F. Jaramillo, ChemSusChem 8 (2015) 3512–3519.
[229] H. Zhu, S. Zhang, Y.-X. Huang, L. Wu, S. Sun, Nano Lett. 13 (2013) 2947–2951.
[230] R.B. Levy, M. Boudart, Science 181 (1973) 547–549.
[231] S.T. Oyama, The Chemistry of Transition Metal Carbides and Nitrides, Academic, Blackie, 1996.
[232] D. Kim, J. Resasco, Y. Yu, A.M. Asiri, P. Yang, Nat. Commun. 5 (2014) 4948.
[233] D. Kim, C. Xie, N. Becknell, Y. Yu, M. Karamad, K. Chan, E.J. Crumlin, J.K. Nørskov, P. Yang, J. Am. Chem. Soc. 139 (2017) 8329–8336.
[234] X. Chen, S. Shen, L. Guo, S.S. Mao, Chem. Rev. 110 (2010) 6503–6570.
[235] S. Chen, T. Takata, K. Domen, Nat. Rev. Mater. 2 (2017) 17050.
[236] C. Xie, C. Chen, Y. Yu, J. Su, Y. Li, G.A. Somorjai, P. Yang, Nano Lett. 17 (2017) 3798–3802.
[237] M.E. Grass, S.H. Joo, Y. Zhang, G.A. Somorjai, J. Phys. Chem. C 113 (2009) 8616–8623.
[238] J.C. Park, J.U. Bang, J. Lee, C.H. Ko, H. Song, J. Mater. Chem. 20 (2010) 1239–1246.
[239] S. Mezzavilla, C. Baldizzone, A.-C. Swertz, N. Hodnik, E. Pizzutilo, G. Polymeros, G.P. Keeley, J. Knossalla, M. Heggen, K.J.J. Mayrhofer, F. Schüth, ACS Catal. 6 (2016) 8058–8068.
[240] T.R. Hellstern, J. Kibsgaard, C. Tsai, D.W. Palm, L.A. King, F. Abild-Pedersen, T.F. Jaramillo, ACS Catal. 7 (2017) 7126–7130.
[241] D. Wang, T. Hisatomi, T. Takata, C. Pan, M. Katayama, J. Kubota, K. Domen, Angew. Chem. Int. Ed. 52 (2013) 11252–11256.
[242] D. Zheng, X.-N. Cao, X. Wang, Angew. Chem. Int. Ed. 55 (2016) 11512–11516.
[243] M. Xing, B. Qiu, M. Du, Q. Zhu, L. Wang, J. Zhang,Adv. Funct. Mater. 27 (2017), 1702624.
[244] Z. Li, L. Mo, Y. Kathiraser, S. Kawi, ACS Catal. 4 (2014) 1526–1536.
[245] Z. Li, S. Kawi, Catal. Sci. Technol. 8 (2018) 1915–1922.
[246] M. Zhao, K. Yuan, Y. Wang, G. Li, J. Guo, L. Gu, W. Hu, H. Zhao, Z. Tang, Nature 539 (2016) 76–80.
[247] K.M. Choi, K. Na, G.A. Somorjai, O.M. Yaghi, J. Am. Chem. Soc. 137 (2015) 7810–7816.
[248] I. Wheeldon, S.D. Minteer, S. Banta, S.C. Barton, P. Atanassov, M. Sigman, Nat. Chem. 8 (2016) 299–309.
[249] M. Baalousha, J.R. Lead, Nat. Nanotechnol. 8 (2013) 308–309.
[250] J.-H. Park, H. Jeong, J. Hong, M. Chang, M. Kim, R.S. Chuck, J.K. Lee, C.-Y. Park, Sci. Rep. 6 (2016) 37762.
[251] R.D. Glover, J.M. Miller, J.E. Hutchison, ACS Nano 5 (2011) 8950–8957.
[252] Y. Shen, M.Y. Gee, A.B. Greytak, Chem. Commun. 53 (2017) 827–841.
[253] J.D. Bass, X. Ai, A. Bagabas, P.M. Rice, T. Topuria, J.C. Scott, F.H. Alharbi, H.-C. Kim, Q. Song, R.D. Miller, Angew. Chem. Int. Ed. 50 (2011) 6538–6542.
[254] P. Kunal, E.J. Roberts, C.T. Riche, K. Jarvis, N. Malmstadt, R.L. Brutchey, S.M. Humphrey, Chem. Mater. 29 (2017) 4341–4350.
[255] L. Zhang, G. Niu, N. Lu, J. Wang, L. Tong, L. Wang, M.J. Kim, Y. Xia, Nano Lett. 14 (2014) 6626–6631.
[256] M.E. Cueva, L.E. Horsfall, Microb. Biotechnol. 10 (2017) 1212–1215.
[257] J.M. Byrne, H. Muhamadali, V.S. Coker, J. Cooper, J.R. Lloyd,J. R. Soc. Interface 12 (2015), 20150240.

Pit Losch is an Alexander von Humboldt fellow at the Max-Planck-Institut für Kohlenforschung. He was a visiting scholar in Prof. M. Cargnello's laboratory at Stanford University within the frame of a Fulbright fellowship. He received his PhD in chemistry from Strasbourg University in 2016. His research interest focuses on nanomaterials, micro- and mesoporous materials and catalysis.

Weixin Huang received his Ph.D. from University of Notre Dame in 2018 and joined Prof. Matteo Cargnello's group at Stanford University the same year as a postdoctoral scholar. His research focuses on the development of nanomaterials for the removal of hydrocarbons from contaminated gas streams.

Emmett Goodman is a fourth year National Science Foundation Graduate Research Program fellow working with Matteo Cargnello at Stanford University. He received his bachelor's degree from Caltech in Chemical Engineering. Emmett's research focuses on synthesizing and studying the catalytic effects of interparticle interactions in powder catalysts.

Cody J. Wrasman is a fourth year Ph.D. student in the lab of Prof. M. Cargnello. He attended The University of Minnesota – Twin Cities as an undergraduate. His research focuses on the use of dilute alloys for selective oxidation catalysis.

Alexander Holm received his Ph.D. in chemical engineering from Stanford University in 2018, and is currently working as a post-doctoral scholar, also at Stanford University, in the laboratory of Professor Matteo Cargnello. His research interests include self-assembly, nanomaterials, catalysis and photocatalysis.

Andrew Riscoe is a National Science Foundation Graduate Research Program fellow working towards his PhD under the direction of Prof. M. Cargnello. He received his BS in Chemical Engineering at the University of Colorado in 2012 before working in the lithium battery industry at CoorsTek Fluorochemicals. His research interests include nanomaterials, microporous polymers and biomimetic catalysis for energy applications.

Jay A. Schwalbe received his B.S. in Chemical Engineering at Cornell University before joining Stanford as a Ph.D. student with Prof. M. Cargnello. His research focuses on electrocatalytic processes for sustainable production of fuels and chemicals, such as the conversion of nitrogen into ammonia.

Matteo Cargnello received his Ph.D. in Nanotechnology in 2012 at the University of Trieste (Italy) and he was then a post-doctoral scholar at the University of Pennsylvania (Philadelphia) before joining the Faculty at Stanford in 2015, where he is currently Assistant Professor of Chemical Engineering, and, by courtesy, of Materials Science and Engineering, and Terman Faculty Fellow. In his research group, uniform and tailored nanocrystals and nanostructures are synthesized, studied and used for energy and environmental applications through catalytic processes, with emphasis on how to precisely control nanoarchitectures to understand and exploit interactions between well-defined building blocks.